Global Vulnerability Mapping of Coastal Zones Prone to Saltwater Intrusion

Master of Science Thesis
by
Aisyah Fairuz Salsabila

Supervisors
Dr. Michael McClain

Mentors
Dr. Yangxiao Zhou
Dr. Gualbert Oude Essink

Examination committee
Dr. Michael McClain
Dr. Yangxiao Zhou
Dr. Gualbert Oude Essink

This thesis is submitted in partial fulfilment of the requirements for the academic degree of

Master of Science in Water Science and Engineering
IHE Delft Institute for Water Education, Delft, the Netherlands

Master of Science in Environmental Engineering
Instituto Superior Técnico, Universidade de Lisboa, Portugal

Master of Science in Hydro Science and Engineering
Technische Universität Dresden, Germany

IHE Delft

August 2022

Global Vulnerability Mapping of Coastal Zones Prone to Saltwater Intrusion

Master of Science Thesis
by
Aisyah Fairuz Salsabila

Supervisors
Dr. Michael McClain

Mentors
Dr. Yangxiao Zhou
Dr. Gualbert Oude Essink

Examination Committee
Dr. Michael McClain
Dr. Yangxiao Zhou
Dr. Gualbert Oude Essink

This research is done for the partial fulfilment of requirements for the Master of Science degree at the
IHE Delft Institute for Water Education, Delft, the Netherlands.

Delft
28/08/2022

Although the author and IHE Delft Institute for Water Education have made every effort to ensure that the information in this thesis was correct at press time, the author and IHE Delft do not assume and hereby disclaim any liability to any party for any loss, damage, or disruption caused by errors or omissions, whether such errors or omissions result from negligence, accident, or any other cause.

Abstract

Saltwater intrusion (SWI) has been a global issue in recent decades. It is worsened by the rapid rate of climate change and high population growth. It threatens groundwater supply in the cities along the coastline because of the risk of higher salinity in the water. Thus, this study aims to create a map of vulnerability to saltwater intrusion in the coastal zones based on the governing indicators. It could be achieved with the goals of evaluating relevant indicators that determine the vulnerability to seawater intrusion, developing a method to combine multiple indicators for vulnerability mapping, and testing the indicators' sensitivities. This study used 16 indicators that embodied both natural and anthropogenic factors. Vulnerability mapping uses a weighted average method, adapted from GALDIT method. The results were generated per continent and then merged to obtain a global vulnerability map, showing that around 40% of the coastal zones worldwide have extreme vulnerability, mainly in the coastal zones with high human interventions. This includes South and Southeast Asia, the eastern coast of China, the Arabian Peninsula, the northern coast of Europe, the east coast of the UK, the Mediterranean coast, the west coast of North America, and small regions scattered on the west coast of South America. The indicators were tested with two sensitivity tests to see their influence on the map. The most influencing indicators are groundwater abstraction, aquifer type, and the distance from the coastline. Some mitigation measures are needed to reduce the severe impact of saltwater intrusion in the coastal zones. Since the governing effect of saltwater is not only from the natural elements but also anthropogenic elements, thus integrated coastal zone management would be more efficient for overcoming the issues.

Acknowledgements

Table of Contents

List of Figures

List of Tables

Abbreviations

Chapter 1   Introduction

1.1 Research Background

Saltwater intrusion (SWI) is a natural process that is not only a result of the anthropogenic activity but is also related to climate change (Jakovovic et al., 2016; Post et al., 2018; Trabelsi et al., 2016). Accumulating pressures from different drivers on coastal aquifers is causing groundwater salinity, now and in the future, leading to varying schemes of events. An important driver is climate change, which is expected to seriously affect the coastal area in many ways, such as sea level rise (SLR), high tides, storm surge, ice sheet melting, climate variability, etc. (Taylor et al., 2013). In this study, the climate change drivers that will be considered are sea level rise and storm surge. Sea level rise can directly cause further saltwater intrusion in the long term, while storm surges usually happen seasonally due to high tides (Muis et al., 2016). Both processes could generate land inundation over the coastal zone, where it could cause saline vertical downward infiltration, which resulting vertical upward saline exfiltration into groundwater aquifers causing saltwater intrusion(Oude Essink, 2001).

On top of that, climate change also brings other problems. For example, higher evapotranspiration rates and lower evapotranspiration in certain areas following with lower precipitation rate can cause higher salinity in the topsoil horizon (IPCC, 2021). Higher precipitation rates and land use change could also lead to erosion (Hassani et al., 2021). Geology is also a substantial indicator because coastal zones mainly consist of alluvium deposits, rich in clay material that limits groundwater recharge due to impaired permeability (e.g., Zamrsky, 2013). Zamrsky et al. also describe other vital indicators, e.g., the water needs. The demand for freshwater in the coastal zone is prominently high, especially in Asia. It is in the range of 500 - 1000 km3/year in the coast of India, Bangladesh, and China, while on the other coastal cities, the water demand varies from $10 - 200 \text{ km}^3/\text{year}$.

Many areas along the global coastline suffer saltwater intrusion issues (Figure 1). These coastlines are densely populated and exploited for natural resources like sand and water. One of the most affected resources is fresh groundwater. With approximately 35% of people in the world living within 100 km of a coast, it is expected that there will be substantial pressure on coastal freshwater aquifers due to groundwater extraction because of human placement in the area (Parizi et al., 2019; Stigter, 2021). Large amounts of groundwater extraction can decrease the piezometric head in aquifers. Groundwater over-abstraction later can increase the salt content of the water to a higher influx of (paleo) saline groundwater. This will eventually lead to unsuitable water quality (the water is being too salty) for drinking, agricultural use, and industry (Pilla & Torrese, 2022; Weerasekera, 2017). Many studies proved that groundwater over-abstraction for agriculture, industrial, recreational, and household needs (Alfarrah & Walraevens, 2018; Ivkovic et al., 2012; Wada et al., 2012; Wu et al., 2020). Urban areas will be seriously affected since the groundwater is often over-abstracted. Population increase linked to a higher rate of urbanization in the world also limits fresh groundwater availability due to groundwater over-abstraction. Infrastructures over land, e.g., buildings and houses, can result in less infiltration leading to sealing and a decrease of groundwater recharge leading to smaller

fresh groundwater volumes. Over abstraction of groundwater in the long term could be developing an upconing of saline groundwater. It also leads to another SWI-related driver: land subsidence (Hendrikx, n.d.; Minderhoud et al., 2017). Land subsidence is not necessarily always caused by groundwater exploitation, but in urban areas, land subsidence is known to be a byproduct of over-exploitation. Then, it could lead to higher susceptibility to land inundation by storm surges.
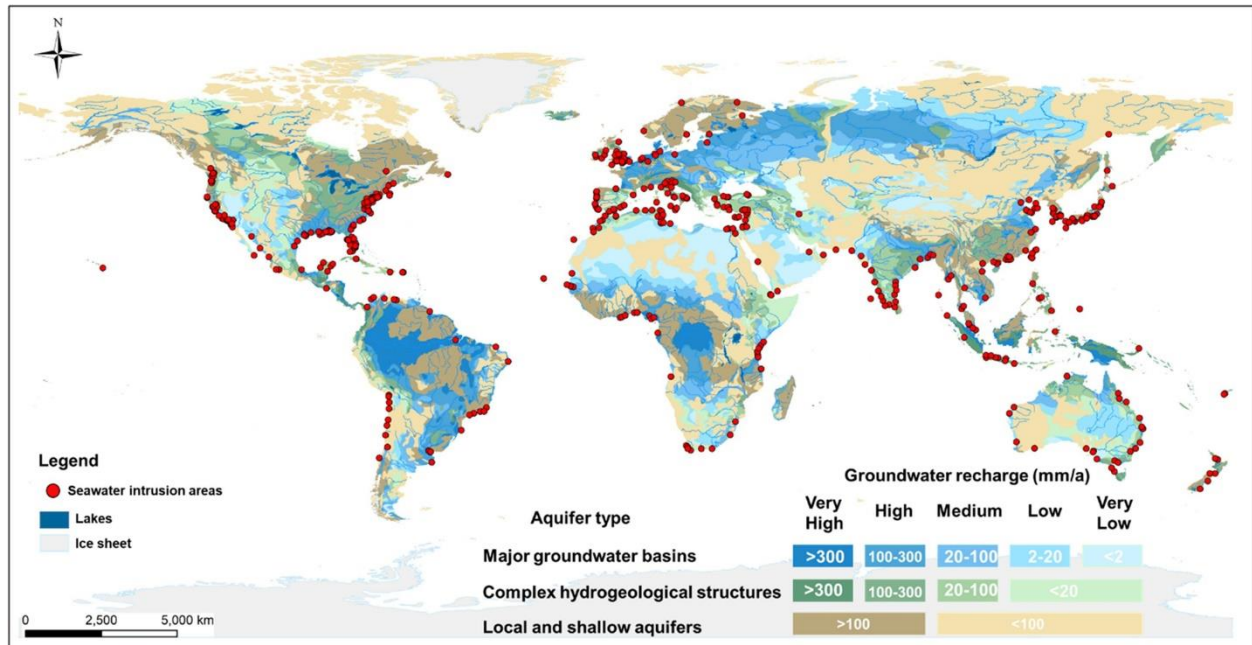
Figure 1. Areas in the coastal zone with reported seawater intrusion problems (Cao et al., 2021)

1.2 Problem Statements

A significant number of world's population resides within 100 km from the coastline and in the same time 67% of the megacities – cities with more than 10 million population – are located in the coastal zones (Parizi et al., 2019; von Glasow et al., 2013). Continuous alteration of what and pressure of what in the coastal zone will have a big effect on the hydrogeological system, leading to salinization of the groundwater system. This study will focus on groundwater salinization induced by three mechanisms: upconing from groundwater abstraction, lateral saltwater intrusion from the seaside, and overtopping or inundation of seawater on coastal zones due to storm surges.

Many studies have proven that excessive abstraction of groundwater causes major issues on coastal water resource management, where aquifer suffers from large piezometric water level drops and seawater intrusion due to higher rates of upconing (Chang et al., 2020; Jakovovic et al., 2016; Mirzavand et al., 2020; Nogueira et al., 2019; Parizi et al., 2019; Tasnim & Tahsin, 2016). Saltwater intrusion from the sea to the groundwater systems is usually determined by the water quality, such as high total dissolved solute (TDS) value in groundwater. These high values make the water not eligible to be drunk. The TDS value in the coastal groundwater system can be ranged from 10,000 mg/L to more than 100,000 mg/L, while according to WHO Guidelines for drinking water quality, the limit of TDS for eligible drinking water is less than 500 mg/L (Mirzavand et al., 2020; WHO, 2003). The high value of TDS indicates that many

coastal aquifers are unsafe since most groundwater in coastal zones suffers from mixing with saline groundwater as the primary process affecting groundwater salinity in the coastal area.

Coastal zones are highly susceptible to storm surges, inundation due to rising sea levels and tsunamis (Vithanage et al., 2012). Overtopping of seawater on the coastal floodplain could increase the groundwater salinity due to infiltrated saline water into groundwater (Mirzavand et al., 2020). Overtopping could repeatedly occur in a year, especially with the climate change effect where a more unstable and extreme climate affects the surface and increases the probability of saline groundwater infiltrating deeper parts of the aquifer. It has been proven that there has been a significant increase in coastal-related natural disasters, such as storm surges and sea level rise (Yu et al., 2016). In addition, the rising and falling of tides on the ocean could give an effect of "push and pull" of the freshwater-saltwater interface more inland with high tides and more seaward as the tides are low (Muis et al., 2016; Paldor & Michael, 2021). This movement highly affects the mixing of fresh and saline groundwater in the coastal aquifer.

In short, the stress occurs in the coastal zones due to natural and anthropogenic drivers, especially in coastal zones with urban development. Nevertheless, only a few studies (e.g. Ivkovic (2012) and Zamrsky (2013)) approach the topic of groundwater salinization of coastal aquifers holistically. Considering several aspects, not only intrinsic properties but also socio-economic aspects, and the impact of the groundwater salinization processes on humans, thus an investigation of the vulnerability to groundwater salinity is relevant. On top of this, a better understanding is also needed to design a mitigation scenario to seawater intrusion, especially for drinking water and agriculture.

1.3 Research Questions

Regarding problems stated in the previous section, it is essential to analyze the vulnerability to salinity on a global scale. To solve these problems, four research questions are determined:

1. Which factors determine the degree of vulnerability of the groundwater to seawater intrusion, for example, geology, geomorphology, and abstractions, and which one is the most important driver?
2. Which method can be applied for the vulnerability assessment using existing (global) mapping databases?
3. How efficient can the global mapping technique be applied in a specific study area?
4. What are the effective mitigating measures for preventing seawater intrusion?

1.4 Objectives

The objectives of this research are the following:

1. To evaluate relevant indicators that determine the vulnerability of seawater intrusion from a water resources point of view;
2. To develop a method to combine different indicators for vulnerability assessment using global datasets;
3. To test sensitivities of indicators on vulnerability index.

1.5 Scope of Study

The scope of this study is chosen as the constraint for this study. These scopes are the following

1. The vulnerability mapping is done at the global scale.

2. The methodology used for seawater intrusion vulnerability mapping is an index mapping method adapted from GALDIT.
3. The source of salinity will be constrained to seawater intrusion.

Chapter 2   Literature Review

In this chapter, we will discuss the literature of basic knowledge to groundwater salinization, vulnerability of coastal zone, and parameters that governing the process of groundwater salinization in the coastal zone.

2.1 Sea Water Intrusion (SWI)

The mondial distribution of water on the Earth accounted to be 1386×10^6 km^3 and accounting to 97.5% of the water on the Earth are seawater and the rest is freshwater, where out of 2.5% of the freshwater (approximately around 35×10^6 km^3), 30% is potentially available as groundwater (Oude Essink, 2001). Groundwater is an essential aspect of life due to its independency of season, high water quality (constant temperature), low storage cost without spatial limitation, and huge available quantities. But the population is growing and the demand for fresh groundwater also is increasing. The high demand for groundwater threatens fresh groundwater availability because groundwater is prone to salinization, especially in coastal aquifers. The most known phenomenon of salinization is seawater intrusion (SWI). This phenomenon occurs in the coastal aquifer where there is a migration inland of seawater into the freshwater coastal aquifer. Some of the important factors to SWI are the height of groundwater level above sea level, hazards due to climate change (e.g. sea level rise), overexploitation of groundwater aquifers, and high abstraction pumping rates (Parizi et al., 2019). Seawater intrusion is not the only reason of salinization in the coastal zone. Several sources induce salinization in groundwater, such as the dissolution of basement rock by fluid, agricultural waste activity, and many others.

In coastal aquifers, there is contact between fresh and saline groundwater at their seaward margins. The freshwater's seaward limit is influenced by the amount of freshwater flowing through the aquifer, the thickness of the aquifer, the hydraulic properties of the aquifer and adjacent confining unit, and the saltwater and freshwater density (Barlow, 2003). The water's density is highly affecting the condition of the contact between fresh- and saltwater or "transition zone", where there's a mixing between two types of water. Due to the higher saltwater density, it tends to sink and sit below the freshwater and form a saltwater wedge. It occurs in the aquifer, landward, and potentially extends tens of kilometers inlandv(Ivkovic et al., 2012; Werner et al., 2013). A transition zone induced a circulation movement of saltwater from the sea to the transition zone and then back to the sea. Figure 2 shows a simplify illustration of the dynamic of coastal groundwater, including the process of upconing. The dynamic of coastal groundwater may seem simple, but in the real picture it is more complex, with a lot of elements influencing it. Globally, the transition zone is moving along with the long-term fluctuation of global sea-level position, e.g., transgression and regression movement of saltwater due to marine water trapped in the sediments (Groen, 2002; Kooi et al., 2000). As the sea level declines, more land will be able to obtain freshwater recharge, pushing the interface away from the land (seaward). On the other hand, as the sea level rises, the interface will be pushed landward because more ground is covered with seawater resulting in seawater infiltration into the freshwater aquifer (Barlow, 2003). Not only horizontal movement, SWI

5

also occurs in vertical movement. Figure 2 shows saltwater moving from a deeper location towards a well due to pumping called "upconing".
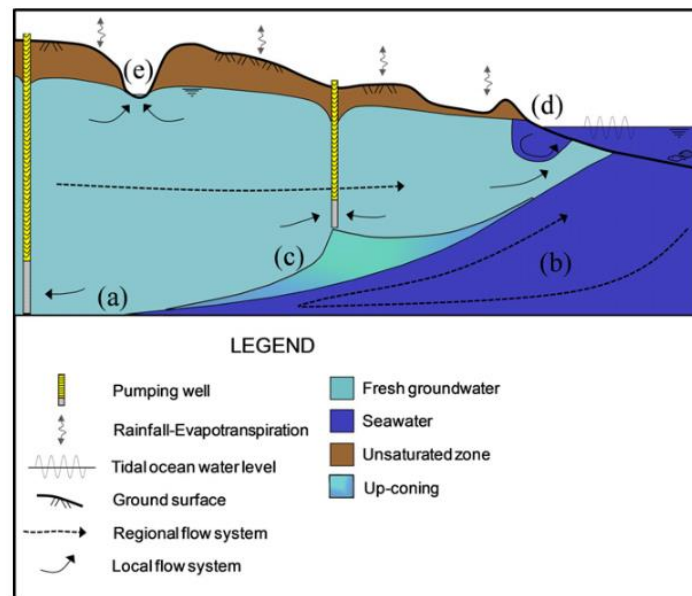
Figure 2. Groundwater flow patterns in unconfined coastal aquifer, showing (a) seawater wedge toe, (b) density-driven circulation in the seawater zone, (c) seawater upconing due to well pumping, (d) coastal fringe processes, such as tidal seepage face and upper seawater recirculation zone, (e) head-controlled surface expression of groundwater (Werner et al., 2013).

Under natural conditions, the groundwater flow in coastal aquifers is highly affected by the saline water flow from the sea. The higher saltwater density can easily change the equilibrium of fresh and saline water interface in the coastal area. Thus, to take into account the density difference, the interface approximation and the depth of fresh- and saltwater interface or transition zone can be computed using Badon Ghijben-Herzberg principle. The relationship estimates the interface based on the density difference between fresh- and saltwater and the thickness of freshwater above sea level, as shown in Figure 3.

Equation 2.1—1 Ghyben – Herzberg principle

$$z = \frac{\rho_f}{\rho_s - \rho_f} h$$

where z is freshwater below sea level, h is freshwater above sea level (hydraulic head), ρ_f is the density of freshwater (1000 kg/m^3), and ρ_s is the density of saltwater (1025 kg/m^3). For a steady state condition, the relationship is described as follow

Equation 2.1—2 Ghyben – Herzberg principle in steady state condition

$$z = \alpha h$$

where according to the density difference in Eq.1 $\alpha = 40$, thus one height unit of fresh groundwater above sea level is equal to 40 height unit of freshwater below sea level. The equation is valid if certain situations comply, which are (Oude Essink, 2001):

- Aquifer is homogeneous
- Hydrodynamic dispersion is negligible,
- Vertical flow in the aquifer is negligible,
- Horizontal flow in aquitard is negligible,
- Saline groundwater is stagnant (no movement), $q_s = 0$.
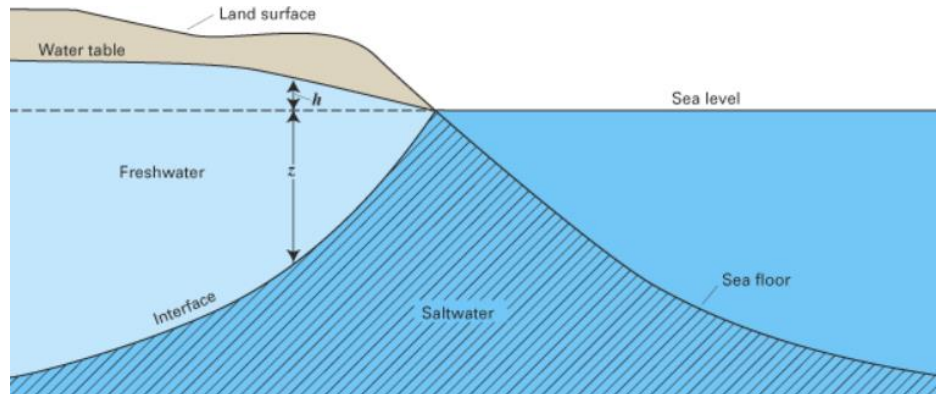
Figure 3. Illustration of fresh- and saltwater interface in the coastal aquifer (Barlow, 2003)

2.2 Groundwater Salinization Sources

In general, salinization sources are divided into two, natural and anthropogenic sources, which will be explained further in sections 2.2.1 and 2.2.2. Many previous studies explained that salinization in coastal is not only the consequence of natural behavior, but human involvement also brings enormous stress to the aquifer. Human activities such as land reclamation and mining of natural resources can increase the potential of salinization in surface water and degrade soil quality as it will be more saline and eventually, the salinity will move downward along with water percolating into the aquifer.

As shown in Figure 4, the threat of groundwater salinization in coastal zones might originate from the subsurface (intrinsic) and the surface (extrinsic). Within the subsurface, the aquifer is threatened by the aquifer characteristic. For example, most coastal aquifers in the world consist of carbonate rock, which has high conductivity, so it can simply conduct water through the aquifer. When the rock formation of an aquifer can pass water quickly, so can sea water. Accordingly, coastal zones are very vulnerable to groundwater salinization due to seawater intrusion into freshwater aquifers just because of the aquifer properties. The thickness of the aquifer is an aspect of subsurface characteristics that should be taken into consideration because the thinner the aquifer, the easier for freshwater to be replaced with seawater in the presence of sea water intrusion event.

Meanwhile, extrinsic factors of salinization can be caused by many other parameters, such as climate change, agriculture, population, land cover, etc. Climate change brings an additional concern to the topic. Furthermore, global temperature rises threaten coastal zones, especially in the polar region, with extreme sea level rise and coastal inundation. With the sudden change in climate conditions, the aquifer may not have enough recovery time from the salinization. Besides climate change, human interaction and development are also extrinsic indicators of vulnerability that need concern. The population growth around the world, especially in megacities, negatively affected the aquifer condition. Conformable with population growth around the world, it increases the amount of water exploitation. Groundwater extraction for different purposes could directly cause saltwater intrusion by causing an upconing into the well.

7
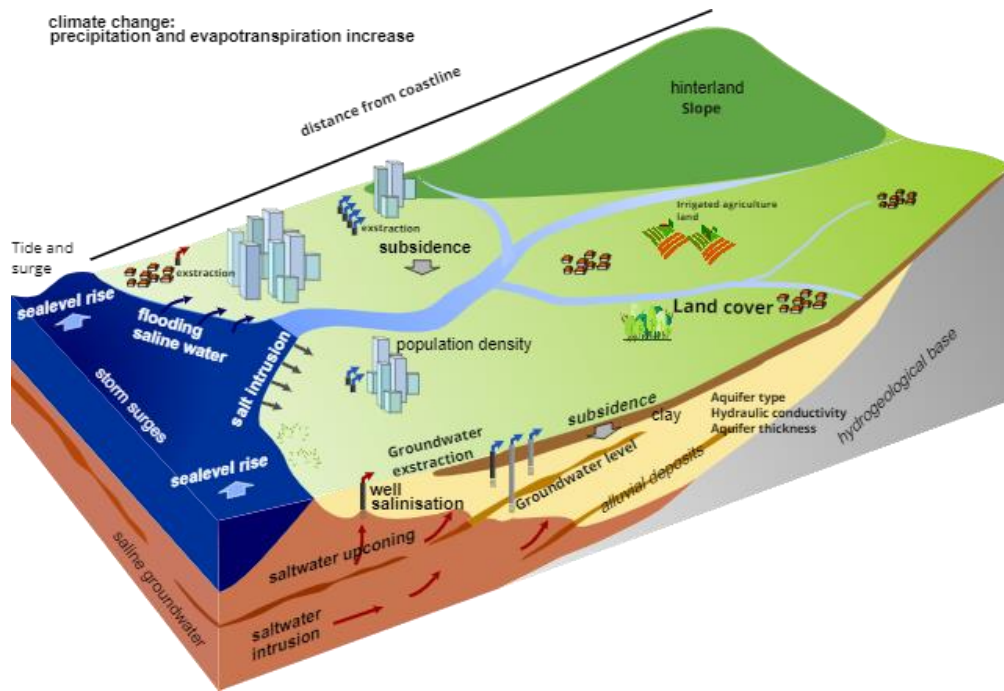
Figure 4. Coastal threat from salinization and salt-fresh water interaction modified from Deltares (2017)

2.2.1 Natural Sources

Many factors affect the fresh, brackish, and saline groundwater distribution. SWI in coastal aquifers is affected by the natural recharge and transport process, mainly the flow of water downward due to gravity (Ivkovic et al., 2012; Mirzavand et al., 2020; Oude Essink, 2001). Natural sources can come from the sea or the continent.

2.2.1.1 Off-shore Sources

Natural sources from the sea can be a condition accumulated over the years, such as connate saline groundwater accumulation in the subsoil that can be related to sea level transgression and regression (Michael et al., 2013; Mirzavand et al., 2020; Nogueira et al., 2019). Transgression and regression events on the sea level over the past millions of years can change the water table to decline and this hydraulic gradient and dynamic equilibrium changed over the geological time (Ivkovic et al., 2012; Mirzavand et al., 2020). Seawater will infiltrate the subsoil when the saltwater inundates floodplain (low-lying) areas relatively over a long time. Due to higher saltwater density, it will move downward on the bottom of the aquifer and create a saltwater pocket (Nogueira et al., 2019). Since coastal aquifers are usually composed of alluvium deposits that consist of fine sediments such as silt and clay, it has a high adhesion force that attracts water to soil particle, which means that it has low hydraulic conductivity. It leads to poor flushing (freshening) ability of the shallow aquifer (Nogueira et al., 2019). The residual of saltwater in deep sedimentary formations will be stored in this marine environment. On top, residual connate water can also be originated from evaporated continental or marine water buried at a shallow depth and then percolates to groundwater aquifer (Mirzavand et al., 2020). This condition mostly happens in arid or semi-arid areas, including the polar region.

Other sea-sourced salinization drivers are sea-level rise (SLR) and tide. As an impact of current climate change, IPCC has reported that there will be a rising sea level up to 1 m by 2100 due to ice sheet melts (IPCC, 2021). This means there will be a higher likelihood of seawater migration to the land, increasing the change in the distribution of fresh-brackish-saline

groundwater. Other than that, tidal behavior may lead to a "push and pull" movement – landward and seaward direction of high and low tides, respectively – contributing to the mixing of fresh and saltwater in the transition zone, resulting in a brackish water (Ivkovic et al., 2012; Oude Essink, 2001). Extreme tide behavior, e.g., cyclones and storms, can create incidental flooding by saltwater. When these events occur, many coastal areas will be inundated by saltwater for a short time. Consequently, flushing of saltwater could occur, leading to a higher groundwater salinity in the coastal aquifer (Mirzavand et al., 2020; Zamrsky, 2013).

2.2.1.2 Continental Sources

Continental salinization sources are associated with the evaporation of land surface, dissolution of evaporites mineral, geothermal activities, and osmotic activities in subsoil (Mirzavand et al., 2020; Nogueira et al., 2019). Coastal aquifers are rich with calcite ($CaCO_3$) and halite (NaCl) minerals. A high evaporation rate leads to more concentrated minerals in the subsoil and dissolved to recharge zones as it is highly soluble in water, thus, it increases the groundwater salinity due to ion exchange in the water (Mirzavand et al., 2020; Nogueira et al., 2019). The processes behind the movement of ions are called hydrodynamic dispersion. The concentration gradient drives molecular diffusion, which also induces the development of fresh and saltwater interfaces. Flowing water will create a mixing due to the magnitude and orientation difference of velocity vector in aquifer pore called hydrodynamic dispersion (Oude Essink, 2001). The dissolved matter displacement by dispersion is proportional to groundwater's velocity. Both mechanical dispersion and molecular diffusion influence the concentration difference.

The volcanic rock environment usually has a higher potential for SWI due to the existence of preferential flow in the aquifer. In this environment, groundwater tends to be more mineralized, especially in potential geothermal areas where the groundwater temperature is often high and creates a high mineralization reaction. This water is usually called hydrothermal water. This water is often rich in chloride, bromine, fluoride, sodium, arsenic, and other minerals that could harm fresh groundwater quality (Mirzavand et al., 2020).

The hydrogeological setting of coastal aquifers is critical to assessing the vulnerability of salinization in groundwater. The rate of seawater intrusion is affected by freshwater boundary conditions, specified flux or specified head. The specified flux boundary condition describes the adequate thickness of the unsaturated zone to provide space for water-table rise (Michael et al., 2013). The water table conditions are differentiated into two types, recharge-limited and topography-limited (Figure 5). Most coastal zones worldwide are topography-limited, accounting for around 46.8% to 77.9% (Haitjema & Mitchell-Bruker, 2005; Michael et al., 2013). These two different types of water tables behave differently from SWI. Topography-limited systems are less vulnerable to sea level rise than recharge-limited systems because the hydraulic head on fresh water inland cannot react with the increased head in the sea (Michael et al., 2013).
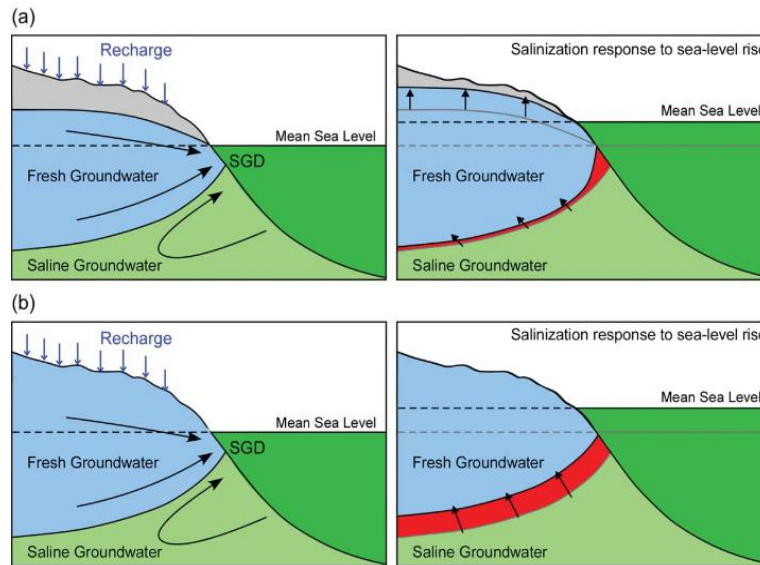
Figure 5. Conceptual model of coastal groundwater aquifer for (a) recharge-limited and (b) topography-limited system. Left figure describes the initial hydraulic condition, groundwater flow, and submarine groundwater discharge (Michael et al., 2013)

2.2.2 Anthropogenic Sources

It is undeniable that human activity highly interferes with groundwater dynamicity, which it influences the distribution of freshwater and saltwater in the subsoil. Most activities that affect groundwater are groundwater extraction, domestic and wastewater effluents, agriculture wastewater, and natural source mining activities (Mirzavand et al., 2020; Oude Essink, 2001; Werner et al., 2013). The following activities are often resulting local salinization of groundwater.

1. Groundwater Extraction

One of the most critical factors is groundwater extraction. Groundwater extraction can induce saltwater intrusion, especially in the coastal aquifer. Extraction can generate upconing in the coastal aquifer due to the discharge of freshwater, causing saltwater to move upward as well as a tremendous amount of hydraulic head drawdown and it has become the biggest issue in the world. Regarding groundwater extraction, the most critical parameter that controls seawater toe below groundwater is the seaward hydraulic gradient, where it will shift to risky conditions and excessive groundwater extraction can bring out a high amount of groundwater discharge to the sea (Parizi et al., 2019; Werner et al., 2013). Excessive pumping of groundwater can induce land subsidence due to the lowering of piezometric heads, as happened in several cities in the world, e.g. Jakarta, Tokyo, Los Angeles, Florida, and many other towns, and induce inland movement of salt water wedge (Oude Essink, 2001).

2. Wastewater Effluent

Wastewater effluents mostly originate from urban areas. In the household sector, the use of detergent salt is becoming a concern due to its effect to the salinization of groundwater (Mirzavand et al., 2020). Groundwater can also be contaminated by sewage system seepage, electronic waste, septic tank or underground storage tanks, and industrial effluents (Brindha & Schneider, 2019). The biggest concern of urban areas, especially in industrial areas and waste disposal facilities, is the contamination of heavy metals, e.g., lead, cadmium, chromium, and mercury (Brindha & Schneider, 2019; Michael et al., 2013). Salinization due to mining often appears near mining pits or oil and gas fields. In oil and gas fields, groundwater is vulnerable to salinization from mud brine in the drilling process and in oil and gas fields in the fluid

10

extraction process (Mirzavand et al., 2020). Open mining pits, surface disposal, and injection wells from the geothermal production field also possibly salinize the groundwater.

3. Agriculture Activities

Agriculture activities give rise to groundwater as well as soil salinity due to use of pesticides and fertilizers. These substances usually leave some residues that plants are not taking and remain in the soil, such as NO_3^-. As the precipitation infiltrates the soil, the substances also move downward, which can later percolate to groundwater aquifer or salt flushing. In the semi-arid and arid regions, groundwater is more prone to salinization because of capillarity rise. Salt is being transported to the surface and the salt concentration on the surface increases as evaporation takes place, resulting in saline groundwater close to the surface (Mirzavand et al., 2020; Nogueira et al., 2019). Salinization in the agriculture sector is influenced by several factors: the salt balance in the soil (input and output), irrigation water quality, and the rate of fertilizer usage (Mirzavand et al., 2020). Salinization in agricultural land also affects crop yield (decreasing crop yield). In the worst case, it causes the crop to die and more salt-tolerant crops are planted to compensate the dying crops (Oude Essink, 2001).

2.3 Vulnerability Assessment

Vulnerability is a term that researchers use to assess the susceptibility of an object to a particular action. Vulnerability is defined as a condition resulting from physical, social, economic, and environmental factors or processes, which then can enhance the susceptibility of a population to be influenced by a hazard, thus it should be recognized as a key indicator of the seriousness of environmental problems (Adger, 2001; ADRC, 2005). A study by Schanze (2016) proposed a relationship between vulnerability, hazard, risk, and exposure (Figure 6). It indicates that vulnerability is an interrelation component that should include several aspects simultaneously. The vulnerability concept of areas is a function of the social element's value, susceptibility, and coping capacity (Schanze, 2016). Thus, the interrelation concept of vulnerability, including social, economic, and physical factors and impact, should always be considered as we make a study for vulnerability.
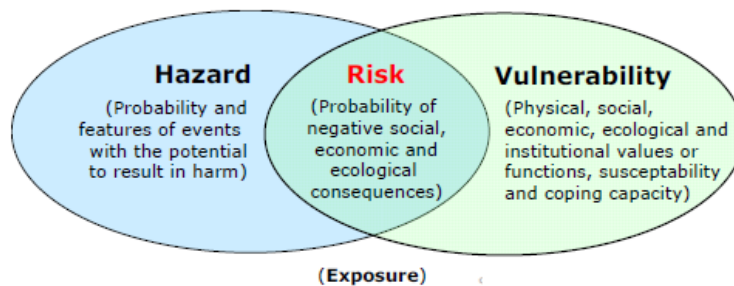
Figure 6. A proposed concept of vulnerability (Schanze, 2016)

The susceptibility of an area to a specific hazard determines how people need to react and mitigate the threat. The vulnerability to salinizaiton was first introduced in 1960 based on a case of sea water intrusion in the Middle East to raise attention to groundwater contamination (Vrba & Zaporožec, 1994). The study of salinization vulnerability helps policymakers in the field of water management to "protect, mitigate, and remediate" the contaminated groundwater with a combination of hydrogeological and hydrochemical as well as socio-economical aspects translated into a map that will help policymakers to create a sustainable utilization of groundwater (Fatema, 2019; Ivkovic et al., 2012). This study will be concentrated on the index-based method with the help of numerical modeling for deeper understanding. The result of vulnerability mapping will benefit the policymaker in managing groundwater utilization.

11

Vulnerability assessment on a global scale is done by choosing several indicators that are affecting groundwater salinization, not only intrinsically but also extrinsically. Figure 4 compile some of the indicators or factor that are well known for salinity intrusion vulnerability assessment, such as intrinsic properties of the aquifer, topography, social and economic aspect, climate, etc (Ivkovic et al., 2012; Michael et al., 2013; Morgan & Werner, 2015; Werner et al., 2013; Zamrsky, 2013). There are three well-known vulnerability assessment techniques, which are the index-based method or overlaying statistical and numerical modeling method (Fatema, 2019). This study uses an index-based method to assess the vulnerability. The index-based method is a qualitative method that can be applied to analyze vulnerability mapping in the coastal zone that may involve both intrinsic properties of the aquifer and the extrinsic parameter that could affect the aquifer vulnerability(Baena-Ruiz et al., 2018). Both intrinsic and extrinsic aspects need to be evaluated because groundwater can be contaminated due to human activities and physiographic characteristics, e.g., geology and water level. The most widely used index-based method is GALDIT which was developed by Chachadi et al. (2007), applying six hydrogeological properties of an aquifer that will be elaborated more in the next section.

GALDIT is one of an overlay and index-based vulnerability method that was designed significantly for seawater intrusion (SWI), which stands for the indicators that were used for the calculation. There are six indicators/factors required for the assessment, which are (G) groundwater occurrence based on the lithological unit of the aquifer, (A) aquifer hydraulic conductivity obtained from pumping test or laboratory work, (L) depth to groundwater level based on the piezometric observation in the wells, (D) distance to shore that can be obtain from remote sensing analysis, (I) impact of the existing status of seawater intrusion obtained from hydrochemical ratio, e.g. Cl^-/HCO_3^-, and the most important factors: (T) thickness of the aquifer as the SWI toe is highly depend on the saturated zone and the hydraulic conductivity, which can be obtained from well log data (Chachadi & Lobo-Ferreira, 2007; Fatema, 2019). These indicators are weighted, ranked, and prioritized through a decision-making process. Chachadi & Lobo-Ferreira (2007) discussed in detail of how to execute GALDIT. In this method, the importance of weight and ratings of an indicator is determined beforehand, where a higher number indicates higher vulnerability to salinization. The indicators have a fixed index that reflects the importance of SWI. After weight and rank are assigned, GALDIT Index is computed based on *Equation 2.1—1*.

<div align="center">

Equation 2.3—1 GALDIT index

$$GALDIT = \frac{\sum_{i=1}^{6}(Wi \; x \; Ri)}{\sum_{i=1}^{6} Wi}$$

</div>

where Wi is the weight and Ri is the rank of (i[th]) indicator (Chachadi & Lobo-Ferreira, 2007). The numerical index is then clustered into a similar class of vulnerability in the map (e.g. low, moderate, and high), which can later be defined as the exposure level.

2.4 Previous Research

Vulnerability mapping to salinization of groundwater in the coastal aquifers has been applied in different places of the world on a local or regional scale (Barik et al., 2021; Chang et al., 2019; Fatema, 2019; Ivkovic et al., 2012; Lobo-Ferreira et al., 2005; Luoma et al., 2017; Michael et al., 2013; Parizi et al., 2019; Seenipandi et al., 2019; Sinaga et al., 2011; Tasnim & Tahsin, 2016; Zamrsky, 2013). Most of them used GALDIT method or modified the method according to their need, e.g., Parizi et al. (2019) and Damayanti & Notodarmodjo (2021). The vulnerability was assessed based on several indicators or mechanisms that cause the salinization of groundwater aquifers, such as climate change (Hassani et al., 2021; Luoma et

al., 2017) and anthropogenic activities, e.g., groundwater pumping (Barik et al., 2021; Oude Essink, 2001; Tasnim & Tahsin, 2016) and agriculture (Nogueira et al., 2019).

Even though there are a lot of studies discussing vulnerability to salinization in groundwater, there are still a few numbers of studies that analyze groundwater salinization worldwide. A study that deliberated on worldwide salinization explains that tsunamis affecting low-lying planes and evaluate the SWI potential on the coastline both using index-based vulnerability and numerical methods (Zamrsky, 2013; Zamrsky et al., 2020). Another global assessment of salinization vulnerability was done by Michael et al. (2013), where they used only one factor of salinization, which is sea level rise (SLR) because SLR has a big impact on the local and regional hydrogeological conditions of coastal aquifers. The study estimates salinization distribution based on water table types, recharge-limited and topography-limited. Based on their findings, the recharge-limited water table shows a minimal rate of salinization, almost negligible. The study concluded that approximately 77.9% of the world's coastal aquifers are vulnerable to salinization.

Some studies, such as (Fatema, 2019; Mirzavand et al., 2020; Nogueira et al., 2019), used a hydrochemical analysis and isotope tracers to analyze the vulnerability to salinization in groundwater as well as groundwater origin. Based on their study, the most significant cause of salinization is seawater intrusion, both horizontal and vertical, indicated by the high Cl^- and HCO_3^- concentration in several places in the study area. Some regions also show a freshening process where the sample shows the composition of Na^+- HCO_3^- water type.

Chapter 3   Material and Methodology

3.1 Overview

Several studies have been done to assess the vulnerability of coastal aquifers to seawater intrusion using in-situ or ex-situ methods. Recently, more methods are using remote sensing data to calculate vulnerability by weighting and ranking. One of the methods is GALDIT, developed by Chachadi et al. (2007) and Paulo Lobo Ferreira et al. (2005). The method was developed based on the hydrogeological properties that affect the potential of seawater intrusion. Furthermore, the parameter that is used in GALDIT technique will be added with a few more indicators to show how the other factors are affecting coastal zone vulnerability to salinization, especially from seawater intrusion.

The election of other indicators that will be used is based on literature reviews and a trial and error, so we know which additional factors are more influencing coastal zone salinization. Vulnerability is one element that influences the risk in cooperation with hazard or threat. In this case, the indicators chosen are clustered to vulnerability and hazard of the saltwater intrusion phenomenon. The two elements – hazard and vulnerability – can result in risks influencing the coastal aquifer. Hence, indicators are also clustered into three categories: vulnerability, hazard, and risk (Figure 7).
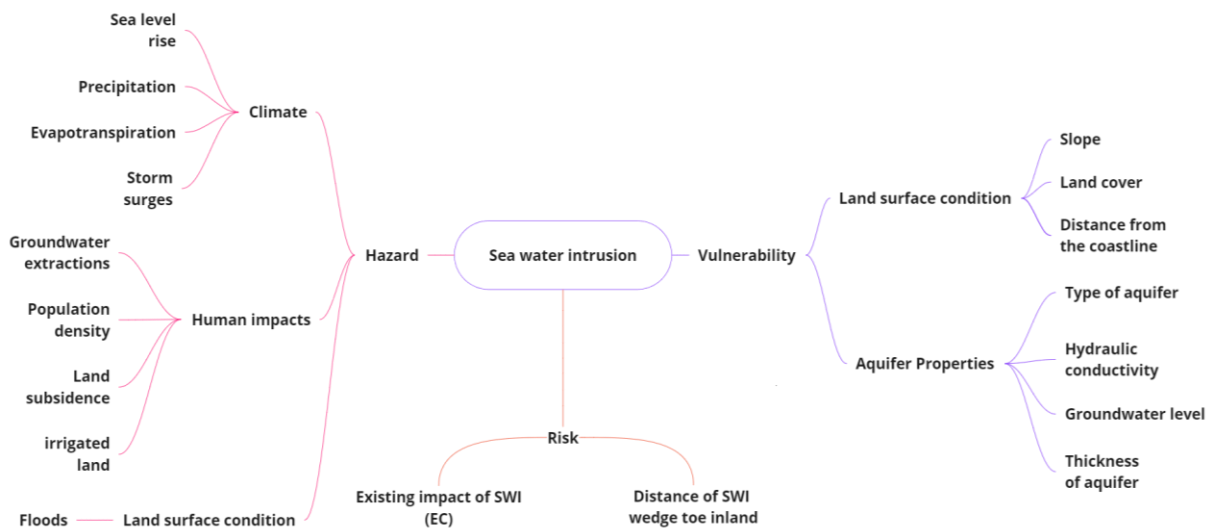
Figure 7. Clustered indicators to vulnerability, hazard, and risk.

General approach of this study can be seen in Figure 8. The study will start by collecting data as mentioned. Data are processed and formatted, which are later assigned to ranking and weighting for each raster layer and then overlayed and calculated for the vulnerability index based on each indicator's importance. Vulnerability indexes are adapted to create a vulnerability mapping to salinization on a global scale. Then the map is evaluated and validated based on the field data. This study case is analyzed based on the salinization mechanism and further, it will be modeled into a simple conceptual model. The vulnerability map will be used to evaluate the impact of salinization on agriculture, water resource, and health.
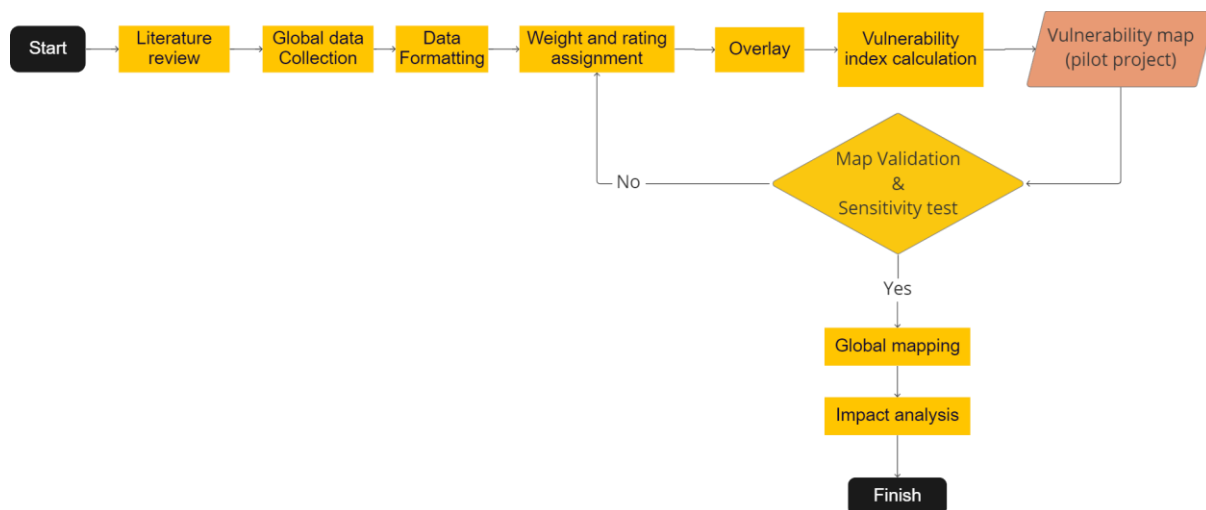
Figure 8 Research methodology flowchart

3.2 Workflow

3.2.1 Data Collection

This research needed a set of variables to assess the vulnerability of groundwater in the coastal zone to salinity for intrinsic properties from the groundwater aquifer itself and extrinsic properties that might affect the vulnerability of groundwater to salinization. The first step in this research is to obtain datasets from different sources (both open source and secondary data). As mentioned in the previous sub-section, there are potentially 18 indicators or parameters that could affect the vulnerability of groundwater aquifers in the coastal zone to salinization. Table 1. Shows the detail of datasets that were used for the research along with the references.

Table 1. Database overview

No	Datasets name	Description	Reference	Data Type / Resolution
1	WHYMAP-GWR	Global groundwater resource map	Richts, 2011	Vector
2	GLHYMPS	Global hydrogeology maps: Global permeability dataset	Huscroft et al., 2018	Vector
3	WTL	Global groundwater level	Verkaik, 2021	Raster / 30-arc second
4	EAT	Global estimated aquifer thickness	Zamrsky et al., 2018)	Vector
5	Groundwater salinity	Global groundwater quality; based on electrical conductivity data (EC)	Thorslund & van Vliet, 2020	Vector
6	Distance from the coastline	Approximation of inland distance from the coastline	-	Raster / 60-arc min

7	Slope	Global slope derived from GMTED2010 data and SRTM4.1	Amatulli et al., 2018	Raster / 30-arc second
8	Land cover	Global discrete land cover	Buchhorn et al., 2020	Raster / 3.5-arc second
9	Sea level rise	Change of sea level rise in near term projection (2021 – 2040)	Gutiérrez et al., 2021)	Raster / 60-arc min
10	Precipitation	Monthly precipitation near term projection (2021 – 2040)	Gutiérrez et al., 2021)	Raster / 60-arc min
11	Population	Population density value	Gutiérrez et al., 2021)	Raster / 60-arc min
12	Well abstraction	Groundwater abstraction and water demand	(Sutanudjaja et al., 2018; Zamrsky et al., 2021)	Vector
13	GMIA v5.0	Global Map of Irrigation Areas	Siebert et al., 2015	Raster / 5-arc minute
14	Natural Earth Coastline	Global coastline – distance from the coastline	Natural Earth, 2022	Vector
15	Flood risk data	Global flood risk data by country	Luo et al., 2015	Vector
16	Potential evapotranspiration	Global Aridity Index and Potential Evapotranspiration (PET)	Zomer & Trabucco, 2022	Raster / 30-arc second
17	Storm surges	Global storm surges and extreme sea levels	Muis, 2016	Vector
18	Land subsidence	Global land subsidence map	Erkens & Sutanudjaja, 2015	Raster / 5-arc minute
19	Coastal SEAWAT model	SEAWAT model in coastal zone (COSCAT region)	Zamrsky et al., 2021	Vector

1. Aquifer type

According to the GALDIT method, to assess the vulnerability of coastal aquifers to salinization, aquifer type classification was needed to characterize the behavior of seawater intrusion in coastal areas depending on different aquifer types. In this case, the global dataset available for aquifer type is called "WHYMAP and Groundwater Resource (WHYMAP-GWR)" with a scale of 1:25,000,000, as shown in Figure 9. This dataset classified aquifer type into four different types based on groundwater resources: groundwater in major groundwater basins, groundwater in a complex hydrogeological structure, groundwater in areas with local

and shallow aquifers, and groundwater in carbonate rock region (Richts et al., 2011). Groundwater in major groundwater basins is groundwater that is invested in a sedimentary basin that already proves to have a good record of groundwater exploitation. Groundwater in a complex hydrogeological structure is groundwater resources with a very productive aquifer in heterogeneous complex earth structures (folded and faulted regions). Groundwater in areas with local and shallow aquifers has a limited groundwater resource due to its origin, where the aquifer is developed into the alteration zone of bedrock and creates an overlaying structure of shallow layers of weathered bedrock. Carbonate aquifer is most likely located in the highly karstic condition. Based on the aquifer type classified in the map, the vulnerability importance is rated based on the ability of the formation to pass water (permeability) and the recharge rate of the region is disregarded to make straightforward calculation. To simplify and elaborate more of the geological condition of the coastal condition, the aquifer types from WHYMAP-GWR are rephrased as follows:

Table 2 WHYMAP-GWR aquifer type rephrasing for vulnerability mapping

WHYMAP Aquifer Type	Rephrased Aquifer type
Groundwater resources in carbonate rock region	Aquifer of carbonate (karstic) rocks
Groundwater resources in major groundwater basins	Aquifer of sand and gravels
Groundwater resources in a complex hydrogeological structure	Aquifer of sandstone and limestone
Groundwater resources in area with local and shallow aquifers	Aquifer of weathered bedrocks
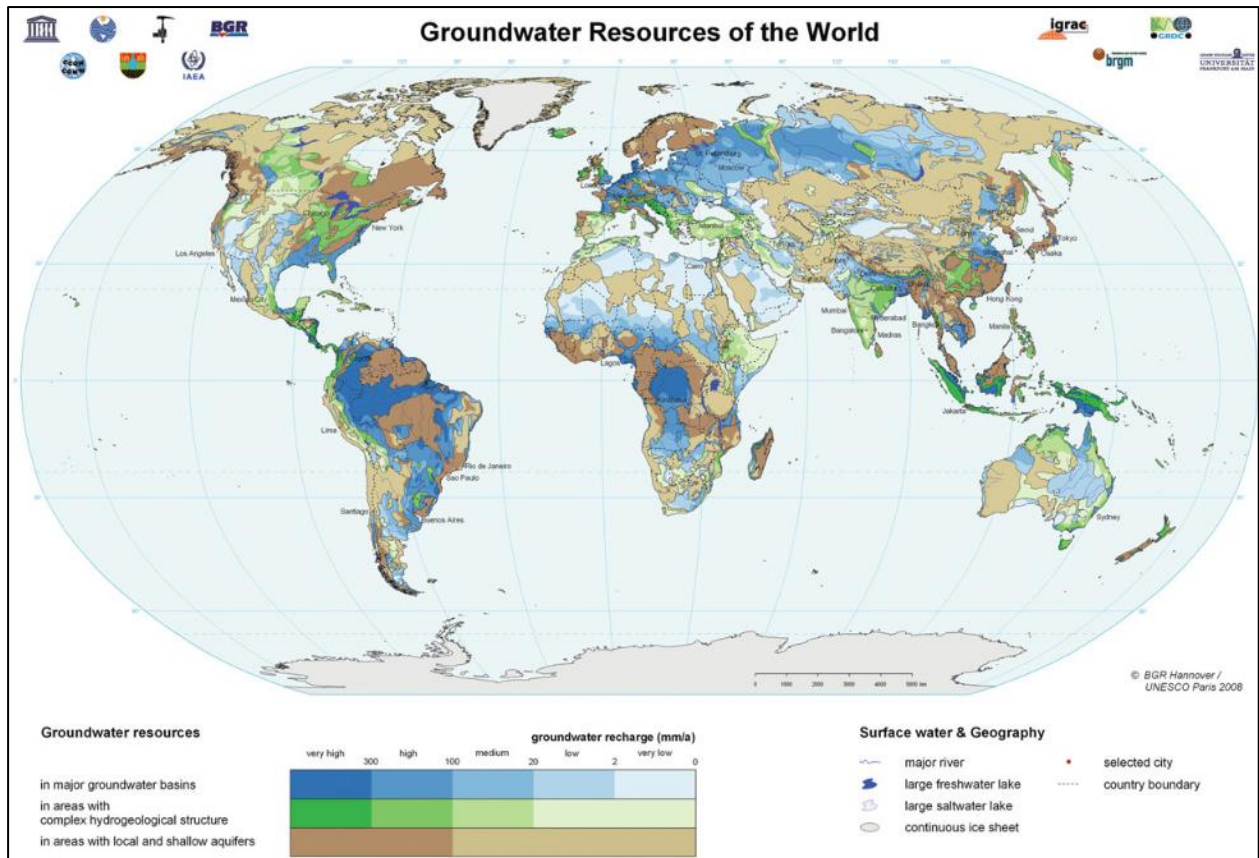
Figure 9. Global groundwater resource map with different groundwater recharge classifications, which later to be defined as aquifer type thematic layer (Richts et al., 2011)

2. Hydraulic conductivity

Hydraulic conductivity is one of the essential parameters of an aquifer. In most seawater intrusion cases, hydraulic conductivity following groundwater flow is usually applied to predict the length of seawater wedge toe. Groundwater flow is driven by how big the hydraulic conductivity is thus, high hydraulic conductivity results in a higher vulnerability to seawater intrusion. Hydraulic conductivity is highly variable over the short distance and lithology formation (Costall et al., 2020; Gleeson et al., 2011, 2014). Therefore, hydraulic conductivity is chosen as one of the parameters to assess the vulnerability of coastal aquifers to salinization. Hydraulic conductivity of aquifers around the world can vary from 10^{-13} through 1 in m/s (Freeze & Cherry, 1979), where the highest value is the unconsolidated sediment, and the lowest is fine-grained sediment that acts as the aquitard hydraulic conductivity (Gleeson et al., 2014). Due to this wide range of data, a high-resolution map of hydraulic conductivity is needed to map the vulnerability.

This study uses a permeability distribution across the globe created by Gleeson et al. (2011). They have compiled permeability data worldwide based on the local-scale saturated terrestrial lithologies called GLHYMPS. Figure 10 shows the logarithmic permeability (log *k*) and is classified by hydro-lithology with a 95% confidence level. The permeability compiled in the map was intrinsic (*k*). Since the permeability is in logarithmic value, we need to convert it to hydraulic conductivity using *Equation 3.2—1*.

Equation 3.2—1 Hydraulic conductivity relationship with intrinsic permeability, the density of water, gravitational acceleration, and viscosity

$$K = \frac{k \, \rho \, g}{\mu}$$

Where K is hydraulic conductivity (m/s), k is the intrinsic permeability, ρ is density of water (1000 kg/m^3), g is gravitation acceleration (9.8 m/s^2), and μ = is water dynamic viscosity (0.001 Pa s).
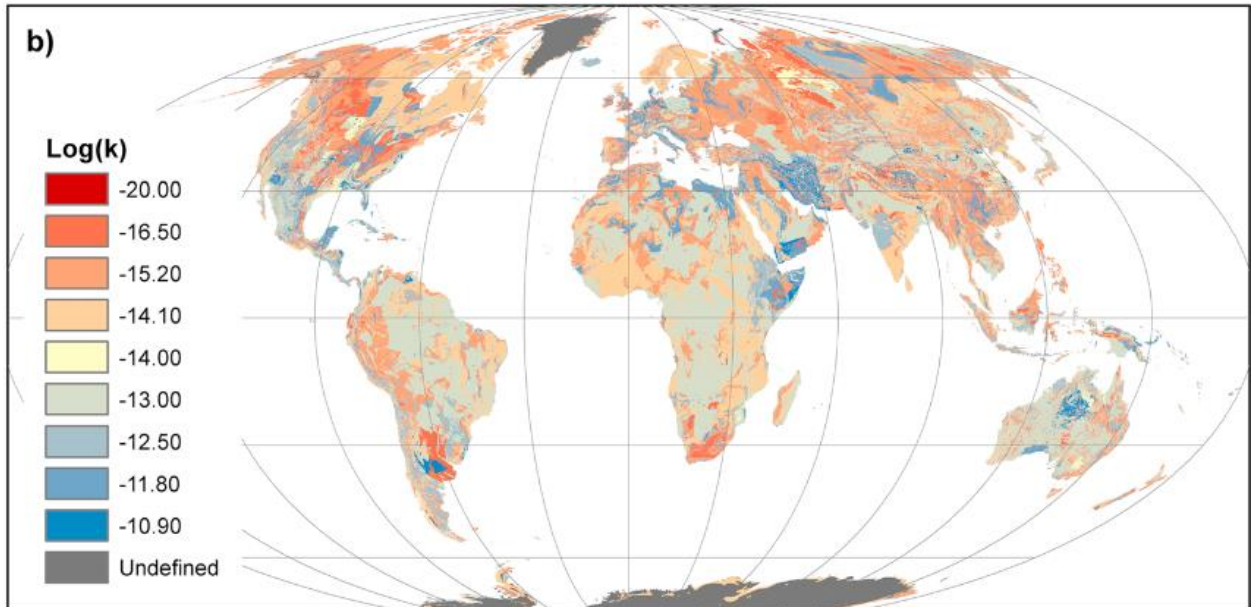
Figure 10. Global logarithmic intrinsic permeability (log k) map unaffected by permafrost region (Gleeson et al., 2014)

Thus, the result for hydraulic conductivity calculation can be seen in Table 3. Conversion result and the respecting hydrolithology categories as well as the hydrolithology related to the value. The hydraulic conductivity (K) is rated based on how well the aquifer can conduct water. So, the higher the K value, the higher the rated value. In short, higher K resulting higher vulnerability.

Table 3. Conversion result and the respecting hydrolithology categories

Log(k) (m^2)	Hydraulic conductivity (K) (m/s)	Hydrolithology
-13	9.8E-07	Unconsolidated
-10.9	1.2E-04	Coarse-grained unconsolidated
-14	9.8E-08	Fine-grained unconsolidated
-15.2	6.2E-09	Silicate sedimentary
-12.5	3.1E-06	Coarse-grained sedimentary
-16.5	3.1E-10	Fine-grained sedimentary
-11.8	1.55E-05	Carbonate
-14.1	7.78E-08	Crystalline
-12.5	3.1E-06	Volcanic

3. Groundwater Level

Few studies have globally mapped groundwater tables with good resolution of data (Fan et al., 2013; Verkaik et al., 2021). Verkaik et al. (2021) created a global high-resolution groundwater model on 1 km x 1 km scale. This model is a follow-up to the previous PCR-GLOBWB model by Sutanudjaja et al. (2018). The groundwater level in the coastal zone is mainly classified into shallow aquifers since topography can highly influence the groundwater table. Figure 11 shows the distribution of groundwater levels varies in different parts of the world, ranging from -116 m.a.s.l. to more than 2000 m.a.s.l. Distinguished data distribution is shown in the desert area, where almost all of the site has deep groundwater. Shallow groundwater is randomly distributed worldwide, primarily in low-elevation areas (not mountainous areas). However, there is an anomaly for the data in Greenland, where the data is 0 m.a.s.l on the entire island. This anomaly could be the result of a lack of data in the region.

The groundwater level impacts the vulnerability where the shallow groundwater level is considered to have a higher susceptibility to salinization. In contrast, the deeper groundwater level is less prone to salinization. Especially in regions with negative groundwater levels, indicating the groundwater level is below the mean sea level. This condition is very hazardous to the groundwater because it can be more susceptible to salt flow either from above or sides.
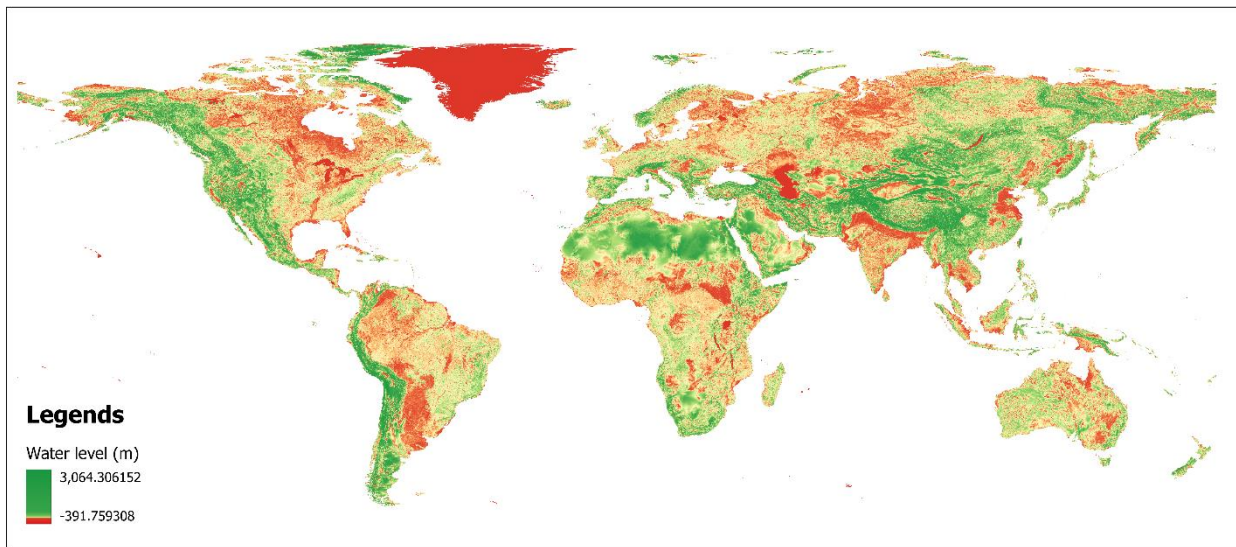
Figure 11. Groundwater level dataset for global scale with a resolution of 0.1 degrees (altered) adapted from Verkaik et al. (2021)

4. Estimated Aquifer Thickness (EAT)

Coastal vulnerability to seawater intrusion is primarily affected by the hydrogeological condition on the local and regional scale. The estimated aquifer thickness dataset is obtained from the work of Zamrsky et al. (2018), where they compiled several other open-sourced datasets, including topography, soil and sedimentary deposit thickness, global groundwater model, lithological map, and global coastline. The model represents coastal aquifer thickness in the area without the permafrost (Figure 12). From this database, we understand that the thickness of aquifers in coastal zone areas ranged from 1 to 5245 m. The saline transport modeling they also executed shows that the thinner aquifers, the saltwater can intrude more easily and upconing phenomena in the low-lying area can be found (Zamrsky et al., 2018). With a thicker aquifer, it was not as prone to salinization as it had a higher chance for the remediation process to freshen the salt intruded into the aquifer. Therefore, the thinner aquifer is more vulnerable in this case than the thicker aquifer.
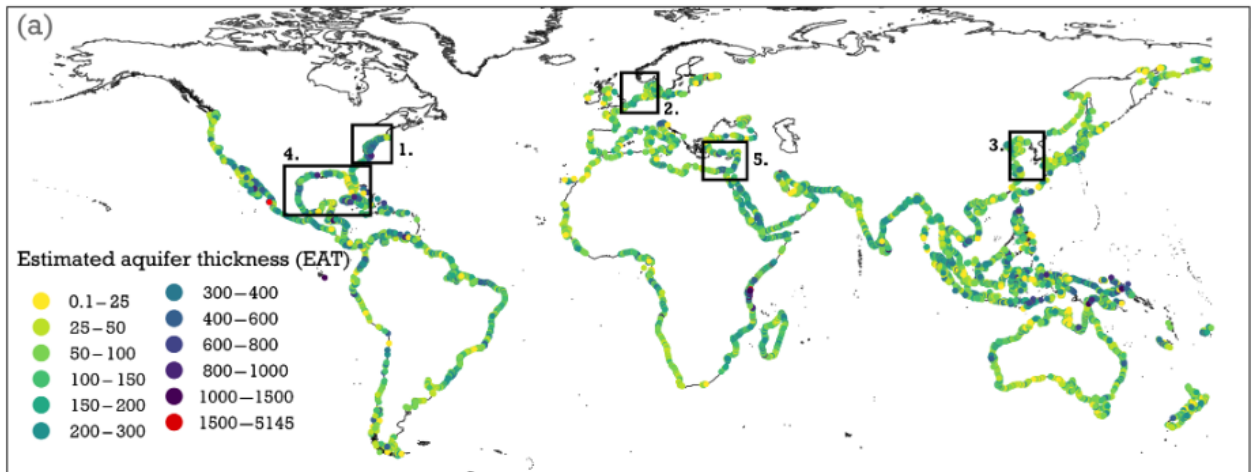
Figure 12. Global estimated aquifer thickness (EAT) in meters (m) along the coastline excluding permafrost region (Zamrsky et al., 2018)

5. Groundwater salinity

The salinity dataset is obtained from Thorslund & van Vliet (2020) work. The data is a combination of surface and groundwater measurement data sources covering local, regional, and global scales from 1980 - 2019. The salinity data shown in the database is electrical conductance (EC) obtained both from the direct measurement from a sampling station or through a conversion from TDS, especially for groundwater datasets. As you can see in Figure 13, the distribution of groundwater salinity is sparse around the world, where most of the data is located in the USA and Australia with more than 10,000 data collection stations, also some parts of Europe, South Africa, and South America. Only little data is collected in Asia – in Cambodia and Bangladesh. In this study, the dataset that was taken into consideration is only the mean EC collected from the groundwater sampling source (Figure 13). The groundwater EC data ranged from 0 µS/cm to more than 3000 µS/cm.
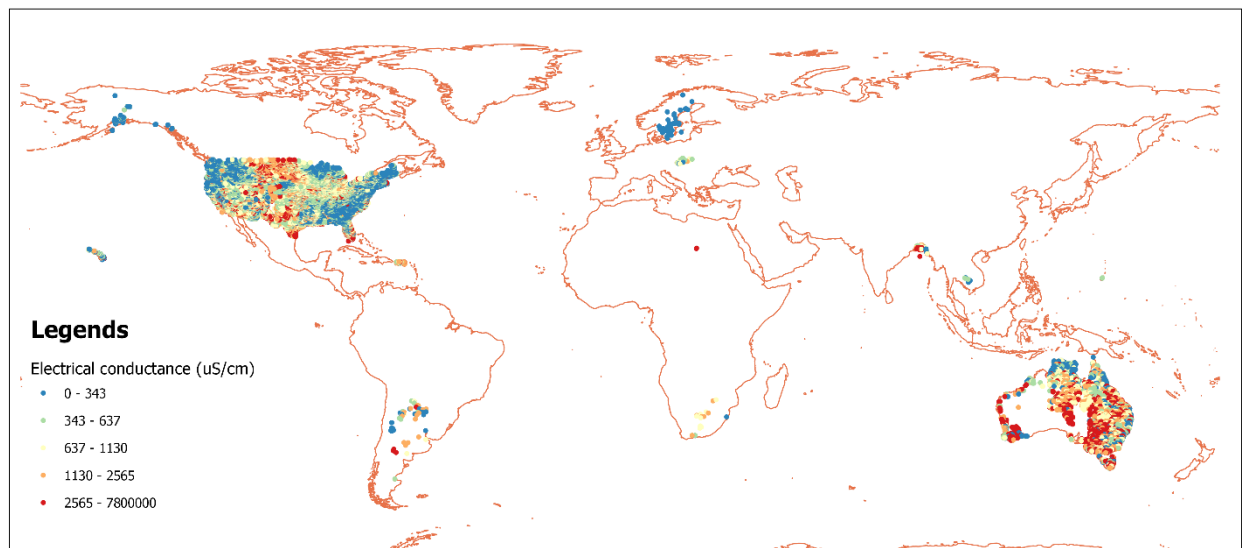
Figure 13 Distribution of mean electrical conductance (EC) for groundwater dataset points across the world (extracted from Thorslund & van Vliet (2020))

6. Distance from the coastline

Distance from the coastline is considered an important indicator for seawater intrusion in the coastal zone because usually, the development of megacities is in the coastal zone areas, as it is also one of the components to consider in the seawater intrusion vulnerability method

(GALDIT) (Allouche et al., 2017; Chachadi & Lobo-Ferreira, 2007; Chang et al., 2019, 2020; Moghaddam et al., 2017; Parizi et al., 2019). Distance from the coastline is calculated perpendicularly from the shoreline and it has been proven by Chachadi & Lobo-Ferreira (2007) that it could bring a significant effect on SWI. Therefore, distance from the shoreline is weighted with high value. As the distance from the coastline increases, the vulnerability rating should also be reduced and vice versa.

This dataset is generated from the Natural Earth Coastline (see section 3.2.2). The approximate distance from the coastline chosen was 50 km. This distance was selected to cover all parts of the coast worldwide, including deltas, estuaries, etc. As shown in Figure 14, the raster dataset is generated to 0.1-degree resolution to satisfy the necessity of 50 km coastal zone proximity and to accommodate the computer program.
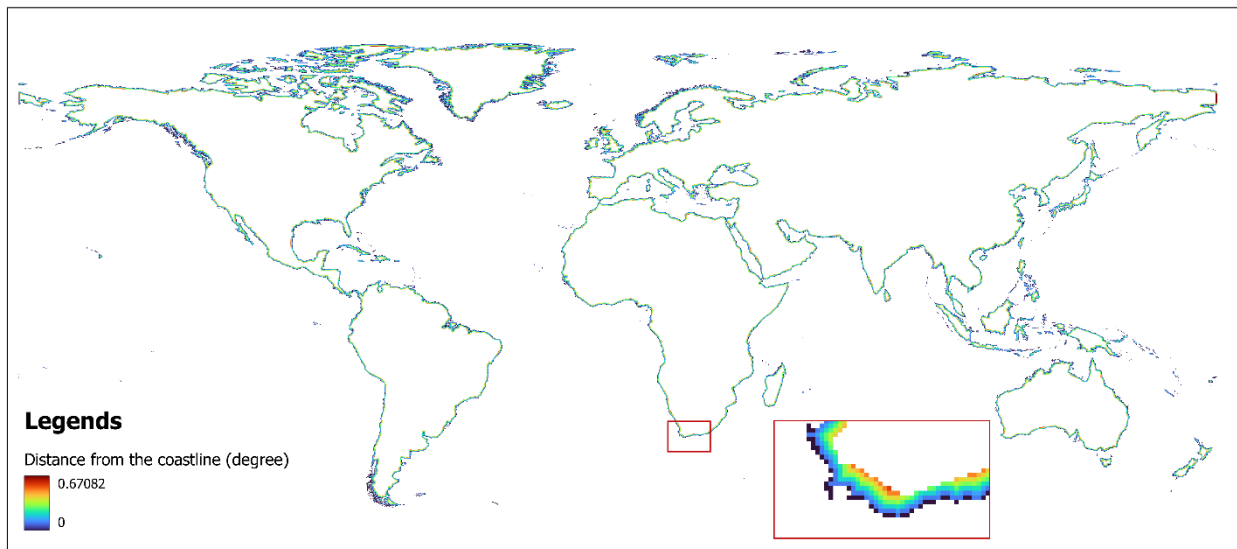
Figure 14. Distance from coastline generated from Natural earth coastline dataset with a resolution of 0.1 degrees (1 degree = 11 km)

7. Slope

The topography of an area is highly affecting the behavior of water flow, where most of the water levels in the world are topography-influenced (Haitjema & Mitchell-Bruker, 2005). Moreover, the coastal zone, where most low-lying areas are located, is highly impacted by the progression of the sea waves. If the slant of a site is low, which is usually indicated as a flat area, thus it is prone to transgression and regression movement of sea level. This phenomenon will affect the salinity of groundwater over time. Therefore, a flat area in the coastal area is prone to salinization if no mitigation action is taken. Thus, the area with a lower slope (flatter) has a higher vulnerability rating than the steeper area.

As shown in Figure 15, most of the surface land in the world mostly has a relatively flat surface. The noticeable steep slope is located in the mountainous region, e.g., in the Himalayan and Andes Mountains. Most coastal areas have a fairly flat slope (<10%). Some exceptions are in some parts of the world where it was the place where tectonic plates met (subduction or collision). For example, the western part of Sumatra Island, Indonesia, as shown in the inset of Figure 15, has a steepness of >40%. The western part of the South America continent is also distinguished for its steep slope due to its mountainous geomorphology.

23
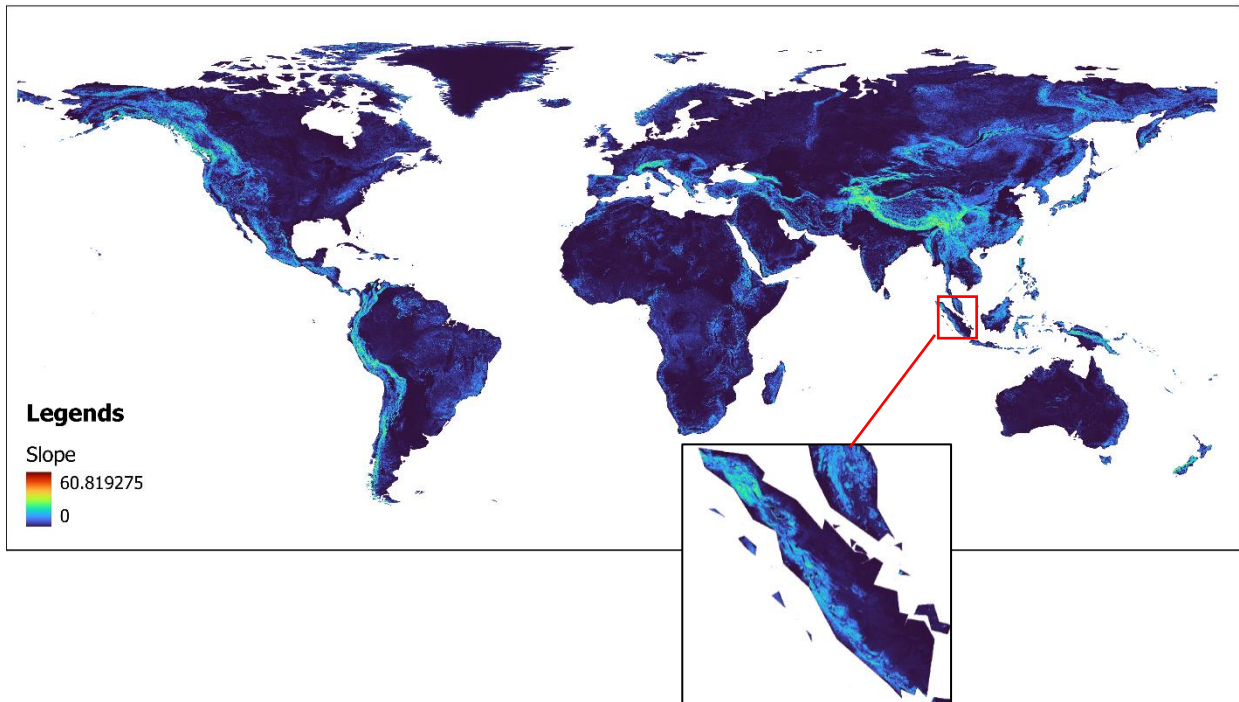
Figure 15. Global slope database in percentage (%) (Amatulli et al., 2018)

8. Land cover

Land cover data are obtained from the Copernicus database, including the vegetation type as well as the land surface coverage type. Figure 16 shows the global distribution of land cover with 23 discrete classes on a 100 m scale (Buchhorn, Bruno, et al., 2020). For simplification of the project, the raster is upscale to 0.1-degree resolution and some land cover with similar characteristic are grouped based on the susceptibility of a land cover type to an event of salinization and its potential to increase the degree the vulnerability, thus resulting in five different categories as follows:

- different types of forests are clumped into one category,
- the land covers water bodies into a single category (wetlands, permanent water bodies, and snow & ice),
- Shrub, herbaceous vegetation, and moss & lichen are grouped into uncultivated land
- Built up area
- Bare / sparse vegetation

Evergreen needleleaf closed forest	Shrubland
Deciduous needleleaf closed forest	Herbaceous vegetation
Evergreen broadleaf closed forest	Herbaceous Wetland
Deciduous broadleaf closed forest	Moss & lichen
Mixed closed forest type	Bare / sparse vegetation
Unknown closed forest type	Cropland
Evergreen needleleaf open forest	Built-up
Deciduous needleleaf open forest	Snow & ice
Evergreen broadleaf open forest	Permanent Water Bodies
Deciduous broadleaf open forest	Ocean
Mixed open forest type	No input data available
Unknown open forest type	

Figure 16. Global dynamic land cover map created by Copernicus Global Land Operation in 100 m scale with 23 discrete classes (Buchhorn, Bruno, et al., 2020)

9. Sea level rise (SLR)

Sea level rise has proven to show a massive impact on the coastal area (e.g., Michael et al., 2013; Tebaldi et al., 2021; Zamrsky et al., 2018) and it has been worsened by the increasing rate of groundwater depletion that can contribute to SLR (Wada et al., 2012). SLR has happened before, but with an additional driver — climate change —it has brought more danger to human lives. IPCC report projected that sea level change with current climate change with business as usual (RCP 8.5) would rise up to 2 m (IPCC, 2021). Sea level rise is worse in the low-lying areas (often deltaic areas), e.g. the Netherlands, Guyana, and Bangladesh, and the oceanic islands. Melting of Greenland and the West Antarctic ice sheet is the most immense contribution to a significant SLR in the future (Nicholls & Klein, 2005). This likelihood is considered an extreme event and might happen to certain coastal zones if the current rate of climate change is maintained. With sea level rise threatening coastal zone, there is also an implication threat due to SLR, which is a potential of coastal overtopping that will speed up groundwater salinization (Almar et al., 2021). Therefore, SLR is one component that needs to be included in assessing the vulnerability of the coastal zone to salinization, where a higher SLR value will result in a higher vulnerability to SWI.

The dataset was obtained from IPCC interactive atlas (https://interactive-atlas.ipcc.ch). The dataset chosen was the baseline data in the near-term projection (2021-2040) to illustrate the current condition of sea level rise. Based on Figure 17, a high SLR rate is mostly in the sub-tropical region, where it was impacted by the ice-melting event in of the permafrost. Meanwhile, in the tropical regions, the sea-level rise change is not as extreme as in the sub-tropical area.
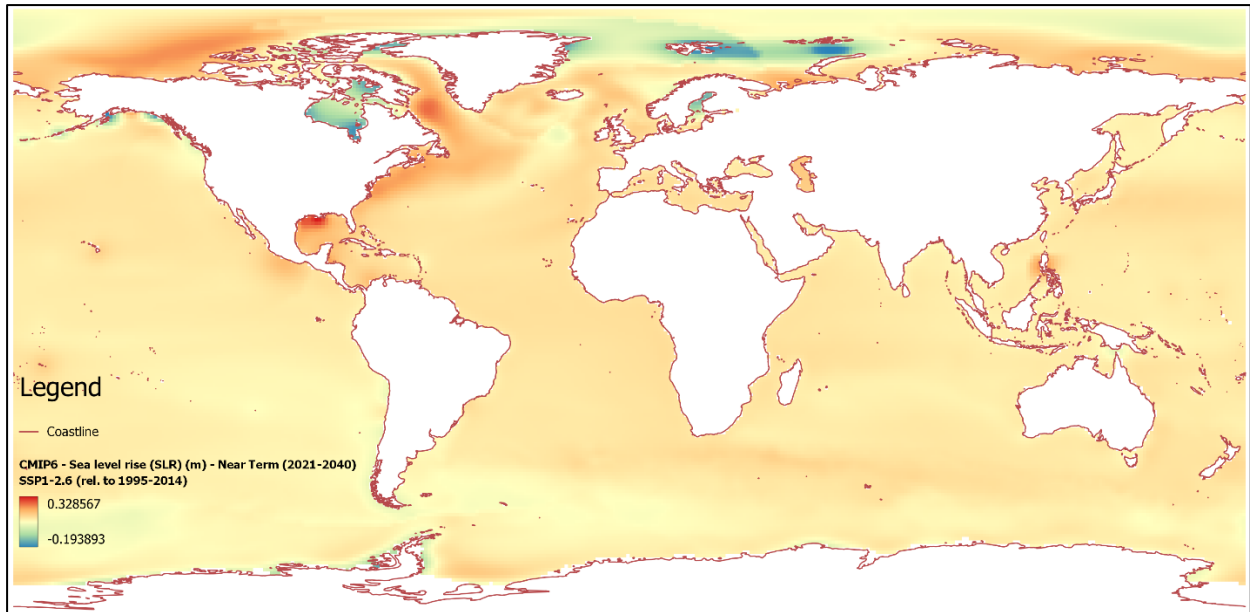
Figure 17. Global sea level rise (SLR) change in meters (m) adapted from IPCC 6th report relative to 1995-2014 in near-term projection (2021-2040) with scenario SSP 1-2.6 (Gutiérrez et al., 2021)

10. Flood (Flood risk projection)

Land inundation data was obtained from a flood interactive map platform in World Research Institute (WRI) called Aqueduct Global Flood Analyser. This database is historical coastal flood data with a return period of 10 years. The global dataset is clipped into the coastal zone of 5 km. As shown in Figure 18a, The value of coastal floods is not significant globally but distributed in the local region. For example, in the region of Bangladesh and Southern India, as highlighted in Figure 18b, the surrounding may not have a significant value of flood inundation, but in the coastal urban area of Bangladesh, the risk of the flood was projected to be as high as 3.7 decimetres (dm). The potential of flood in coastal zone may be induced by several drivers, such as overtopping (Almar et al., 2021) and land subsidence (Erkens & Sutanudjaja, 2015). Therefore, in this database, land subsidence and SLR are considered in the model.

Due to the overtopping hazard caused by sea-level rise, flood in the coastal zone is an essential driver to the salinization of fresh groundwater aquifers in coastal areas. Overtopping could drive coastal flooding that happens only temporarily and in a localized area (Almar et al., 2021). The contribution of tide and waves from the sea is also an important aspect of the overtopping event. Therefore, in this coast flood dataset, higher inundation risk means a higher vulnerability of an area to salinization.
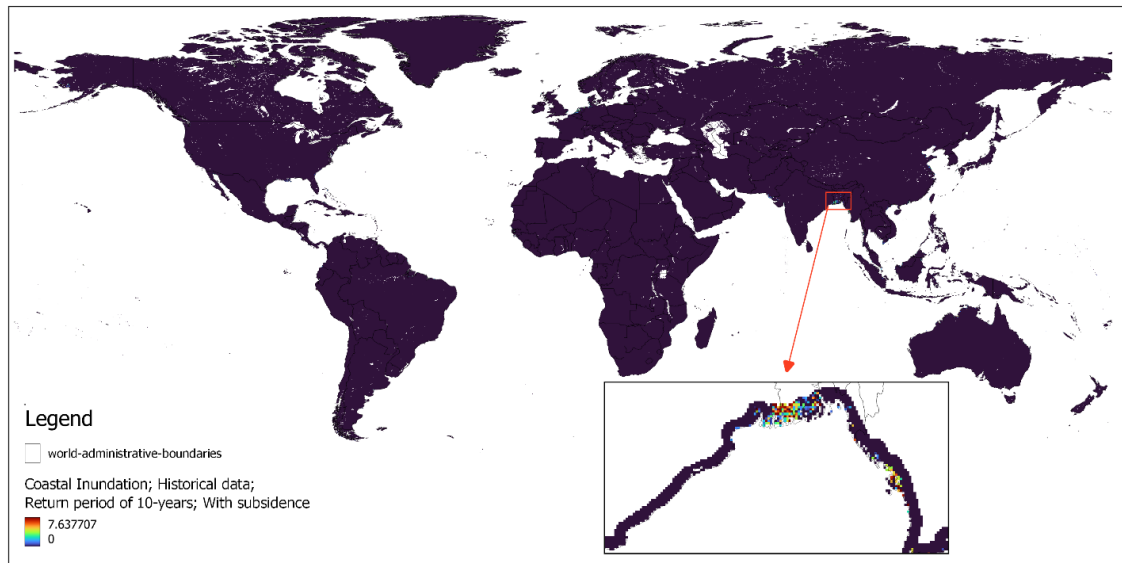
Figure 18. Flood Risk Map in depth (dm) with the historical data model, return period of 10 years, and subsidence included. Compliment with highlighted area in Southern Bangladesh (Luo et al., 2015)

11. Storm Surges

Storm surge is one of the important parameters that significantly impact salinization in coastal zones. One of the concerning matters among the researchers is storm surge. Storm surges are a rise of sea level induced by low atmospheric pressure and high intensity of the wind, which may cause coastal flooding (Muis et al., 2016). Storm surge may only happen in a short period, but a high tide that surges further inland could affect the hydraulic interface of fresh- and salt-groundwater. This disturbance brings an enormous effect on the equilibrium of the interface and could increase the vulnerability of fresh groundwater to sea-water intrusion. Consequently, the higher tide and surge amplitude cause higher coastal zone vulnerability to salinization.

The dataset for storm surge is called GTSR (Global Tide and Surge Reanalysis), created by Muis et al. (2016). The GTSR dataset has certainty for estimating the global exposure of coastal flooding. Based on the simulation, due to the tide and surge, 1.3% of the population lives under the threat of 1 in 100-year floodplain (Muis et al., 2016). As shown in Figure 19, the high intensity of tide and surge is located between 30° and 60° N, a major conflict zone between polar and tropical climates.
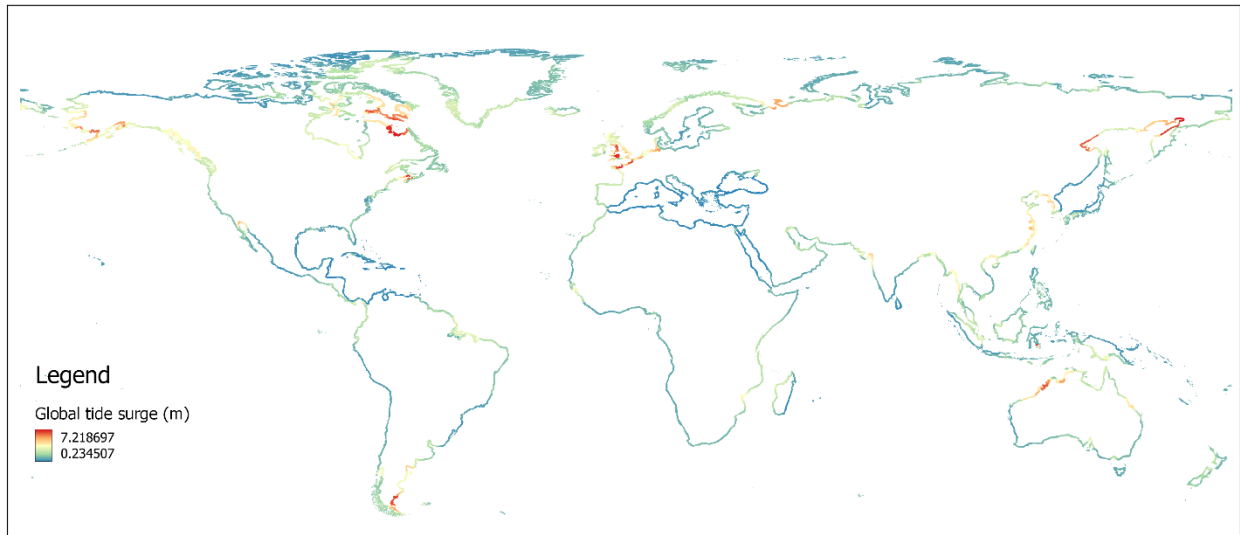
Figure 19. Global tide surge in meters adapted from Muis et al. (2016)

12. Land Subsidence

The land subsidence dataset was acquired from the work of Erkens and Sutanudjaja (2015). The global scale land subsidence data is essential for policymakers and scientists to raise awareness about this existing and growing phenomenon. Land subsidence is a phenomenon connected to groundwater extraction, usually concentrated in urban areas. With higher extraction of groundwater, the groundwater reserve can be depleted as so with the pressure inside the formation, thus the land above could slowly sink due to the weight ad unbalance of pressure. The land subsidence is mostly in the area with typically soft material formation (e.g., clay or unconsolidated sediment). It explains the "hotspot" in the map as shown in Figure 20, which is located in several coastal cities, e.g., Jakarta. The subsidence rate in the area could reach up to 1 m / year.

Meanwhile, most of the area does not have a significant value (~ 0 m/year). Therefore there is only a few distinguish spots are noticed. This dataset explains the current situation and projection of a sinking area's future condition, 2030-2050-2080 (Erkens & Sutanudjaja, 2015). This prediction could help the policymakers to assess the development of socio-economic in regard to a natural phenomenon in urban areas.

The dataset is generated based on an integrated hydrogeological and water resource model — PCR-GLOBWB — created by multiple researchers in The Netherlands (de Graaf et al., 2015; Sutanudjaja et al., 2018) and the map resulted is in 5 arc minute spatial resolution for a period of 1958-2010. In the making of the dataset, the PCR-GLOBWB is combined with the MODFLOW groundwater model to create a better monthly spatio-temporal groundwater head change model, which is then used as an input in the land subsidence model (Erkens & Sutanudjaja, 2015).
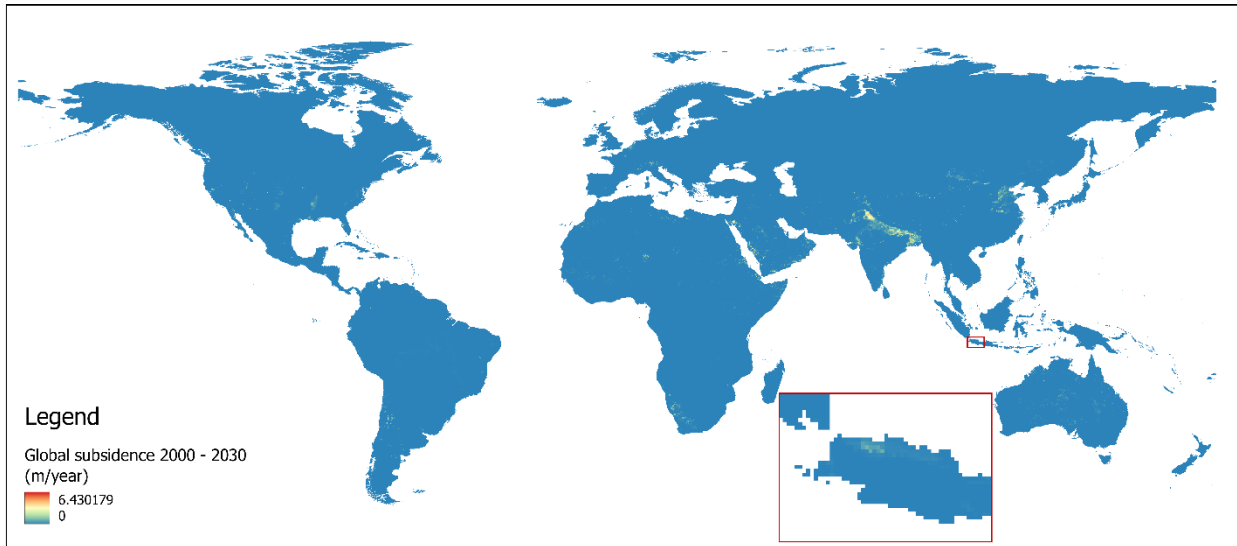
Figure 20. Global land subsidence distribution clipped to 50 km coastal zone (Erkens & Sutanudjaja, 2015)

13. Population density

The population density dataset tells us how many people are in a square kilometer. The data was obtained from IPCC interactive atlas with near-term projections relative to 1995-2014. As can be seen in Figure 21, the densest area is located in the urban area, such as in Jakarta, where it can reach more than 7500 persons per km^2. This population density is projected to increase significantly in future years, especially in the existing urban area. The increasing population around the world would bring many more problems, especially water issues. It is made worse by the geographic location of some urban areas, such as in arid areas where water resources are limited. Based on IPCC 6th report, in long-term projection, there will be more than 9000 persons per km^2. This means that most of the urban areas will be overcrowded and there will be barely enough resources to feed everyone (IPCC, 2021). Consequently, as population density increases, so will the vulnerability to salinization.
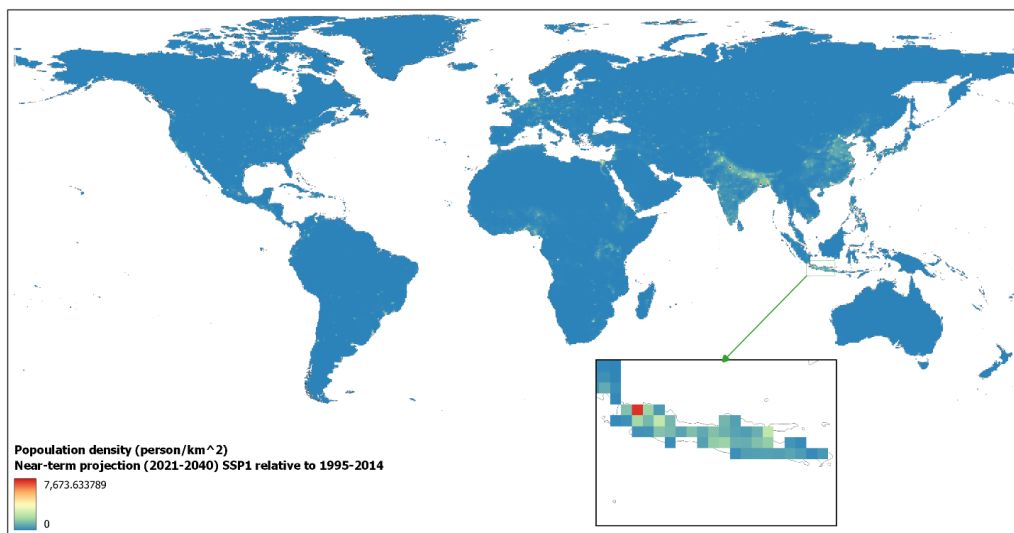
Figure 21. Global population density map (person/km^2) adapted from IPCC 6th report (Gutiérrez et al., 2021; IPCC, 2021)

14. Irrigated land

29

The irrigated land uses groundwater was chosen to see the effect of irrigation from groundwater resources. This dataset was obtained from Siebert et al. (2015), where they assessed irrigated land from 1900 to 2005. Based on the projection of almost one century, many regions have increased irrigation use (relative to 1950). The most significant increase is located in Australia and Oceania, Southeast Asia, Middle and South Africa, Central America, and eastern Asia (Siebert et al., 2015).

The dataset in Figure 22 shows a scattered distribution of irrigation areas using groundwater. Some regions use a lot of groundwater as the source of irrigation water, such as North America, the middle and east part of South America, most of Europe, and the east and south of Asia. Moreover, the archipelago countries, e.g., Indonesia and the Philippines, use groundwater as their irrigation resource in most agricultural land. Even though the value of groundwater usage is not as high as in other countries, the constant use of groundwater for irrigation in agrarian land could cause a problem for freshwater storage for human use. Therefore, the area that irrigates their land using a considerable amount of fresh groundwater is more vulnerable.
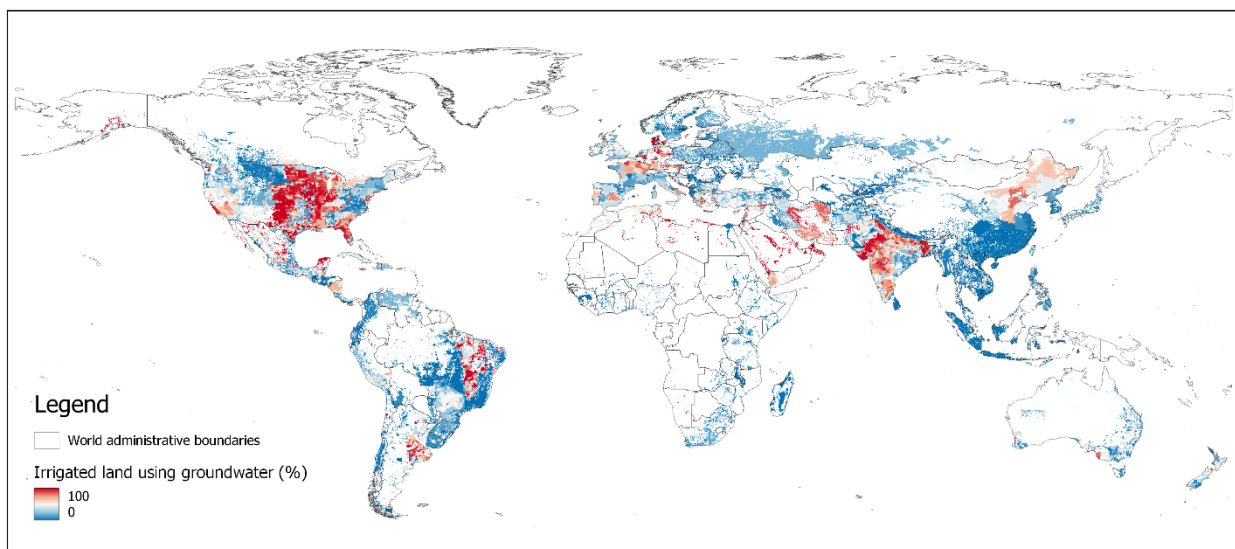
Figure 22. Global irrigated land area (in percentage) that uses groundwater as water resources (Siebert et al., 2015)

15. Groundwater extraction

Groundwater abstraction data is originally from the work of Sutanudjaja et al. (2018), which was then modified to the coastal zone area by Zamrsky et al. (2021). This estimated groundwater extraction is a part of PCR-GLOBWB global hydrological model. The model was created in a buffer area of 200 km inland and excluded the permafrost area to simplify the model. The high abstraction is usually in cooperation with the high value of the population in an area. Thus, in urban areas the groundwater is usually overexploited. The over-abstraction of groundwater in a dense area, moreover in the coastal zone, could increase the risk of saltwater upconing and reduce the volume of freshwater abstracted. Consequently, the possibility of salinization of an aquifer is higher, as is the vulnerability.

The dataset in Figure 23 shows that the groundwater abstraction in the coastal zone in Asia has greater value than any other continent. The highest abstraction is shown in the south Asia region (India, Bangladesh, and Myanmar), which ranges between 25.5 km^3/year and 29.6 km^3/year. In addition to that, the eastern part of China also shows a moderate rate of groundwater abstraction (~14 km^3/year). In the others parts of the coastal zone of the world, the value of groundwater abstraction is considered as low (dark blue area). On the Africa continent, there is no data region in the desert area.
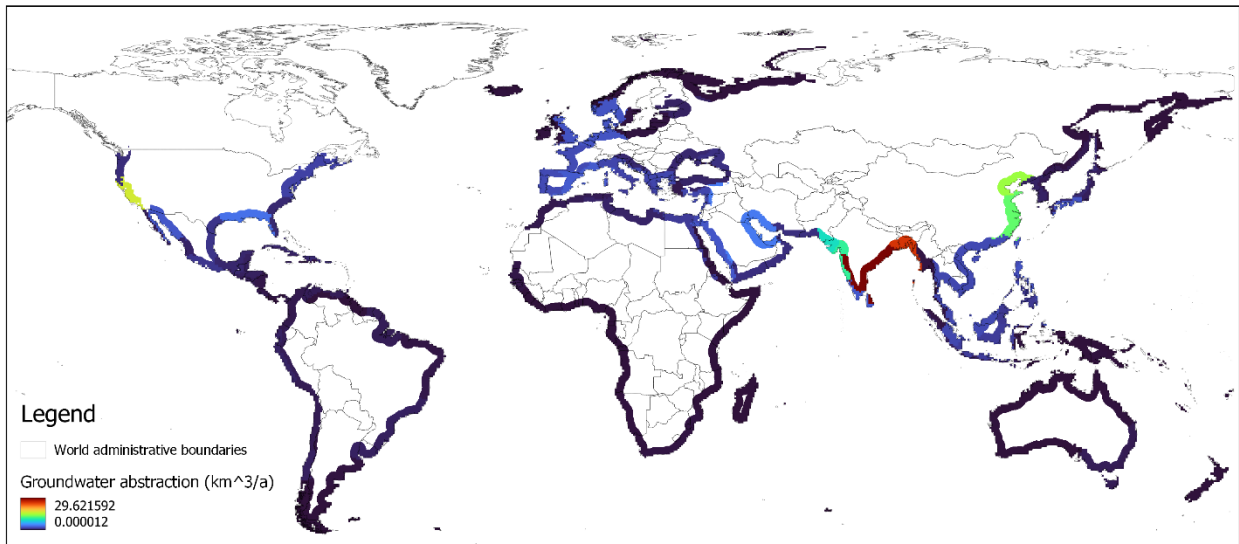
Figure 23. Groundwater extraction (km³/year) excluding permafrost region (Sutanudjaja et al., 2018; Zamrsky et al., 2018)

16. Precipitation

Precipitation data is obtained from the interactive atlas map composed of IPCC. The database is based on the latest IPCC report (AR6) with baseline data from 1995-2014. Near-term projection most likely describes the current climate condition of the world. Based on Figure 24 illustrate the projection of precipitation (in depth) in a day. It is shown that the equator area has the highest precipitation rate, caused by the low-pressure atmosphere. Increased precipitation in the tropical area brings both good and bad to the region. As in the tropical climate, most of the countries are developing countries, which do not have a good infrastructure, thus could result in a flood in urban areas. The good side is that the precipitation has a high rate of recharge. High recharge resulting lower possibilities of salinization. Especially in the coastal zone area, precipitation can help to reduce the rate of SWI further inland.
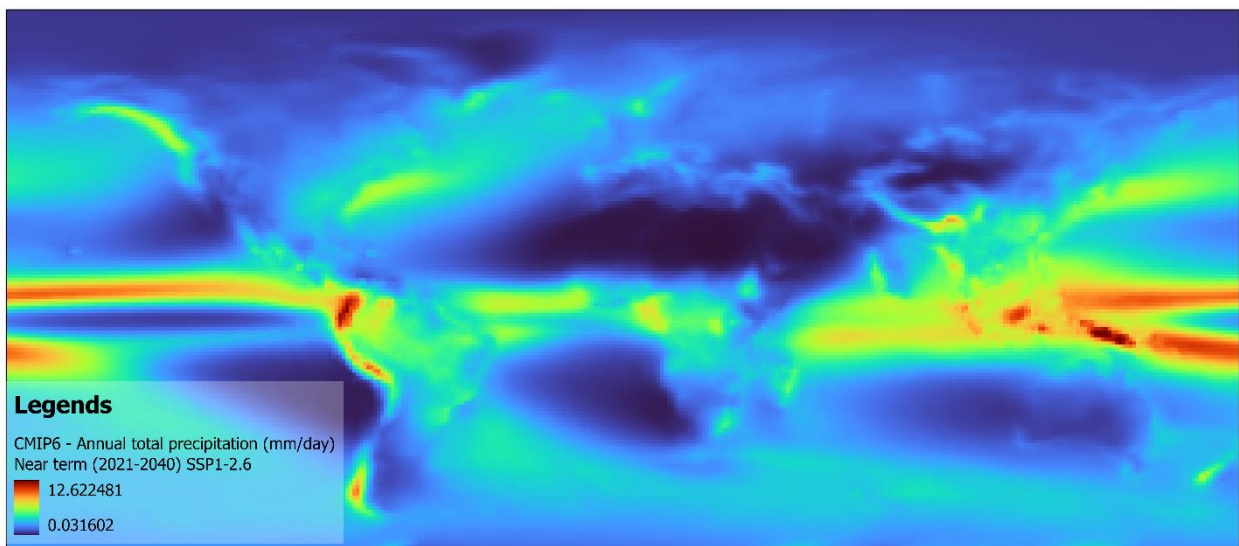
Figure 24. Global precipitation data adapted from IPCC 6th Report with near-term projection (2021-2040) SSP 1-2.6 scenario (Gutiérrez et al., 2021)

17. Evapotranspiration

Evapotranspiration (ET) is an important aspect of soil water balance. A region with a very strong ET rate could impact the soil salinization of the soil due to a high evaporation rate. In

31

this study, the dataset that was used is potential evapotranspiration (PET based on Penman-Monteith Method (*Equation 3.2—2*).

Equation 3.2—2 Penman-Monteith method

$$PET = \frac{0.408 \; x \; \Delta \; x \; (R_n - G) + \gamma \frac{900}{T_{avg} + 273} \; x \; u_2 \; x \; (e_s - e_a)}{\nabla + \gamma(1 + \frac{r_s}{r_a})}$$

Where:

PET is the evapotranspiration for a reference crop (mm/day)

Rn is the net radiation (MJ / m^2 day)

G is soil heat flux density (MJ / m^2 day)

T_{avg} is mean daily air temperature at 2 m height (^{o}C)

u_2 is the wind sped at 2 m height (m/s)

es is the saturation vapour pressure (kPa)

ea is the actual capour pressure (kPa)

es – ea is the saturation vapour pressure deficit (kPa)

Δ is the slope vapour pressure curve (kPa / ^{o}C)

γ is the psychrometric constant (kPa / °C)

rs is the bulk surface resistance (m/s)

ra is the aerodynamic resistance (m/s)

The dataset shows the global distribution of potential evapotranspiration (PET). It shows that the highest PET is located in arid regions, especially in desert areas (e.g., the Saharan desert in northern Africa). These arid regions are usually located in sub-tropical climate region, with less precipitation and dry weather. This high PET is also illustrated in the middle of Australia, where desertification also occurs. The high PET indirectly indicates a higher chance of an aquifer being salinized. Therefore, high PET indicates a higher vulnerability to seawater intrusion in the coastal zone.
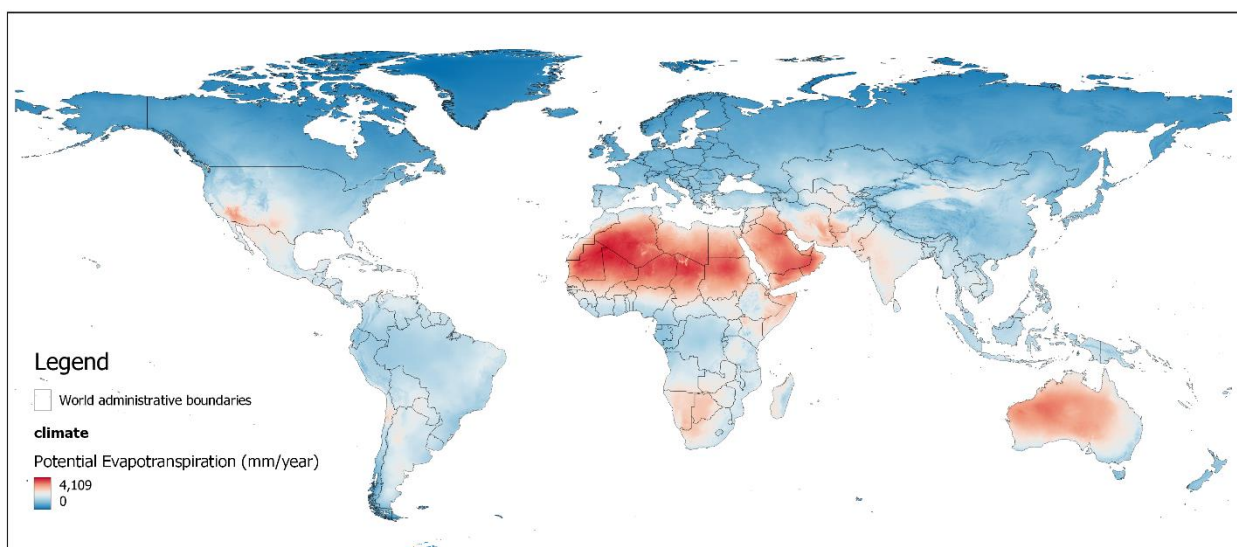
Figure 25. Potential evapotranspiration (PET) on a global scale in mm/year (Zomer & Trabucco, 2022)

18. Sea water wedge toe

Sea water wedge toe is the main indicator to evaluate salinization risk. In most coastal megacities, the condition of the SWI wedge is concerning, in addition to upconing phenomenon due to groundwater extraction. For example, on the northern coast of Jakarta, people are having trouble finding freshwater sources due to the high rate of salinization. Studies show that the indication of saltwater intrusion could reach up to 3 km inland from the coast, where the water sampling shows that the water type in several sampling well is Na-HCO3 and Na-Cl (Setiawan et al., 2017; Wijaya et al., 2019). This evidence shows that seawater intrusion in coastal megacities is very concerning and threatens human health.

In this study, the data for seawater intrusion is obtained from two types of data, analytical and numerical models. Analytical data is obtained from the calculation of Badon Ghijben-Herzberg principle in *Equation 2.1—1* and *Equation 2.1—2*.

3.2.2 Layer's Spatial Formatting

The datasets needed to be in a raster format to assign weight and rank to each layer according to the criteria range. The conversion of vector data was done using GIS. Some data need to be formatted to be used further in the process.

i. Creating a coastal zone dataset

The coastal zone was determined based on a few considerations, for example, the possibility of tide and sea surge reaching further inland through storm events, sea-level rise, and deltaic deposition of some big deltas (e.g., Mekong Delta), and land subsidence in coastal megacities. Therefore, even though GALDIT recommended a coastal zone of 5 km, in this research, we expand further to 50 km. Generation of coastal zone was done using buffer tools. This ruling of the coastal zone threshold also considered the wide variety of coastal zones worldwide. With the generated coastal zonation, raster data was clipped to the coastal zone accordingly so that we only assess the interest area. This particular step is time-consuming due to the large size of datasets. Some data with very fine resolution, such as land cover data, took a day and a half to clip the raster data. Meanwhile, for not moderately fine resolution data, clipping could take faster.

ii. Interpolation and distance generation

a. The proximity tool is used to generate the discretization of distance from the coastline dataset. The proximity tool created discrete proximity of distance to the furthest coastline boundary with a pixel size of 0.1° x 0.1°. This dataset is generated using the natural earth coastline dataset following the coastal zone area we created beforehand. Due to its 0.1-degree resolution, roughly equal to 11 km width and length per raster pixel, it is easy to differentiate how far the criteria range would be.

b. Some vector data were in point features. So, it needs to be interpolated to fill the coastal zone. Some data that are required to be interpolated are aquifer thickness and salinity data. The interpolation method that was chosen was IDW (Inverse Distance Weighted). This method simply assumes that the things close to each other are more akin to those that are further apart (ArcGIS, 2022). The method was chosen because the data are sparsely distributed and due to the limitation of file size, IDW gives the fastest result with good estimation.

iii. Rasterize data

Some data are obtained in vector format as shown in Table 1. All datasets are needed in raster format to comply with the requirement of calculating the vulnerability map. This step was done

because, in raster format, we can assign the pixel as we wanted so all data can be in the same pixel, so because we can change the resolution, raster data size is usually not as large as vector data.

iv. Uniformity of raster resolution

Some raster data that was obtained from the source were either in very fine resolution (0.001 degrees) or very coarse resolution (1 degree). The difference in each resolution could create an anomaly in the map result, either it is too coarse that some data areas are not included, or it is too fine so that the map creates a pattern according to the finest resolution. This may cause a misalignment of the map interpretation. Therefore, all raster maps are converted to the same pixel resolution, which in this project is 0.1 degree.

3.2.3 Layers Weight and Rating Assignment

The weight and rating system was developed based on expert knowledge and adapted from some literature reviews on weighting and rating systems for salinization vulnerability (e.g. GALDIT). However, some changes and adjustments were made to create the ratings based on expert judgment. Each layer was weighted from 1 to 5 and classified into a rating system from 1 to 10. In order to reach the most detailed result of vulnerability mapping, the cluster is also weighted to its importance, where aquifer properties are 4, land surface condition is 5, human impact is 5, and climate is 3. The detailed weighting and rating system for the layers are shown in Table 4.

Table 4. Clustered indicators with assigned weight and rating

Sub-Cluster	Weight	Layers	Weight	Criteria/range	Rating Value
Aquifer properties	**4**	Type of Aquifer	5	Aquifer of (karstic) carbonate rocks	10
				Aquifer of sand and gravel	8
				Aquifer of sandstone and limestone	6
				Aquifer in weathered bedrock	4
		Hydraulic conductivity (m/s)	3	$10^{-03} - 10^{-01}$	10
				$10^{-05} - 10^{-03}$	8
				$10^{-07} - 10^{-05}$	6
				$10^{-09} - 10^{-07}$	4
				$10^{-11} - 10^{-09}$	2
		Water Level (M.a.s.l)	4	-30 - 0	10
				0 - 10	9
				10 - 20	7
				20 - 40	5
				40 -80	3
				>80	1
		Aquifer thickness (m)	2	0-50	10
				50-100	8
				100-200	6
				200- 400	5
				400-600	3
				>600	2
Land surface condition	**5**	Slope (%)	4	0 - 2	10
				2 - 6	8
				6 - 10	5
				10 - 15	3

				> 15	2
		Distance from the coastline (m)	4	0 - 50	10
				50 - 100	9
				100 - 500	7
				500 - 1000	5
				1000-5000	3
				>5000	1
		Land cover	2	Cropland (agriculture)	8
				Forest	7
				Bare/sparse vegetation	5
				Shrub, herbaceous plant, moss, and lichen (uncultivated land)	4
				Wetland, reservoir, snow, and ice	3
				Build-up areas	2
		Coastal Inundation/flooding hazard (dm)	3	3 - 5	10
				2 - 3	9
				1 - 2	7
				0 - 1	5
Climate	**3**	Sea-level rise (m)	5	0.1 - 0.3	6
				0 - 0.1	3
				-0.1 - 0	1
		Precipitation (mm/a)	4	0 - 50	8
				50 - 100	7
				100 - 500	5
				500 - 1000	3
				1000 - 3000	1
		Evapotranspiration (mm/a)	2	2000 - 3600	8
				1000 - 2000	7

				500 - 1000	5
				100 - 500	3
				0 - 100	2
		Tide surges (m)	4	6 - 7	9
				4 - 6	7
				2 - 4	5
				0 - 2	3
Human Impact	**5**	Well extraction rate (km3/yr)	5	10 - 30	10
				1 - 10	8
				0.5 - 1	6
				0.2 - 0.5	4
				0 - 0.2	3
		Population density (person/km2)	4	1000 - 7000	10
				100 - 1000	8
				10 - 100	5
				0 - 10	3
		Land Subsidence (m/year)	3	3 - 5	8
				2 - 3	6
				1 - 2	5
				0.5 - 1	4
				0 - 0.5	3
		Area of irrigated lands with groundwater (%)	3	75 - 100	10
				50 -75	6
				25 - 50	4
				0 - 25	2

3.2.4   Vulnerability Calculation and Mapping

Creating a vulnerability map is one of the critical aspects for the policymaker to understand the threat and risks of an area. This study was done with a vision so that we can help some policymakers to create mitigation measures for seawater intrusion, which is now a common problem in the coastal zone. All process of mapping and calculation is done using QGIS. Vulnerability calculation is done by an index mapping approach using the weighted average (*Equation 3.2—3*) adapted from GALDIT method, where ratings and weights are applied to each indicator. In this study, instead of using only six indicators, there are 16 indicators used, as indicated in Table 4. Then the ratings and weight assigned to each indicator and criteria were used to calculate the vulnerability index on the coastal zone, which later can be used as a first approximation of the coastal condition.

Equation 3.2—3 Vulnerability index relationship derived from GALDIT method

$$Vulnerability\ index\ = \frac{4}{17}\ x\ \left[\frac{\sum_{i=1}^{4} w_i^{AP} AP_i}{14}\right] + \frac{5}{17}\ x\ \left[\frac{\sum_{i=1}^{4} w_i^{LS} LS_i}{13}\right] + \frac{3}{17}\ x\ \left[\frac{\sum_{i=1}^{4} w_i^{C} C_i}{15}\right] + \frac{5}{17}\ x\ \left[\frac{\sum_{i=1}^{4} w_1^{HI} HI_i}{15}\right]$$

where w_i is the weight for each indicator corresponding to each cluster (AP: Aquifer Properties, LS: Land Surface Condition, C: Climate, HI: Human Impact), AP_i, LS_i, C_i, HI_i is the rating assigned to each class in aquifer properties, land surface condition, climate, and human impact cluster.

In order to make the analysis of vulnerability easier, the mapping was done on a continental scale, which are six continents: Africa, Australia and Oceania, Asia, Europe, North America, and South America. The indicators were first overlayed and calculated for each cluster, resulting in four maps of vulnerability according to the group (human impact, aquifer properties, land surface properties, and climate). Afterward, all clusters were mapped together, thus creating a vulnerability map of the coastal zone to salinization.

3.2.5   Sensitivity Analysis

Sensitivity analysis was done to analyze how each indicator contributes to the groundwater's vulnerability to salinization. There are two types of sensitivity analysis: single parameter sensitivity test and map removal sensitivity test (Allouche et al., 2017; Babiker et al., 2005; Seenipandi et al., 2019). These two methods are based on statistical analysis to express their sensitivity.

3.2.5.1   Single Parameter Test

The single parameter test is a statistical sensitivity computation developed by Napolitano and Fabbri (1996). It compares the theoretical weight that was assigned to the vulnerability indicators based on expert judgment with the effective or real weighted value of a parameter or indicator in each pixel (Allouche et al., 2017; Seenipandi et al., 2019). This sensitivity test was done to examine the effect of each parameter on the vulnerability index. The test calculates the effective weighted value of indicators using *Equation 3.2—4*.

Equation 3.2—4 Single parameter test

$$W = \frac{P_r P_w}{V}\ x\ 100 \qquad Eq.\ 1$$

where P_r is the rating of the indicator, P_w is the weight of each indicator, V is the total vulnerability obtained from Eq. 5, and W is the effective weighted value.

3.2.5.2 Map Removal Test

The map removal test was done by excluding one or more indicator layers from the vulnerability index calculation. The map removal test itself calculates an indicator's influence on the vulnerability index using *Equation 3.2—5*.

Equation 3.2—5 Map removal test

$$S = \frac{\left(\left|\frac{V}{N} - \frac{V'}{n}\right|\right)}{V} \; x \; 100$$

where S is the sensitivity of a particular parameter, V is the unperturbed vulnerability index, V' is the perturbed vulnerability index, and N and n are the number of layers used to calculate V and V', respectively. The unperturbed vulnerability index is the original vulnerability index with all parameters included, while the perturbed vulnerability index is the vulnerability index computed using reduced indicators. Theoretically, this method tells us to remove one or more indicators one by one at a time until there is only 1 data left (Seenipandi et al., 2019). But, this method was unlikely to be done since there were 16 datasets. Therefore, to simplify the removal test, a statistical correlation test was done first to see if any indicators were insignificant to the vulnerability index calculation result.

3.2.5.3 Correlation Test

A correlation test can identify the relation between parameters (Elçi & Polat, 2011; Javadi et al., 2011; Moghaddam et al., 2017). The Pearson correlation test (r) was done using Equation 3.2—6, which will be automatically calculated in the Microsoft Excel program using the '=PEARSON' function. The statistical tools can also describe the statistical summary (mean, minimum, maximum, and standard deviation (SD) value).

Equation 3.2—6 Pearson's correlation relationship

$$r = \frac{\sum (x_i - \bar{x})(y_i - \bar{y})}{\sqrt{\sum (x_i - \bar{x})^2 \sum (y_i - \bar{y})^2}}$$

Where:

    r = correlation coefficient

    x_i = values of the x-variable in a sample

    $\bar{x}$ = mean of the values of the x-variable

    y_i = values of the y-variable in a sample

    $\bar{y}$ = mean of the values of the y-variable

In this study, the significance test used the paired sample *t*-test, where the calculated P-value through the two-tailed significance method was compared to the significance level α of 0.05 (95% confidence) (Elçi & Polat, 2011). For the *t*-test, two hypotheses are needed to achieve: the null hypothesis (H₀) and the alternative hypothesis (Hₛ). Based on the *t*-test result, if $P < \alpha$, then the null hypothesis is rejected, and thus alternative hypothesis is accepted. Based on the significance test result, if an indicator shows $P > \alpha$, that indicator will be removed or excluded from the vulnerability calculation. The null hypothesis (H₀ and alternative hypothesis (Hₛ) were formulated as follows:

    H₀ : the indicators have very little effect on the vulnerability map

    Hₛ : the indicators have a significant effect on the vulnerability map

3.2.6 Data Validation

The map was validated to evaluate the vulnerability map with the actual condition of seawater intrusion. Validation of the map using the risk component of the vulnerability interrelation concept to understand the real risk of SWI. Thus, salinity data, e.g., electrical conductivity (EC) and saltwater wedge toe data, is used to validate the vulnerability map. An approach to estimating the salt wedge toe in the coastal zone under natural conditions by using *Equation 3.2—7* and *Equation 3.2—8*. The calculation is distinguished into two types, according to the aquifer type, which are unconfined or confined aquifers (*Figure 26*). The following formula can be used to calculate the length of the saltwater wedge (*L*) in an unconfined aquifer with an assumption where the saline groundwater is stagnant (Oude Essink, 2001):

Equation 3.2—7 saltwater wedge toe in the unconfined aquifer

$$L = -\frac{q_0}{f} - \sqrt{(\frac{q_0}{f})^2 - \frac{k}{f} D^2 (1 + \alpha) \, \alpha}$$

While the following formula is used to calculate the length of saltwater wedge toe (*L*) in a confined aquifer:

Equation 3.2—8 Saltwater wedge toe in the confined aquifer

$$L = -\frac{k \, D^2 \alpha}{2 \, q_0}$$

Where:

q_0 is natural groundwater outflow at the coastline x = 0 (negative sign) ($L^2 \, T^{-1}$)

f is natural groundwater recharge (LT^{-1})

D is the thickness of the aquifer (L)

α is relative density difference ($\rho_s - \rho_f)/\rho_f$ (−)

k is hydraulic conductivity of the aquifer (L T^{-1})

Natural groundwater recharge is based on data available in the global dataset of direct natural groundwater recharge(Moeck et al., 2020). Relative density difference is the ratio of water density difference and freshwater density, where it's 0.25. The aquifer thickness is based on Zamrsky (2018) database. Hydraulic conductivity is based on the work of Gleeson et al. (2014). As q_0 is obtained from the distance from the coastline multiplied by the natural recharge value.
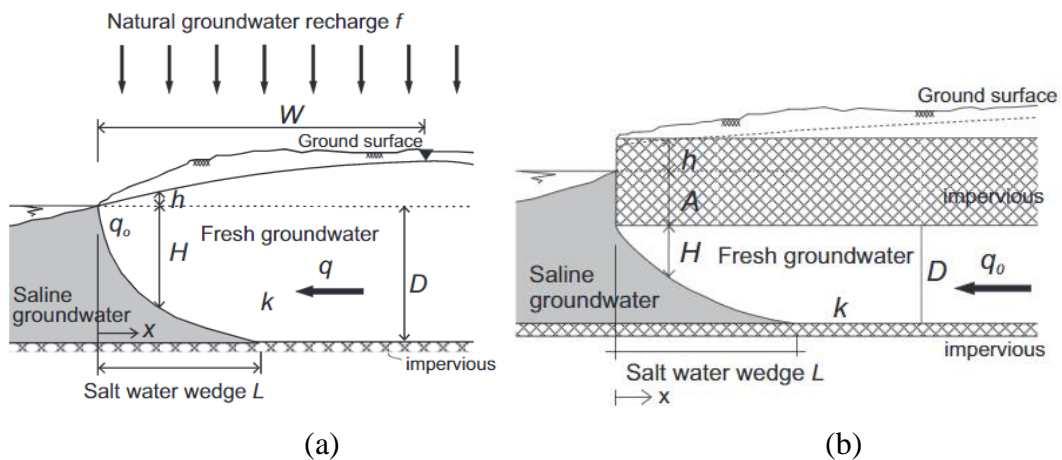

Figure 26. Conceptual model of (a) unconfined aquifer and (b) confined aquifer (Oude Essink, 2001)

Chapter 4   Results

Vulnerability mapping of the coastal zone to salinization is essential for the policymaker to assess and analyze regulations to mitigate saltwater intrusion inland. In this case, intrinsic factors or indicators of the aquifer are not only considered but also extrinsic indicators, such as human activity, land surface conditions, and climate change. Land conditions express pre-condition of the land without human interference, while the human impact is an aftermath condition resulting from human interference. These indicators influence each other and could create different behavior in the vulnerability map. A vulnerability map is composed continentally to understand the impact of the indicators to the vulnerability in the coastal zone.

4.1 Vulnerability Map in Continental Scale

4.1.1   Australia and Oceania

The first continent to be processed was Australia because, fortunately, Australia has the complete data distribution of the indicators, including the EC data. This continent is also considered a pilot project, where all the trial and error were made in this continent to gain the best rating range and weight. Australia has a combination climate on one continent, tropical to semi-arid climate. The climate condition is shown in Figure 27d, where the northern part of Australia indicates a low vulnerability index value. Meanwhile, the middle part of Australia shows a higher index associated with the area's type of climate. The climate index in Oceania (west of Australia Island) shows a low index. Overall, this continent shows the lowest cluster index, probably due to the low weight and ratings assigned to the indicators.

Both Australia and Oceania regions has the effect of human activity shown in some "hotspot" as shown in Figure 27c. The hotspots correspond to urban areas located in the coastal zone, such as Adelaide and Perth, with an index from 1 to 5, approximately. The condition of the land surface index in Australia shows that most coastal zones of Australia have a considerably high index (> 5), which is indicated by the orange to red color (Figure 27b), especially on the coastline pixels. This could be the effect of the high rate and weight of distance to the coastline. Oceania's result shows higher index distribution variability for land surface conditions. The high index was shown in the island's southeast region, which is also a low-lying area. The aquifer properties cluster map shows the highest index value (Figure 27a). This may be due to the high weight assigned to the indicators. The high indexes are clumped in several coastal region areas of the continent. The highest is found in the southern part of the Australia continent with an index of more than 8 and some high indexes are also spotted in the western part of the continent. Oceania region has more variability across the coastal zone, with the highest index on the southeast of the main island of New Zealand.

The vulnerability mapping resulting from the vulnerability index calculation is shown in Figure 28. The map shows a high vulnerability index (dark red color) in most of Australia's coastal zone. A very high vulnerability was shown in the South Australia state, especially in Port MacDonnell and Adelaide. Very high vulnerability also appeared in Perth, Western Australia. Meanwhile, low to moderate vulnerability is shown in New South Wales state coastal zone (green color). Oceania region shows more low vulnerability in the overall area. New Zealand's main island shows low vulnerability in the northern part of the island. On the other hand, the

southern part of the island shows high vulnerability, especially in Christchurch area. This high vulnerability also appears in the north island of New Zealand, especially in megacities of Auckland coastal region.
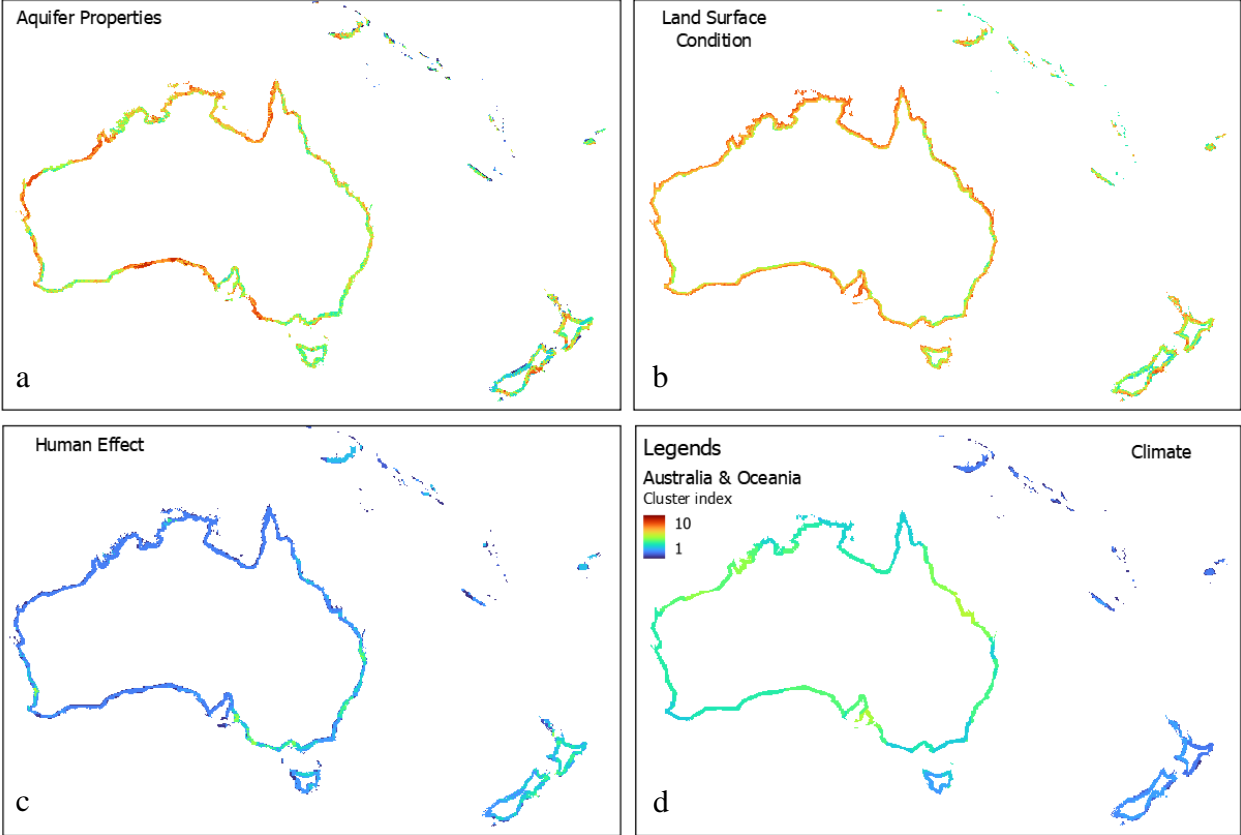

Figure 27. Australia and Oceania cluster (a) aquifer properties, (b) land surface condition, (c) human impact, and (d) climate mapping.
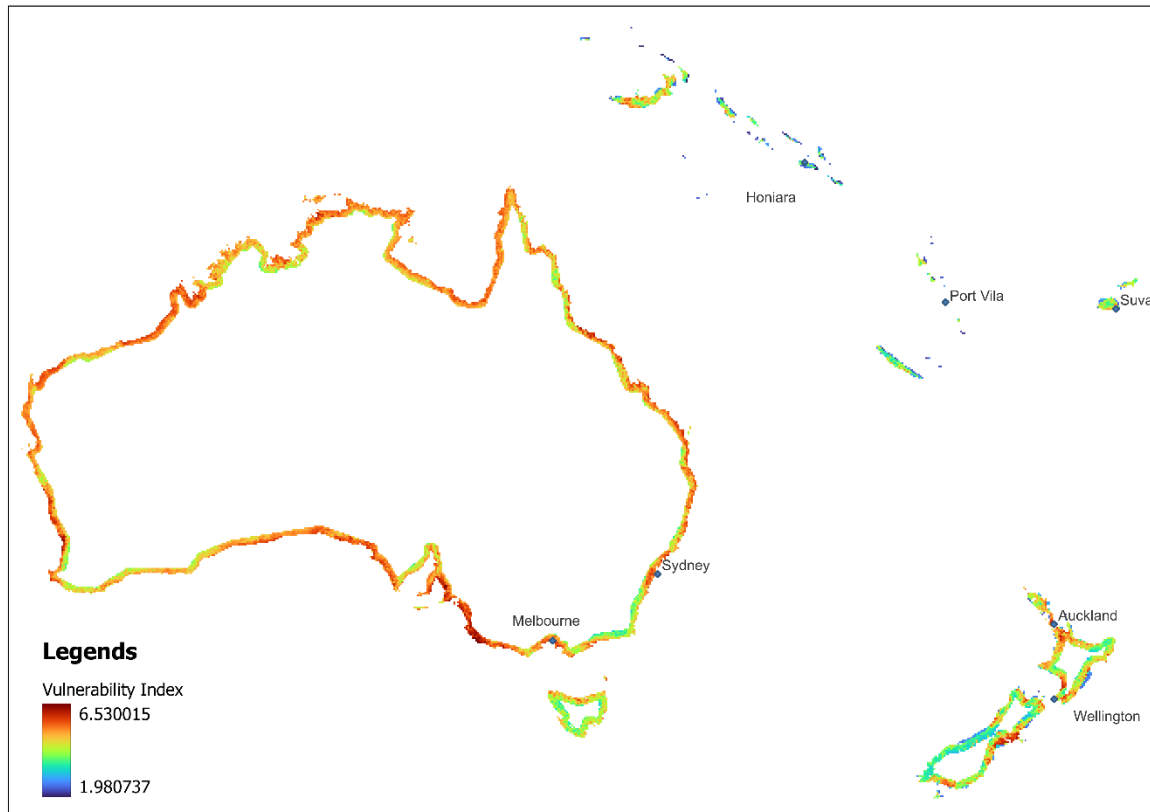
Figure 28. Vulnerability index of Australia and Oceania Continent

4.1.2 Africa

Africa is a continent that is most concerning among scientists due to its arid climate together with lack of water resources recharge. Although Africa has notoriously had poor climate conditions, the climate cluster shows a low index (Figure 29d). But this is supported by the fact that for seawater intrusion, climate alone is not a key indicator that influences seawater intrusion vulnerability. The land surface condition of Africa's coastal zone shows a dominantly moderate to high index, especially in places with a high effect of the distance from the coastline and the slope of the coastal zone (Figure 29b). In contrast, the aquifer properties show multiple high index areas in the north, west, and east of the continent in accordance with the aquifer type of the region consisting of sand and gravel aquifer (Figure 29a).

Human interventions in the coastal zone of Africa show a low index that indicates that in the region, the human impact is not significant to the vulnerability mapping. The Saharan region (west Africa) offers a very low index due to very little human interference in the region and also due to "no data" from several indicators, such as groundwater abstraction (Figure 29c). Compared to other continents, human interference in Africa shows the strongest influence, proved by a higher index in the northern part of the continent (coastal zone of Tunisia, Libya, and Egypt), while the other part shows a low index. The northern part of the continent shows a higher index of human interference because the area has more human activities than the other part of coastal regions in the continent. According to the data acquired, the northern part of Africa is shown to have a higher rate of groundwater abstraction than other parts of the continent.

The condition of the aquifer properties results in the highest effect on the vulnerability index mapped in Figure 31, which shows the impact of the high weight and rating in the vulnerability map. The continent's north, west, and east show some locations with high vulnerability index

(orange to red color with index value >6). This phenomenon indicates that a high weight assigned to aquifer properties indicators and clusters results in a vulnerability map that follows the behavior of the cluster distribution. In contrast, 70% of the other region shows low to moderate vulnerability due to low ratings and indices in all indicators assigned.

Figure 29. Africa cluster (a) aquifer properties, (b) land surface condition, (c) human impact, and (d) climate index mapping
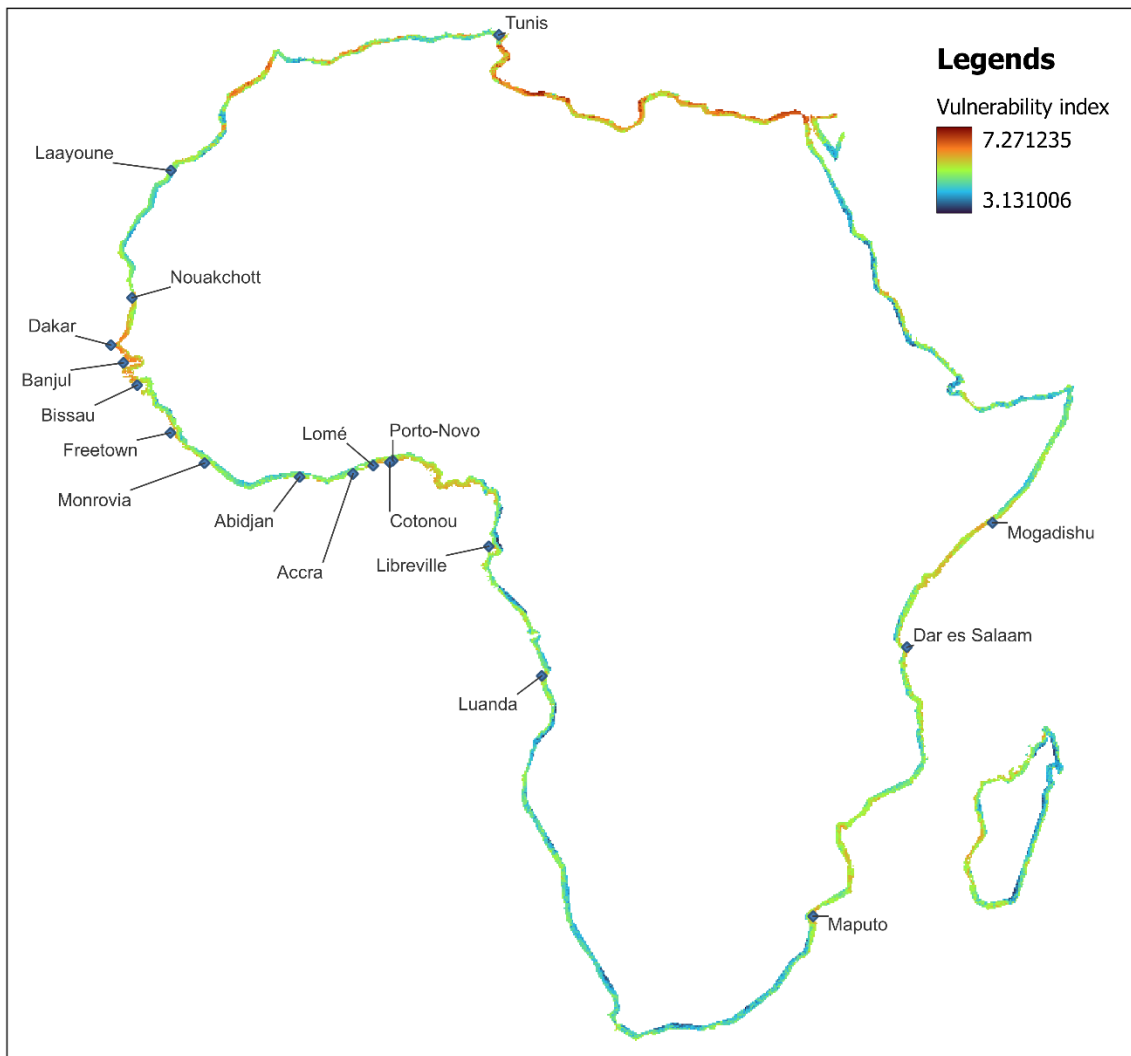
*Figure 30 Africa vulnerability index mapping with the combination of all clusters.*

4.1.3 Asia

Asia has a very high variability among its area in many indicators, such as climate, race, geological formation, and demographic distribution. The variation of the indicators can be seen from the continent's south to the north. Asia is one of the continents that spread over almost half of the world. It is spread over the five major climate types: topical, sub-tropical, temperate, highland, and polar(CIESIN, 2007).

The continent's aquifer properties distribution (Figure 32a) shows a sparse distribution of low to high index. A low index shows the distribution of unconsolidated formation with high hydraulic conductivity and low water level. The most dominant high index is located in the south (parts of Pakistan, India, and Bangladesh), middle-east, east (China), and southeast (Indonesia) Asia. Some regions of Russia in the western part also show a high index of aquifer properties.

The distribution of land surface conditions in Asia is not as homogenous as in Australia or Africa. This is an effect of the geological condition of the continent, where in some regions is a subduction zone for two or more different plates (e.g., Indonesia, Philippines, and Japan). This caused some coastal zones to have a lower index for the land surface condition due to the high slope and less prone indicators. Based on Figure 31b, high vulnerability is clearly shown in the low-lying topography of the continent.

Human impact index mapping emphasizes the condition of the demographic condition of the continent. According to the cluster map in Figure 31c, the northern part of the continent, which has a polar climate, demonstrates very low human activities. The human impact increases gradually to the equator line. A higher index is found in the south Asia country (India and Bangladesh), East China, as well as in the north of Java Island coast. A lower index is also found in Papua and New Guinea Islands due to low human interference on the island.

The continent's climate condition shows that the northern part of the continent has a higher index than the one near the equator line (Figure 31d). The middle-east region shows the highest index due to the arid climate that they suffer. The arid climate causes a higher PET and lowers precipitation causing lower recharge to the aquifer. Meanwhile, in the equator region, there is a high precipitation rate and a low sea level rise rate resulting in a low index.

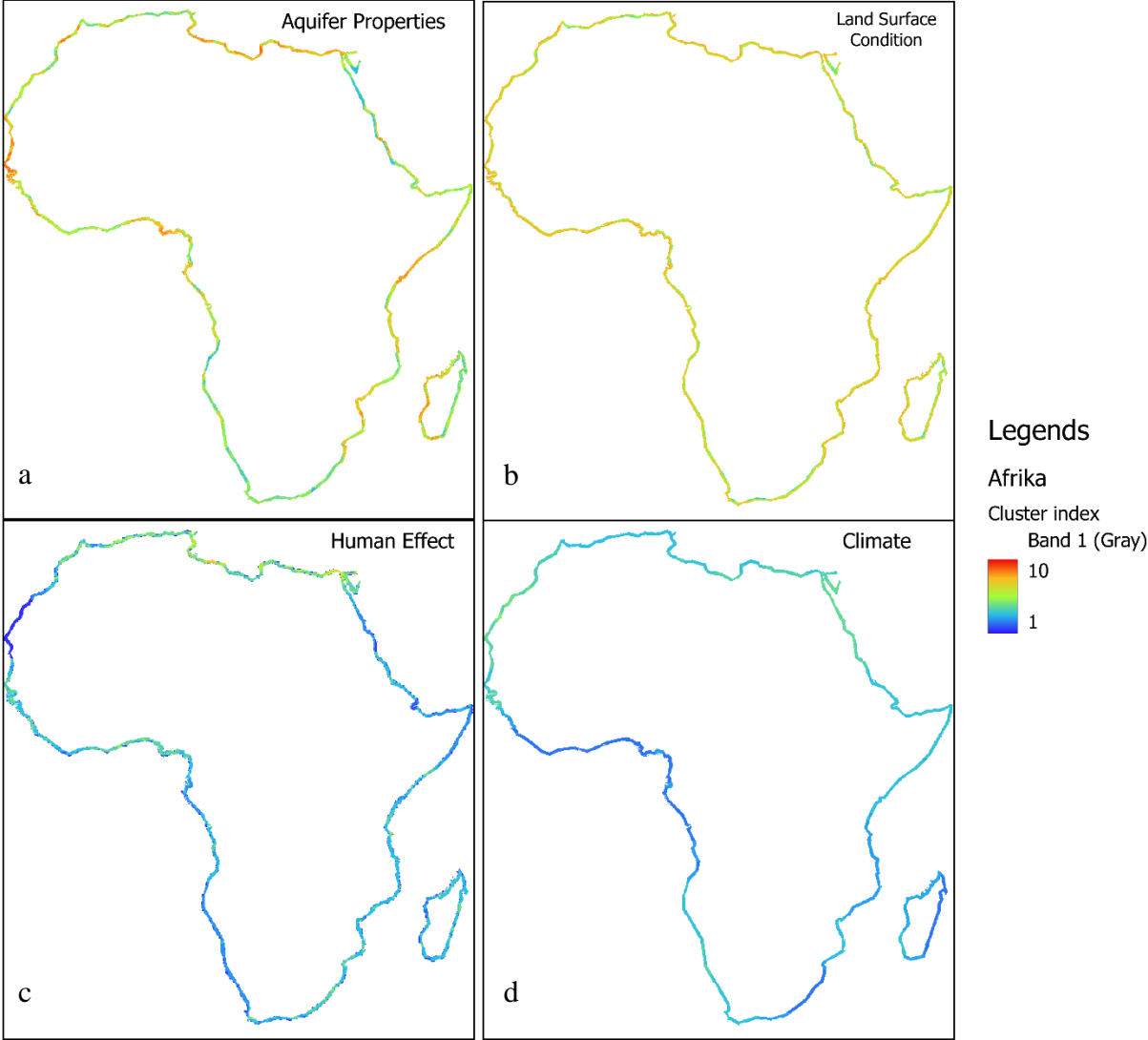*Figure 31 . Asia cluster (a) aquifer properties, (b) land surface condition, (c) human impact, and (d) climate index mapping*
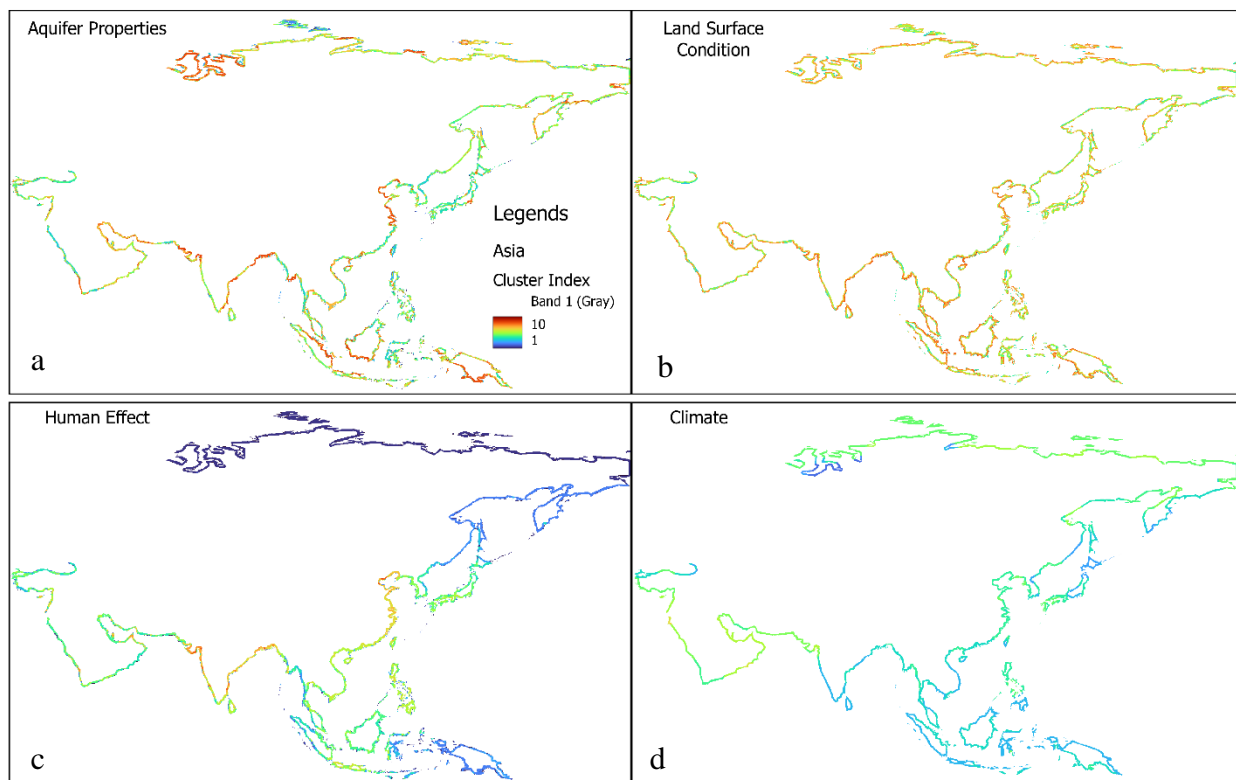
Figure 32 Vulnerability index for Asia continent.

Figure 34 shows the result of vulnerability index mapping for the Asia continent. As a result of a low index from four of the cluster in the northern part of the continent, the vulnerability map also shows a lower index in the northern part (Russia region). Some regions have a significantly very high vulnerability index, such as the coast of Mumbai, Beijing, and Shanghai. Middle east region shows high vulnerability in most populated areas with high resources exploration and exploitation activity (east of the Arab Peninsula). Some region in Southeast Asia shows a distribution of high index in a particular location, such as the Mekong Delta. The north coast of Java Island and the west coast of Sumatra Island also shows a high vulnerability index to salinization.

4.1.4 Europe

Europe is very nurturing of its resources, including water. To accommodate it, Europe creates a Water Frame Director to control the water use in its territory. Thus, this vulnerability mapping in the coastal zone could help the policymaker execute a policy or a treatment. The mapping for the four clusters determined is shown in Figure 33.

a. The aquifer properties cluster map shows a higher index on the northern coast of European countries (The Netherlands, Germany, Poland, and Russia), excluding the Scandinavian region. The Scandinavian coast shows a low to moderate index, in accordance with the aquifer type of the coast, where it mainly consists of igneous rock. Meanwhile, in southern Europe, the distribution of the index varies. For example, Ukraine's southern coast and Venice's coast show a high index, while the west coast of Italy shows a low to moderate index for aquifer properties. The Iberia peninsula (Spain and Portugal) displays a low to moderate index, as well as the other part of the southern coast of Europe. Meanwhile, the islands around the main island do not show significant results for this cluster.

b. The land surface condition of Europe is comparable with the aquifer properties cluster. Northern Europe coast has a relatively high index value, while in the southern it is more

varied in the index value. This behavior shows the imprint of low-lying topography as well as the land cover type of the coastal region that was used as agricultural land.

c. The human impact index value shows a lower index in northern Europe, then increases to the continent's southwest. A moderate to high index is found in countries with megacities in the coastal zones, such as The Netherlands, Germany, Italy, Portugal, and Spain. Densely populated land aligned with land use for agriculture shows a fingerprint on the map. The western part of the UK also indicates a higher index than the left side (comparable comportment as aquifer properties)

d. The climate condition of the continent shows the southern coast of Europe is relatively higher than the northern region. Scandinavian shows a lower index, as well as some parts of Russia. Europe has a moderate to high index caused by the high SLR value in the northern hemisphere. The distribution of the surge gives a dominant pattern to the result.

Figure 33. Europe cluster (a) aquifer properties, (b) land surface condition, (c) human impact, and (d) climate index mapping

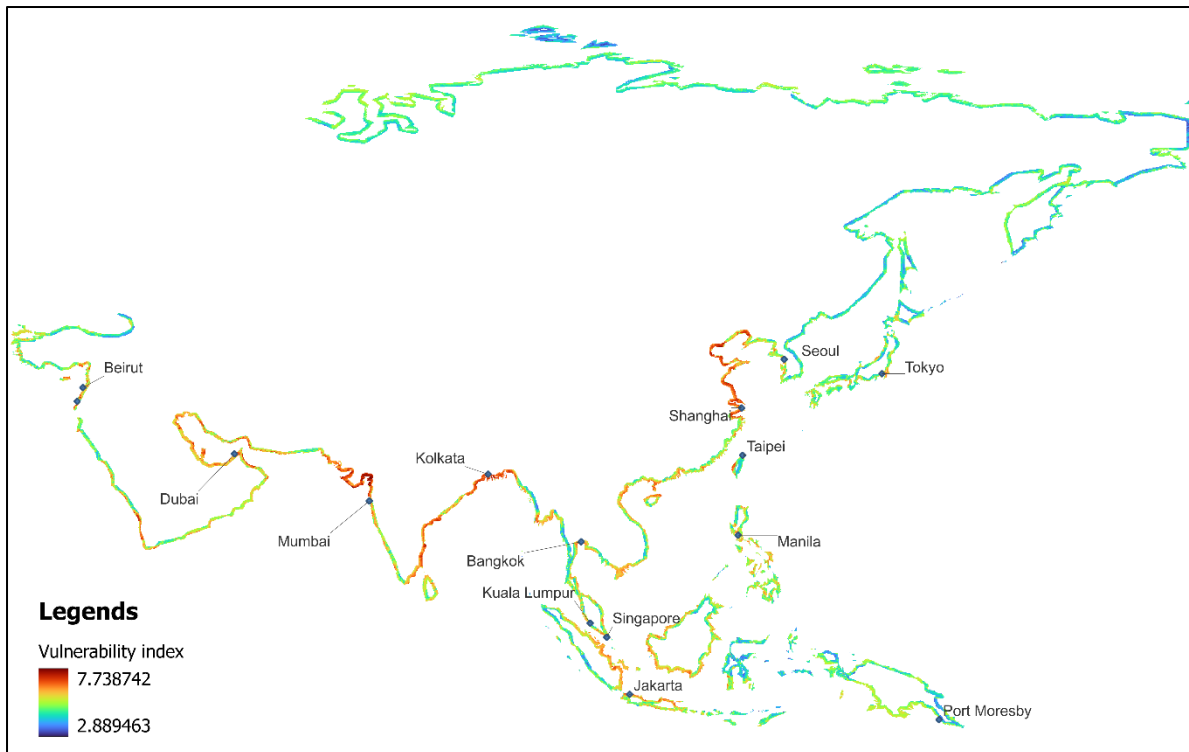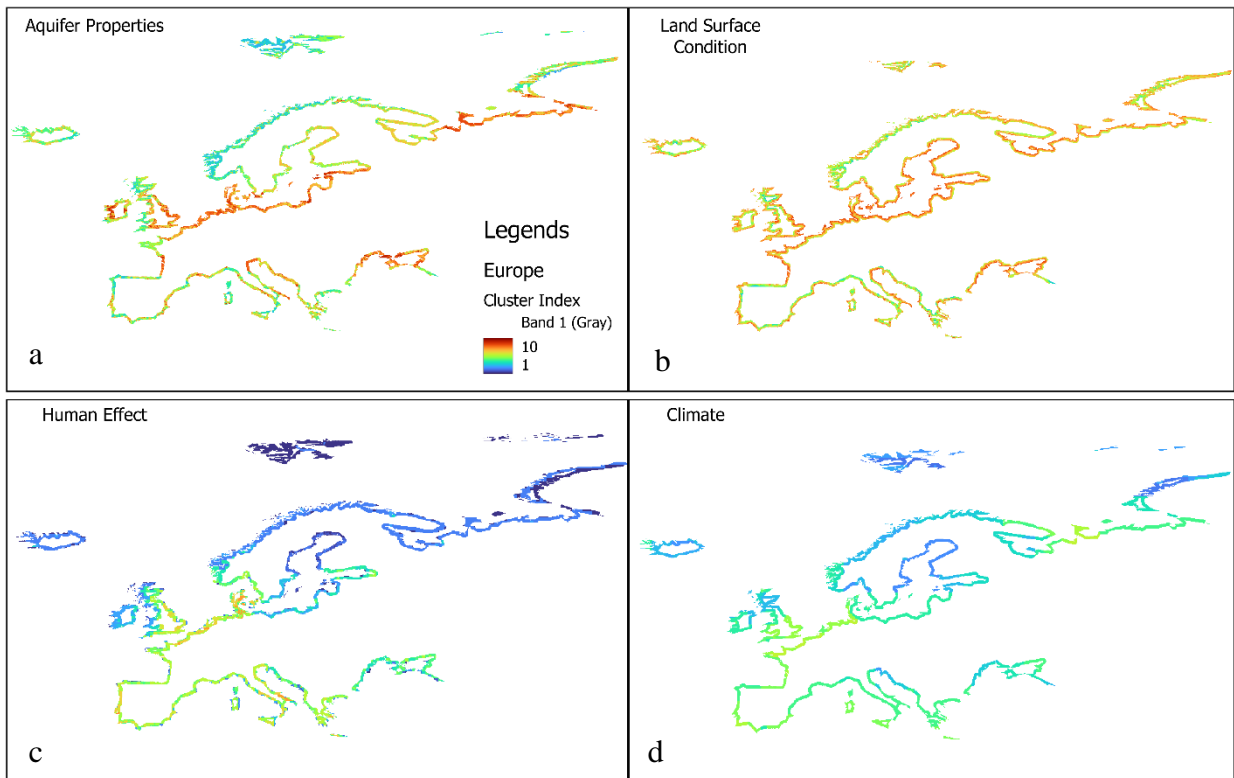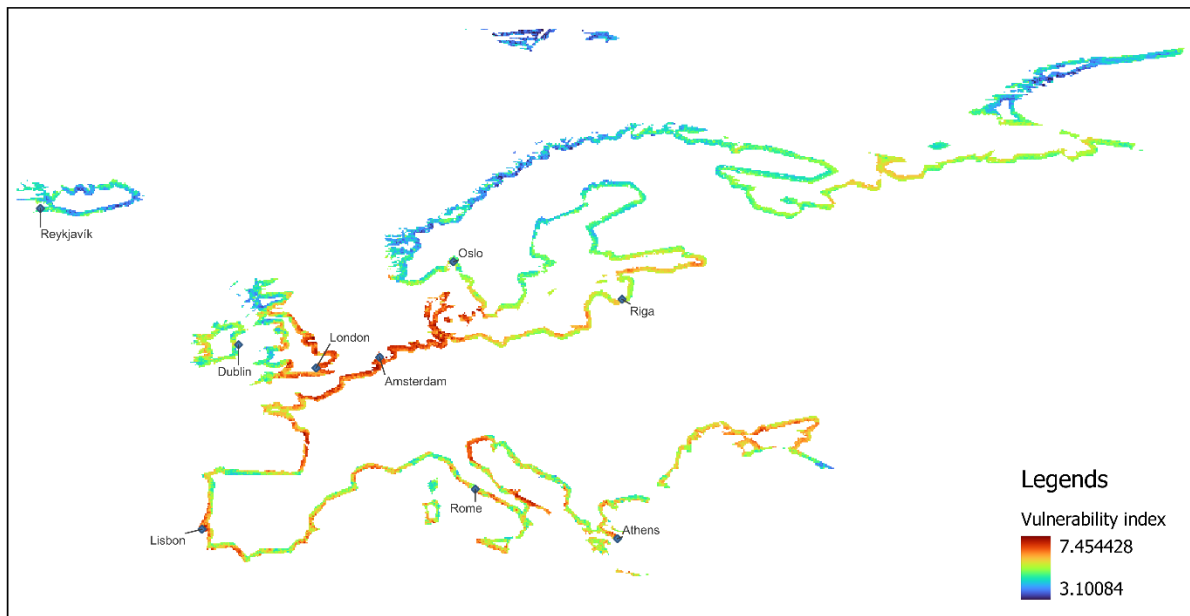*Figure 34 Vulnerability map of the Europe continent*

Figure 36 shows the vulnerability map for Europe. Some regions of the small islands in northern Europe are not showing on the map due to inconsistent data availability. Thus, the final result only shows the fully intersected area between each indicator. The vulnerability map indicates a very high vulnerability index located in the area with a high index on the four clusters result, which is located on the west of the UK, the coast of the Netherland, Germany, France, Venice, southwest of Italy, and Lisbon. On the other hand, the northern part of the Scandinavian region and some parts of Russia shows very low vulnerability due to small human interference.

4.1.5   North America

North America has various natural preconditions and human interfered environments that affect the proneness to salinization of the coastal zone. North America is located in a sub-tropical climate and the northern part of the continent is mostly ice. The result of the four indicators cluster of North America is shown in Figure 35.

   a. Aquifer properties index distribution on the continent shows a scattered distribution, where the highest index is spotted on the northern part (small islands) and the southwest coast, including the coast of Guatemala and Florida. Some region has a low index, such as the south of Alaska and the north of Canada. Other areas have moderate to high vulnerability.
   b. The land surface condition of the continent illustrates the distribution of natural land surface conditions. Similar to other continents, the index value decreases landward. 80% of the region shows a distribution from moderate to high index in the coastal zone, while the rest displays low to moderate vulnerability.
   c. The human impact index in the northern part is very low and mainly moderate to high in the continent's south. The highest human activity impact is located in big cities, such as Los Angeles, Tampa, New York, and New Jersey. Meanwhile, the coast of Mexico, Guatemala, Nicaragua, Costa Rica, and Panama shows moderate index value. However, Greenland has no human impact data since no living person naturally lives there.
   d. The index value for the climate cluster shows a low to moderate index. Some regions have a high index in the estuaries region north of the Gulf of California. It results from a high rate of the surge and the region's aridity.

These clusters are calculated all together with the cluster weight assigned in Table 4, shown in Figure 36. Due to a lack of data on the continent's northern part, the vulnerability index value in the north is low, especially on the northern islands, including Greenland. Low vulnerability is also shown in the south of Alaska, on the coast of the Gulf of Alaska. The highest vulnerability index is spotted on most of the east coast of the USA. In addition, the west coast area of the Gulf of Mexico and the northern coast of Guatemala have very high vulnerability. The Coastal zone of Cuba was also found to have a high to very high vulnerability index.
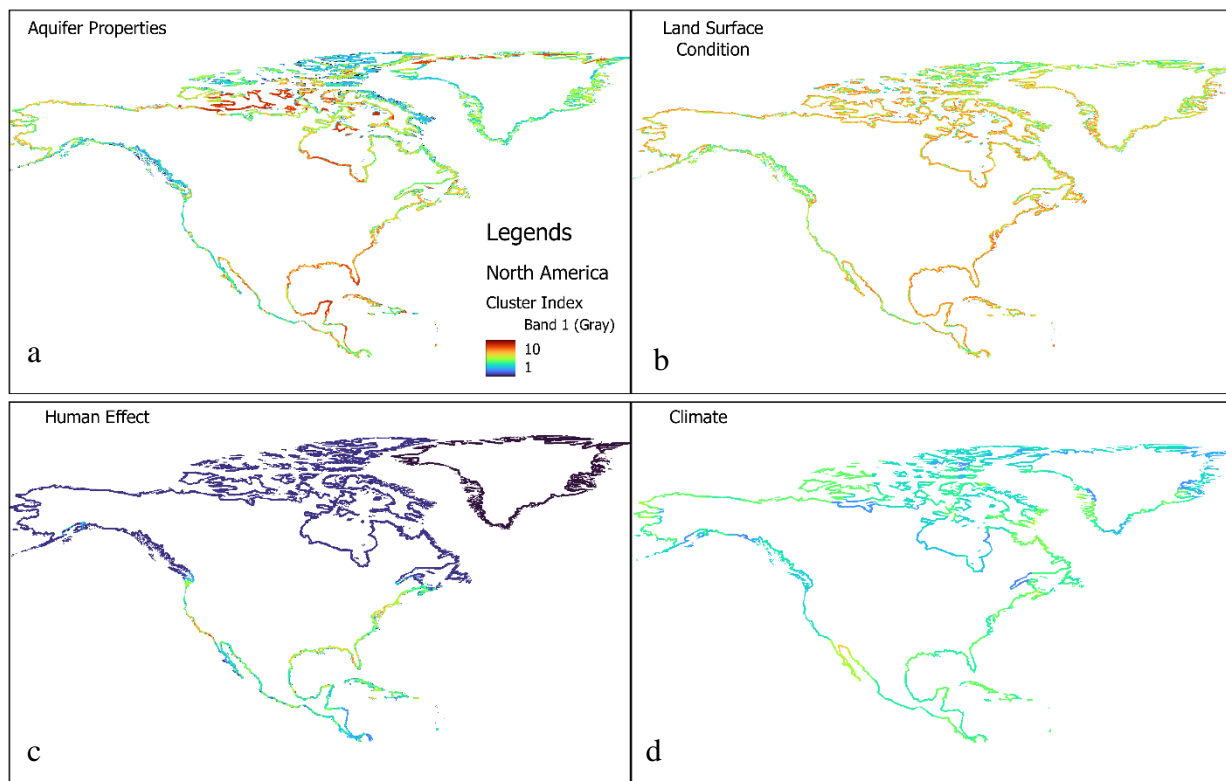

Figure 35. North America cluster (a) aquifer properties, (b) land surface condition, (c) human impact, and (d) climate index mapping
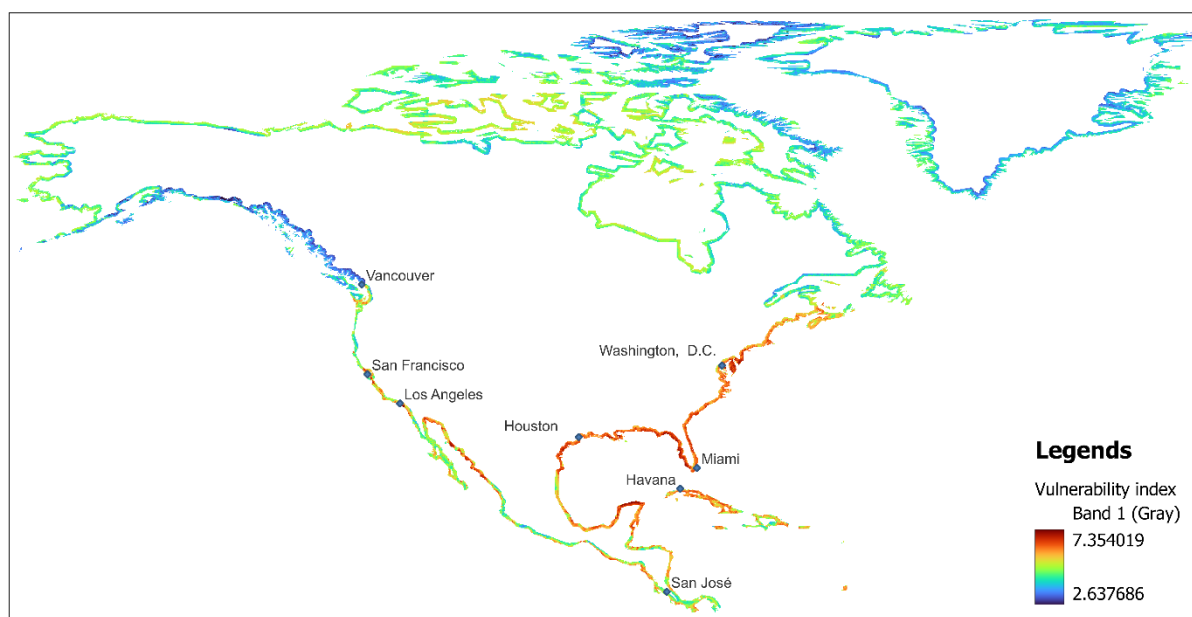
Figure 36. Vulnerability mapping of North America continent

51

4.1.6   South America

South America continent has a warmer climate than northern America. It is located on the equator down to 60 degrees longitude, which tells us that the continent has two climate types: tropical and subtropical. Urban development of the continent is fast growing and predicted to surpass other continents' growth in 2050 by 86% and most of the population lives in the big cities of South American countries (BBVA Research, 2017). The cluster mapping helps us to understand the condition of human and natural influence on the aquifer. Figure 39 describes the cluster mapping result in South America:

a. The aquifer properties index of the continents shows a dominantly high index on the northeast coast and some regions on the southeast coast. Meanwhile, the west coast is mostly low index (light blue to green). West of the mainland has a low index due to the geological condition of the region, where it's one of the collision regions, thus creating a chain of Mount Andes with low permeability rocks. Meanwhile, the east coast is presiding with a low-lying sedimentary area.

b. The mountainous condition on the west and the low-lying land on the east is reinforced based on the land surface conditions. The cluster describes the coastal zone's surface topography and geomorphology. As can be seen in the figure, the west coast has a lower index while the east coast governs with a moderate to high index due to the topographical condition of the coastal zone.

c. Human impact on the continent shows a low index all over the coastal index. Especially in the southern part of the continent shows a very low index due to very little human interference in the area. Some "hotspots" of moderate to high index are shown on the coastal megacities, such as Sao Paolo and Rio de Janeiro in Brazil and on the Buenos Aires coast.

d. The climate cluster shows almost the same behavior as aquifer properties and land surface condition clusters. The northern coast is higher than other regions, and the continent's southeast also has a higher index. The west coast has a low index value, as well as the continent's east coast.
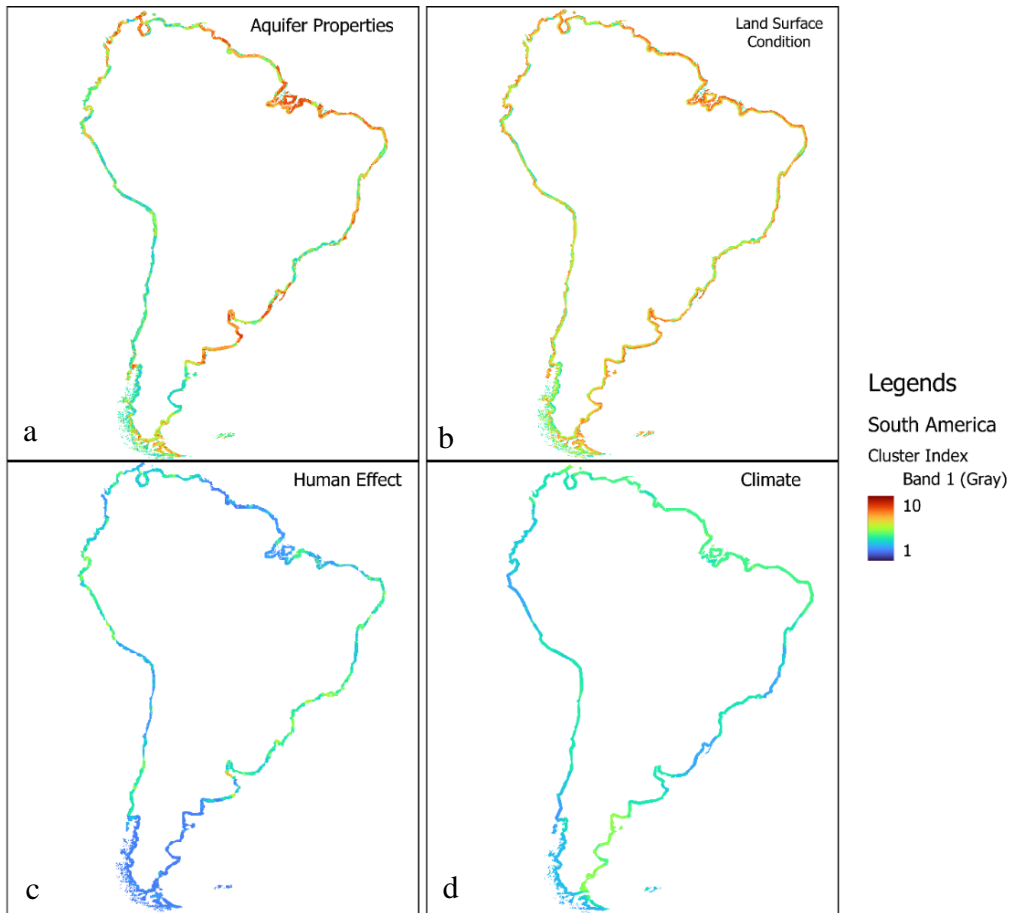
Figure 37. South America cluster (a) aquifer properties, (b) land surface condition, (c) human impact, and (d) climate index mapping

53
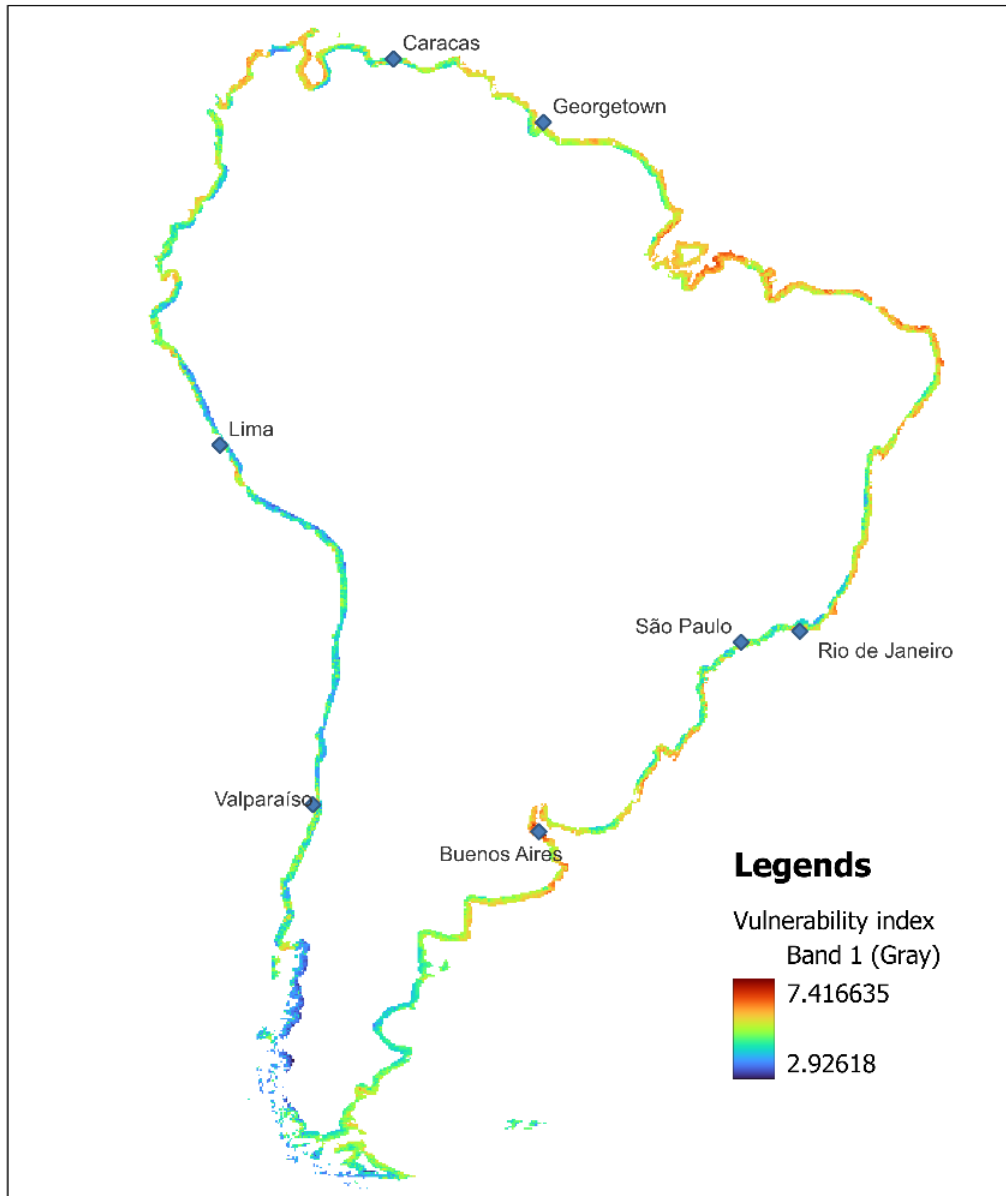
Figure 38. Vulnerability mapping of the South America continent

4.2 Global Vulnerability Mapping

The result was generated per continent. The vulnerability maps of the continents are merged to understand the distribution of vulnerability across the world. The global vulnerability results in a range between 1 through 10 scales (Appendix A. -). Then, the map was reclassified into five categories: very low, low, medium/moderate, high, and extreme vulnerability. Figure 39 shows the global distribution of the coastal zone vulnerability index, which has been reclassified into five categories. High to extreme vulnerability indexes cover around another 40% of the world. Most of the extreme vulnerability pixels are located in the densely populated region associated with cities in the coastal zones. The vulnerability index becomes very high due to the high weight and ratings assigned to aquifer properties indicators supported by the geological condition of the coastal zones that mostly consist of unconsolidated sediments and carbonate environment reinforced by the groundwater level of this region that fall below mean sea level. The high vulnerability index is spread across the globe without any special pattern. On top of that, extreme vulnerability is shown clearly in the region with high human intervention – a highly populated coastal region – located in South (India, Bangladesh, and Guyana) and

Southeast Asia (the Mekong Delta, east coast of Sumatra Island, north coast of Java Island), the eastern coast of China, Arabian Peninsula, the northern coast of Europe (Germany, the Netherlands, and French), the east coast of the UK, the Mediterranean coast, the west coast of North America, and small regions scattered on the west coast of South America (northern coast of Brazil and Buenos Aires coastal zones).

Pixels that show very low vulnerability are located in coastal zones with less human interference and highland topography. The northern part of the world is mostly designated low to medium vulnerability to salinization, which means that those areas are less prone to salinization. The low vulnerability of the region intersects with the low cluster mapping calculation, especially human activity cluster mapping. This behavior shows that human activity could significantly affect the change of groundwater, which could increase the vulnerability of the aquifer to salinization. Very low to low vulnerability areas are dominantly located in the earth's northern hemisphere, where the climate is not convenient; thus, not much population grows in the region. The low vulnerability result is also supported by the land cover of most of the region, which is permafrost, which leads to lower salinization vulnerability since ice is a freshwater source. In addition, lack of sufficient data also assists the lower result, such as groundwater abstraction with no data. Meanwhile, the southern hemisphere does not show any dominant presentation of a certain class, where there are some extreme vulnerability regions and low vulnerability, such as in the west of the southern island of New Zealand.
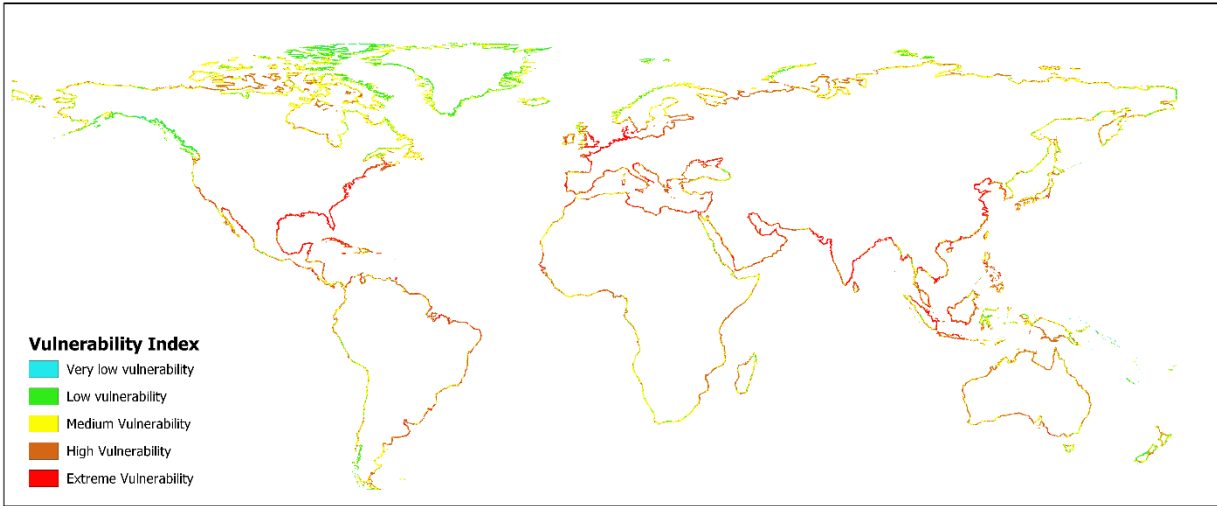
Figure 39. The world vulnerability index reclassified into 5 categories of vulnerability

4.3 Sensitivity Analysis

Sensitivity analysis is done to see how influencing the indicators is. Two types of typical sensitivity analysis were used to identify parameters sensitivity to seawater intrusion: single parameter test and map removal test.

4.3.1   Single Parameter Test

The single parameter test was done to test the sensitivity of an individual parameter to seawater intrusion. Table 5 shows the statistical distribution of the sensitivity calculation. According to the result, the type of aquifer specified as the most sensitive parameter to salinization with the highest mean value, which is 2.2%, followed by groundwater abstraction, which is 1.94%. Meanwhile, the lowest sensitivity indicator is slope with a 0.08% mean value.

Table 5 shows the statistical summary of the single-parameter test. Based on the result, the sensitivity result can be classified the indicators into three categories based on the variation of median and range of the box plot: (a) high variation, (b) medium variation, and (c) small variation (Figure 40). These variations can show us the sensitivity of the indicators to changes. A high variation plot (Figure 40a) describes the sensitivity to changes that can influence the indicators. High variation means that it is most likely to change the result when some changes are applied. The high variation group includes aquifer type, distance to the coastline, groundwater abstraction, water level, precipitation, population, and slope.

On the contrary, a small variation plot (Figure 40c) describes the sensitivity of the indicators that is unlikely to change if some changes are applied. This group has a small median value and a small range of minimum to maximum value, not more than 1%. The small variation group includes aquifer thickness, land subsidence, land cover, and potential evapotranspiration.

Table 5. Statistics measurement of weight theoretical weight (weight assigned) and effective weight.

Indicator layers	Theoretical weight (%)	Effective weight (%)				
		Mean	Median	Minimum	Maximum	SD
Aquifer thickness (m)	8.77	0.71	0.69	0.25	1.25	0.34
Type of Aquifer	5.26	2.20	2.2	1.25	3.14	0.70
Distance from the coastline (m)	7.02	1.46	1.5	0.25	2.51	0.80
Flood (dm)	3.51	1.46	1.5	0.94	1.88	0.36
Groundwater extraction rate (km³/yr)	7.02	1.94	1.88	0.94	3.14	0.80
Hydraulic conductivity (m/s)	7.02	1.15	1.19	0.38	1.88	0.49
Area of rrigated lands with groundwater (%)	3.51	1.04	0.94	0.38	1.88	0.56
Land cover	5.26	0.61	0.56	0.25	1.00	0.27
PET (mm/a)	8.77	0.63	0.63	0.25	1.00	0.29
Population density (person/km2)	7.02	1.63	1.63	0.75	2.51	0.68
Precipitation (mm/a)	3.51	1.20	1.25	0.25	2.01	0.64
Slope (%)	7.02	0.08	0.08	0.02	0.13	0.04
Sea-level rise (m)	8.77	1.05	0.94	0.31	1.88	0.64
Land Subsidence (m/year)	7.02	0.85	0.85	0.56	1.13	0.21
Tide surges (m)	5.26	1.51	1.5	0.75	2.26	0.56
Water Level (M.a.s.l.)	5.26	1.46	1.5	0.25	2.51	0.80

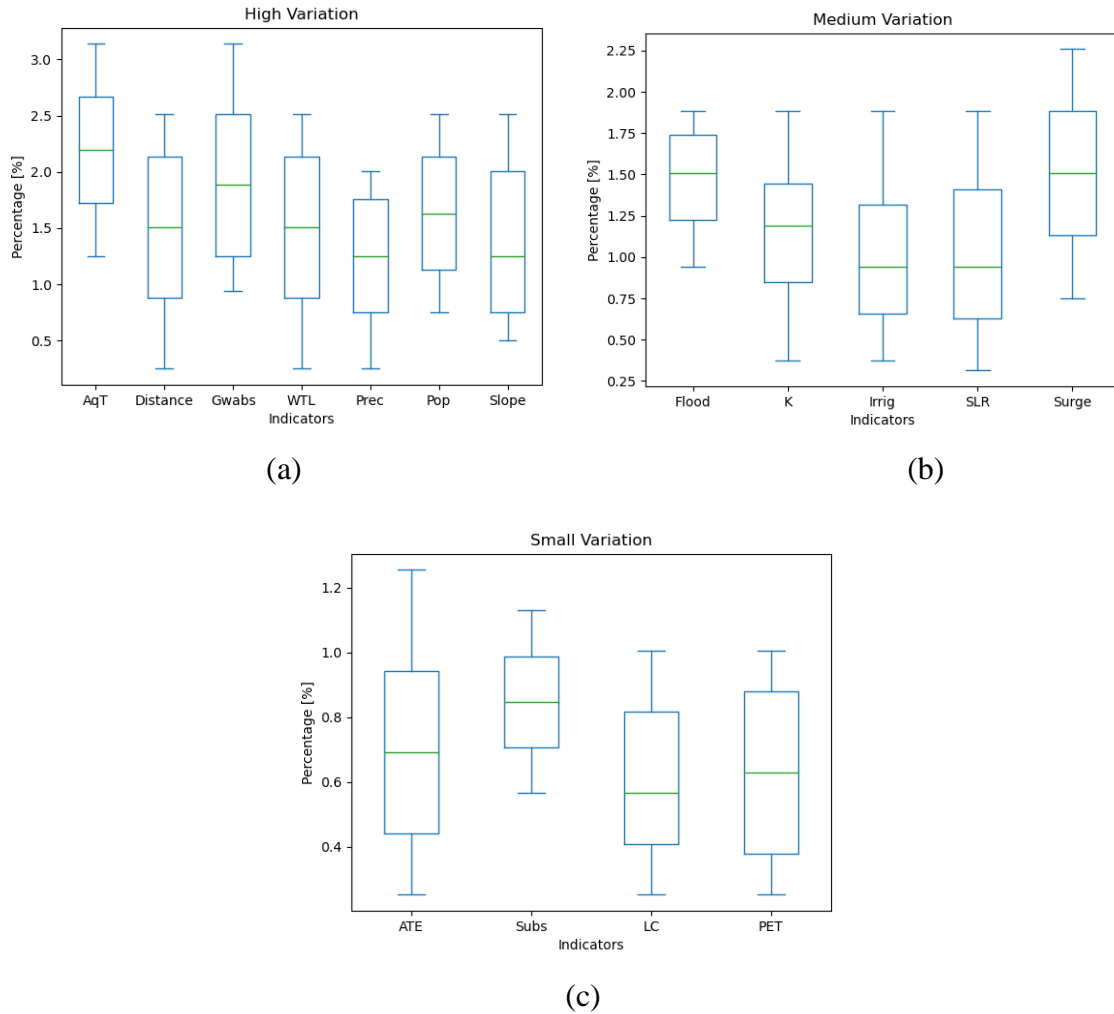(a)   (b)

(c)

Figure 40 Categorize variation of the indicator single parameter sensitivity test. AqT: aquifer type, Distance: distance from the coastline, Gwabs: groundwater abstraction, WTL: water level, Prec: precipitation, Pop: population, Slope: slope, Flood: flood, K: hydraulic conductivity, Irrig: Area of irrigated lands, SLR: sea level rise, surge: storm surges, ATE: aquifer thickness, Subs: Land subsidence, LC: land cover PET: Potential Evapotranspiration

4.3.2   Map Removal Test

4.3.2.1   Correlation Test Analysis

A correlation test was done to see the indicators' relation to the vulnerability index. The correlation test shows the connection between indicators and the significance of the indicators. Indicators whose insignificance is excluded from obtaining the map removal sensitivity test. The test was done per continent to see the relation of each indicator to the vulnerability index regionally (Table 6). Based on the result, some indicators are not significant to the vulnerability result, which is indicated by the coefficient of correlation of less than 0.1. Two dominant indicators exhibit inconsequentiality in most of the continents, which are flood and subsidence. Flood is shown to be non-significance in Australia, Oceania, Africa, North America, and South America. Subsidence is insignificant in all continents except North America. This behavior results from near-zero values in most of the coastal zones and only some pixels that exhibit a significant value of flood and land subsidence despite the higher weight assigned to the indicators. On the contrary, some indicators show a meaningful relation (>0.1) to the vulnerability index in all continents: aquifer type, hydraulic conductivity, area of irrigated lands, land cover, population density, slope, and water level. These indicators strongly relate to

the vulnerability index, evincing that they have a relatively significant influence on the mapping result.

Table 6. Correlation test between the indicators and vulnerability index

| Indicators	Australia	Oceania	Asia	Afrika	Europe	North America	South America
Aquifer thickness (m	0.10	0.15	-0.05*	0.00*	0.16	-0.07*	0.10
Type of Aquifer	0.10	0.74	0.45	0.53	0.47	0.53	0.56
Distance from the coastline (m	0.34	-0.07*	0.29	0.38	0.13	0.19	0.32
Flood (dm)	-0.01*	0.00*	0.10	0.02*	0.10	0.03*	0.03*
Groundwater extraction rate (km³/yr)	-0.10	0.34	0.57	0.38	0.55	0.62	0.06*
Hydraulic conductivity (m/s)	0.38	0.72	-0.18	0.53	-0.22	0.49	0.48
Area of irrigated lands with groundwater (%)	0.31	0.45	0.53	0.40	0.47	0.52	0.38
Land cover	-0.12	0.63	0.37	0.19	0.51	0.47	0.16
PET (mm/a)	0.26	0.72	0.50	0.03*	0.47	0.55	0.36
Population density (person/km2)	0.14	0.34	0.54	0.31	0.64	0.52	0.27
Precipitation (mm/a)	0.29	-0.07*	-0.06*	0.10	0.28	-0.22	-0.17
Slope (%)	0.61	0.84	0.49	0.61	0.44	0.50	0.75
Sea-level rise (m)	-0.01*	0.25	-0.24	0.25	0.50	0.35	0.42
Land Subsidence (m/year)	-0.03*	0.02*	0.08*	-0.07*	0.02*	0.28	-0.04*
Tide surges (m)	-0.08*	0.19	0.19	0.18	0.20	-0.05*	0.02*
Water Level (M.a.s.l.)	0.54	0.46	0.53	0.61	0.41	0.40	0.70

(*) showing the insignificance of the correlation test on the indicators

4.3.2.2 Variation analysis

Map removal test was done by omitting one or more layers of indicators from the vulnerability index mapping and seeing the variation of the change. Figure 41 illustrates the variation distribution of the sensitivity test in each continent due to removing indicators. According to the correlation test, in almost all continents, except Asia and Europe, land inundation (flood) in coastal zone shows its insignificance to vulnerability index mapping. Despite that, the map removal test shows that flood has a large variety, so there is still high uncertainty that could change the result highly. Thus, the sensitivity test shows that flood is an important indicator. Not including land subsidence from the calculation shows its insignificance in almost every continent except North America. The variation of land subsidence in every continent is different. For example, land subsidence shows a small variation in Australia, thus not creating a big change in the vulnerability. Likewise, in Europe, Oceania, Asia, and South America, omitting land subsidence results in higher vulnerability index variation. Despite the different variations, the mean and median values are around 0.4% for all continents except Asia, which is around 0.6%.

Some indicators result in a considerable variation of vulnerability, such as distance from the coastline in Oceania and land subsidence in Europe, resulting in a variation of ~0.8%. A considerable variation of sensitivity shows that removing these indicators brings about a huge change to the vulnerability index, indicating high sensitivity. However, some omitted indicators show a very small range of variation, such as land subsidence in Australia and precipitation in Oceania and Asia. The small degree of variation describes the indicators' small influence as omitted, which means that these indicators have low sensitivity to the vulnerability index, indicating that the indicators are least important in the continent.

There is a unique behavior of potential evapotranspiration (PET) plot in Africa (Figure 41c). It illustrates a very small variation but a very high sensitivity value. High sensitivity value defines the importance of the indicators that can significantly change the value of vulnerability. However, a small range of variation shows that it has a small degree of change to the value of the vulnerability index. Overall, omitting PET in Arica could change the result significantly. Moreover, North and South America continent sensitivity results show similar behavior where the indicator is removed, the changes are significant with high variation (Figure 41f & g). It means that the indicators are essential to the result and better not to be omitted since it creates a significant change to the value.
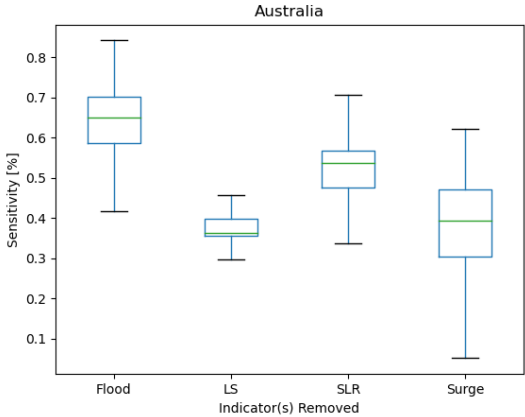
(a)
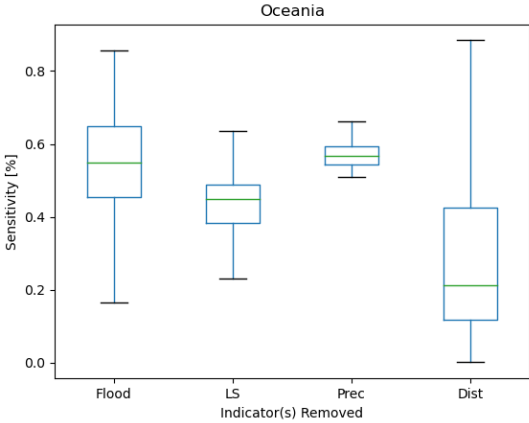
(b)
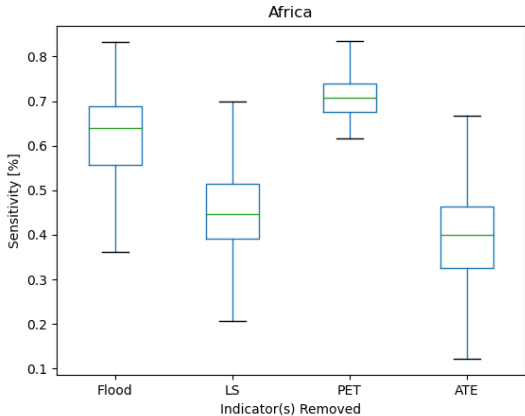
(c)

(d)

(e)

(f)

(g)

Figure 41 Map removal sensitivity test for different continent: (a) Australia, (b) Oceania, (c) Africa, (d) Asia, (e) Europe, (f) North America, and (g) South America. Distance: distance from the coastline, Gwabs: groundwater abstraction, Prec: precipitation, Flood: flood, SLR: sea level rise, surge: storm surges, ATE: aquifer thickness, LS: land subsidence.

Chapter 5   Discussion

5.1 Vulnerability Mapping

Vulnerability mapping of coastal zone prone to salinization is nowadays eagerly needed by policymakers for urban development in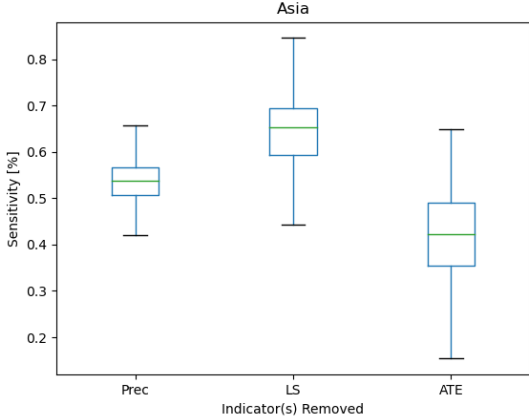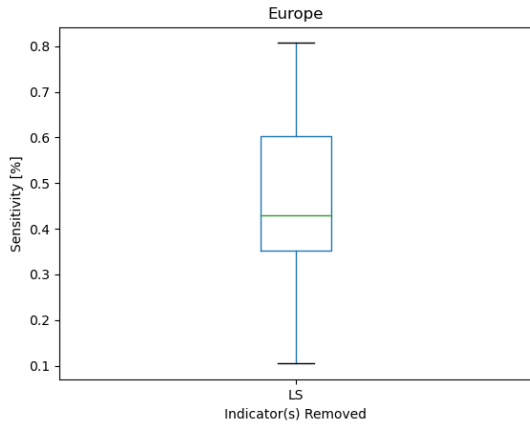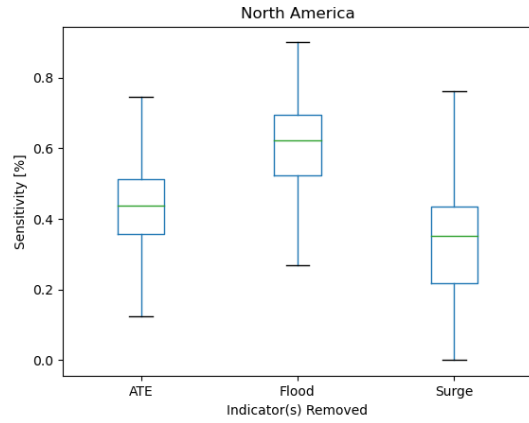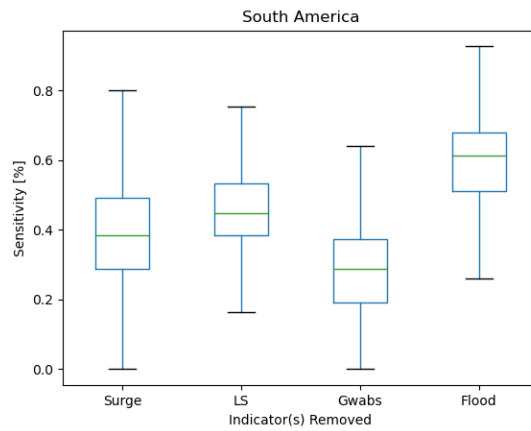 the coastal zones. In order to assess the vulnerability of the coastal zones, components of hazard and risk should also be considered. Figure 7 shows the indicators that include vulnerability, hazard, and risk used in calculating the vulnerability map. The indicators involve intrinsic and extrinsic factor parameters that could govern saltwater intrusion in the coastal zone listed in Table 1. These indicators were comprehensively used to calculate the vulnerability of coastal zone in every continent of the world. Then, continental maps are merged to see the global distribution to obtain global vulnerability. The global result is shown in Figure 39, which exemplifies the distribution of vulnerability in the coastal zone, from very low to extreme vulnerability.

An extreme vulnerability case of salinization in coastal has been found mainly in the coastal megacities and deltas, such as Jakarta and Mekong Delta, respectively (Wijaya et al., 2019; Xiao et al., 2021). Studies have found that high salinity can be caused not only due to natural phenomena (e.g., climate change) but also influenced by human interaction with the groundwater, such as well abstraction and agriculture (Baena-Ruiz et al., 2020; Hassani et al., 2021; Nicholls et al., 2007). High vulnerability pixels are generated from multiple indicators with high ratings, which multiply by their weight. Suppose we trace back the vulnerability index to reclassed pixels of the indicators (Appendix B). In that case, extreme vulnerability areas exhibit a particular pattern of aquifer properties layers, e.g., aquifer type and water level. This indicates that aquifer properties or intrinsic properties still influence the vulnerability mapping of the coastal groundwater aquifer.

On the contrary, climate shows a low impact on the result, given that there are some inconsistencies between the rating value and the result. For example, the tropical region with low precipitation and potential evapotranspiration rating results in a high vulnerability. In contrast, the arid regions with high precipitation and PET rating show a low vulnerability. But some places also show that high climate indicators rating resulting high vulnerability index, such as in the middle east region. Furthermore, indicators have different effects as we analyze each continent. The most significant effect was shown by distance from the coastline. When it was removed, it gave a high sensitivity result, which means that even though the correlation shows an insignificant result, but sensitivity test shows that it has a considerable effect on the vulnerability map. Distance from the coastline also gives a high sensitivity result for a single parameter test. This underlines the importance of the indicators.

The effect of each indicator on the vulnerability mapping is strengthened by the single parameter (Figure 40) and map removal sensitivity test (Figure 41). The single parameter test concludes that aquifer type and groundwater abstraction have the highest effect on the result, emphasizing the pixel imprint of the vulnerability map. On the contrary, the land cover does not significantly impact the result, which could be the result of the low weight assigned to it. Another sensitivity analysis was done, a map removal test, on every continent in addition to the correlation test. The result gives us a deeper understanding of the effect of indicators on vulnerability calculation.

61

Additionally, although flood has been tested to be insignificant to most of the continent's vulnerability map, the sensitivity result shows that it has a high effect on the result, so flood needs to be paid more attention to. However, the removal of land subsidence in Australia shows such low variability, which indicates that it has minimal effect on the vulnerability map. Land subsidence also shows small variability in single parameter test results showing the alignment of the result. The correlation between each cluster and the vulnerability index result shows that aquifer properties and human impact have the highest correlation with the vulnerability index, which is 65% and 68%, respectively. The climate cluster has the lowest correlation value, 27%. However, many studies show that climate could increase the vulnerability to salinization in the coastal zone. In this study, we also consider other clusters that could indirectly result in salinization. Therefore, the climate was given a relatively smaller weight than other clusters, thus providing a smaller contribution to the vulnerability map.

Table 7. Correlation of each cluster index value with vulnerability index

Cluster	P-Coefficient
Aquifer properties	0.65
Climate	0.27
Human impact	0.68
Land surface condition	0.54

Based on the vulnerability map in Chapter 4, the highest mean vulnerability index is found in Europe, followed by Asia, with 5.26 and 5.14 as the mean index, respectively. Meanwhile, the other continents have lower mean vulnerability indexes and are only located in particular areas. For example, on the North America continent, the highest vulnerability is concentrated on the eastern coast of the USA. In South America, Australia, Oceania, and Africa the most heightened vulnerability is scattered in different cities.

Most of the extreme vulnerability in Europe is located on the coast of western Europe, including the Netherlands, Germany, France, and southwestern England. Europe has a highly irregular coastline shape, resulting in a very long coastal zone per unit surface area (Custodio, 2010). Due to concentrated human activities along the coastline, the European coast has suffered significant human alteration, such as lowland reclamation. With the population growth on the European coasts, more problems related to groundwater salinization are surfacing. Moreover, a prominent carbonate aquifer along the southwest of England, northern France, and the Mediterranean coast increases the coastal vulnerability to salinization (Chen et al., 2017; Custodio, 2010). The coasts of the Netherlands and north Germany mostly reside of coastal flatlands with sandy sediments, resulting in higher vulnerability to salinization due to aquifers filled with saltwater bodies (Custodio, 2010). Moreover, coastal development for human habitation led to land subsidence and groundwater abstraction along the coast. Intensified climate change effect in Europe also brings more enhancing vulnerability along the coast. Due to climate change, sea level rise is the highest threat to Europe's coastal zone, where it is estimated to rise 2 – 4 times over the century, and more frequent storm surges will occur (Nicholls & Klein, 2005).

High to extreme vulnerability in Asia is concentrated in low-lying areas, mostly in deltaic morphology due to its susceptibility to climate change, especially sea level rise and human modification that stressed the delta plain. East, South, and Southeast Asia coastal plains (incl. deltaic plains) are notoriously known for their dense population. Hence, many people are prone to disaster risk, such as flood and storm surges, which will composite the impact of climate

change (Nicholls et al., 2007). The largest population delta in Asia is located in Ganges-Brahmaputra Delta on Guyana and Bangladesh coast. It is projected that in 2050 there will be more than 1 million people will be affected by the climate change effect in three mega deltas, following the Mekong delta (Vietnam) and Nile delta (Egypt) (Nicholls et al., 2007). Urban settlement on the coast of India resulting a high number of people living on the coast, approximately 14.1% of India's population, especially in Mumbai and Chennai. India, Pakistan, and Bangladesh are threatened by the projected sea level rise and increase in cyclonic activity due to global warming (Khaleel, 2021). This condition exacerbates the vulnerability of the coastal zone to salinization in South Asia. The situation of Sri Lanka is worse, where almost 80% of the coastal are extremely vulnerable to salinization. A local report shows that most urban and industrial developments are focused on the coastal zones. The observed SLR rate of 3.1 mm/year and the likelihood of gaining high precipitation induced permanent flooding (predicted to cover nearly 25,000 ha of land) and cyclonic storms resulting in the high vulnerability of the island (DMC, 2022). SLR and agriculture activities are proven to trigger coastal salinization expansion inland. Furthermore, Southeast Asia's coastline is one of the most dynamic links in the world, where it shelters an extensive amount of the world's population. A recent study shows that Southeast Asia coastlines are vulnerable to climate change and salinization, including the Philippines regions, the Mekong delta in Vietnam, some parts of Cambodia, North and East of Laos, Bangkok in Thailand, and West and South Sumatra in Indonesia (Noor & Abdul Maulud, 2022).

Furthermore, the result also shows an effect of human activity. Due to human activity in the coastal zone, the coastal systems become more vulnerable to natural disasters, such as reduced coastal slope due to human interventions in infrastructure development along the coastal zones (Noor & Abdul Maulud, 2022). In this study, extreme vulnerabilities pixels are mostly found in coastal zones with high population density, such as Kolkata, Mumbai, Ho Chi Minh City, Doha, Dubai, Naples, Jakarta, Amsterdam, Dakar, New York, Buenos Aires, and many more. It amplifies with irrigated agricultural areas starting to occupy near and along the coastal zones, using groundwater as their primary water source (Minderhoud et al., 2017; Wada et al., 2014). Groundwater extraction for human uses has been a problem for decades worldwide. If this condition is continuously happening, it could disturb the equilibrium of the fresh and salt groundwater interface. The non-equilibrium could substantially enhance the vulnerability of salinization in the coastal zone.

5.2 Map Validation

Map validation is important to evaluate its effectiveness and accuracy for vulnerability assessment. One method for map confirmation is applying qualitative parameters and defining the correlation between qualitative and/or quantitative parameters and the vulnerability index (Kirlas et al., 2022). One of the parameters we used for validation is electrical conductance data composed by Thorslund & van Vliet, 2020 which contains salinization data in most of the prone regions in the world, e.g., Australia, as illustrated in Figure 13. To evaluate the data, a computation R^2 value between groundwater EC and vulnerability index was. The validation process using EC value was done in an area with representative data and reports to validate. For example, Australia, Bangladesh, and the USA coast. However, the EC data did not cover all regions of the world. Thus, other sources were used, such as reports, journals, and the existing salinity model.

Several cities were validated based on previous studies that show cities and deltas with high vulnerability to salinization (Barlow & Reichard, 2010; Bocanegra et al., 2010; Gurmessa et al., 2022; Morgan & Werner, 2015; Nicholls & Klein, 2005; Noor & Abdul Maulud, 2022; Wetzelhuetter, 2013). These cities were exposed to salinity mostly due to climate change affecting urbanization. Figure 42 illustrates the relationship between the vulnerability index in

several coastal megacities with groundwater electrical conductivity data. The regression test result shows 46%, which indicates that the vulnerability index to salinization is in accordance with the fact on the field.

Furthermore, the validation is also done by calculating the natural condition (without human alteration) of saltwater wedge toe (L) using the equation explained in chapter 3.2.6. According to the result in Table 8, coastal cities with high vulnerability index show a significant inland (L) calculated in regions with high vulnerability index. It shows that some regions are showing discrepancies. For example, in Perth, the vulnerability map shows extreme vulnerability, but L value indicates a very small value, 1.28 m inland. This discrepancy shows that the formula did not consider human influence enough to show the saltwater wedge in the real condition as the region has sufficient recharge and such a compact rock formation on the surface that water will not easily pass through. However, the overall result shows a considerable impact of saltwater wedge toe in natural conditions juxtaposed with the vulnerability class.

Table 8. Saltwater wedge toe measurement results in several cities

| Location	Saltwater wedge toe L (m)	Vulnerability class
Bur Said	19.66	Moderate - High
Cape town	1.42	Low - Moderate
Portland	2.48	Low - Moderate
Adelaide	1599.74	High - Extreme
Perth	1.28	High - Extreme
Lagos	637.70	High - Extreme
Dakar	747.42	High - Extreme
Alicante	136.63	High - Extreme
Tel Aviv	142.90	High - Extreme
Washington DC	109.86	High - Extreme
Belem	6.00	High - Extreme
Buenos Aires	16.14	High - Extreme
Port MacDonnell	98.30	Extreme
Amsterdam	66.60	Extreme
Po delta, Italy	113.04	Extreme
Puducherry	144.69	Extreme
Tianjin	112.79	Extreme
Jacksonville	11.97	Extreme
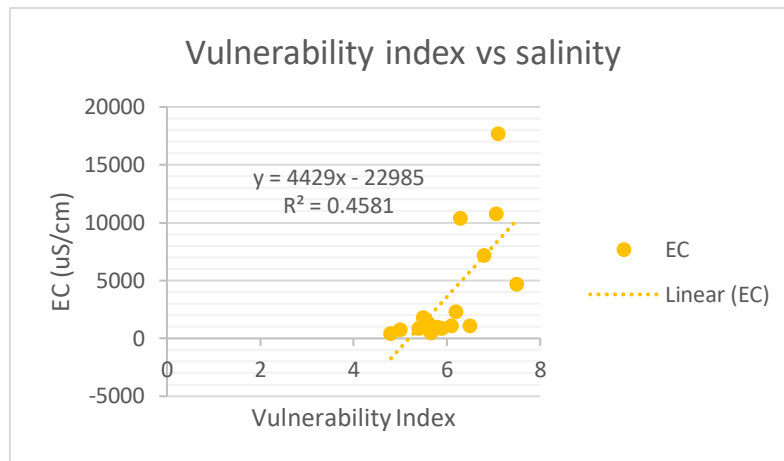
Figure 42. Regression chart between vulnerability index and electrical conductivity (EC)

5.3 Recommendation of Mitigation

As figured that most high to extreme vulnerability is influenced by both natural and artificial caused by human activities. High vulnerability to salinization is located in densely populated coastal zones combined with the supportive condition of aquifer properties (e.g., carbonate formation). Thus, a holistic measure is needed to reduce the effect of coastal salinization. Integrated mentioned refers to the integration of solution that includes all relevant objectives, instruments, policy areas and sectors, disciplines, and terrestrial and marine components. An integrated solution was introduced in 1992 by John Clark in his technical paper about Integrated Coastal Zone Management (ICZM). ICZM is well known for its sustainable approach to overcoming coastal issues with an ecosystem perspective, so not only a single case is addressed but also a compilation of multiple elements that interact with each other. This method includes shot-, mid-, and long-term solutions to reduce the degradation of coastal zone ecosystems and resources. Furthermore, it is a hands-on policy that could also handle resource-use issues to balance short-term economic development and long-term environmental interests (Clark, 1992; Nicholls & Klein, 2005).

Since coastal zones are dynamically evolving, natural, and socio-economically, ICZM must be implemented as a cycle process. It should involve several aspects, e.g., initiation, planning, implementation, and monitoring and evaluation, both on local and national scales. Some actions can be taken to start implementation: protecting people and assets, enhancing sustainability and ecosystem services, economic development, raising awareness, and governance (Dronkers, 2022). Some experts suggest that the program can only run appropriately if the cycle is applied for 5 to 10 years. However, many governments have tried to apply ICZM in their countries, but only a few have successfully run the program comprehensively, including the US and Sri Lanka. Nowadays, many other countries have tried to partially apply ICZM to manage coastal zones, such as Australia, the Philippines, etc. Moreover, European Union is exploring ICZM implementation in several coastal zones in different countries, such as the Baltic Seas. Applying ICZM can only succeed if stakeholders and society are involved in facilitating the management and planning.

Southeast Asia countries are also implementing coastal zone management performed by a government agency and private companies for a complete result without compromising the environment and preparedness for any disaster. Coastal zone management has been implemented in countries known for their coastal degradation, such as Vietnam, Indonesia, Malaysia, Myanmar, and East Timor (Noor & Abdul Maulud, 2022). However, some improvements are still needed in preparation for disaster. Some actions taken for the coastal management are organizing a training program and making a checkpoint post related to the

beach management to ensure that all the management components are always ready (Noor & Abdul Maulud, 2022).

Some technical measures are essential to mitigate saltwater intrusion in the coastal zone, including modifying pumping scheme, artificial recharge, extraction barrier, injection barrier, subsurface, and physical barrier (Javadi et al., 2022; Todd & Mays, 2005). The Netherlands is one of the countries that have superior methods to overcome saltwater intrusion in groundwater. One of the well-known methods that the government proposed is a managed aquifer recharge (MAR) application for drinking water supply by making sand dunes with embedded injected wells to refreshened saltwater in the aquifer (Sprenger et al., 2017; Stuyfzand & van der Schans, 2018). MAR technique to replenish saltwater from aquifers, especially the aquifer storage recovery (ASR) method with injected well, has been applied in different countries all over the world. The subsurface barrier is associated with a hydraulic barrier, especially a negative hydraulic barrier, where it can intercept the saltwater flow by pumping well located by the shoreline with a maintained low head (Pool & Carrera, 2010). Although this method has not been applied in real-world cases, the numerical model showed that this method could be effective in the early stages. The most invasive method to control saltwater intrusion is the physical barrier, e.g., subsurface dam, cut-off wall, and fully penetrating barrier, which requires an ecosystem alteration (Wu et al., 2020).

Chapter 6   Conclusion & Recommendation

Sea water intrusion is an occurring and unavoidable event along the coastal zone even without human intervention. Sea water intrusion is worsened by human activity along the coastline, e.g., groundwater extraction for daily life use or recreation. This study examined the vulnerability of groundwater aquifers in the coastal zone using a weighting and ranking method of several different indicators and complimented with the expression explained in *Equation 3.2—3*. The global vulnerability to salinization map in Figure 39 shows that 40% of the world has extreme vulnerability, indicating that those coastal zones need more attention to address some emerging issues. Most of the extreme vulnerability coastal zones are in the northern coast of Europe, South and Southeast Asia, and the west coast of the US. However, the lowest vulnerability is located in the northern hemisphere of the world, namely Greenland, Scandinavian land, and the northern coast of Russia.

Based on the result, human population and urban development of coastal zone significantly affect coastal vulnerability. This is emphasized by the sensitivity test showing that the groundwater abstraction indicator has the biggest influence on the vulnerability map. In addition to that, aquifer type and distance from the coastline are also governing indicators in deciding the vulnerability of a coastal zone. On the contrary, land subsidence and land cover show the lowest vulnerability map effect. Moreover, the correlation between each cluster with the vulnerability index shows that human impact has the highest impact, followed by aquifer properties. The validation result, it shows that regions with a high vulnerability index already exhibit a further inland saltwater wedge toe in natural conditions.

Consequently, a comprehensive integrated solution is needed to mitigate the saltwater intrusion in the coastal zone. Some countries have tried applying an integrated solution called Integrated Coastal Zone Management (ICZM) because of its holistic approach. Although this method seems to be a dream solution, due to its complexity many countries have not made to finish the program. Instead, engineers propose a partial solution, such as policy-making and technical measures, to create a faster measure. Applying these partial solutions, individually or in combination, could significantly decrease the damage that saltwater intrusion resulting in the aquifer, rather than not doing anything. In short, an integrated measure needs to be applied to reduce the damage from saltwater intrusion. Although technical action is efficient, a policy is still required in order to control the technicality of the measures employed.

During the work of this thesis project some roadblocks are encountered, such as storage limitation and the quality of global data. Therefore, to create higher resolution of the map, a super-computer is needed to handle the large data database. Moreover, numerical modeling is suggested to establish a better understanding of a coastal zone's vulnerability. This numerical model can be done in several places on the world to investigate the condition of groundwater flow and interface equilibrium.

References

Adger, W. N. (2001). Scales of governance and environmental justice for adaptation and mitigation of climate change. *Journal of International Development*, *13*(7), 921–931. https://doi.org/10.1002/jid.833

ADRC. (2005). *Total Disaster Risk Management-Good Practices-Masayuki Kitamoto*.

Alfarrah, N., & Walraevens, K. (2018). Groundwater overexploitation and seawater intrusion in coastal areas of arid and semi-arid regions. *Water (Switzerland)*, *10*(2). https://doi.org/10.3390/w10020143

Allouche, N., Maanan, M., Gontara, M., Rollo, N., Jmal, I., & Bouri, S. (2017). *A global risk approach to assessing groundwater vulnerability*. https://doi.org/10.1016/j.envsoft.2016.11.023

Almar, R., Ranasinghe, R., J Bergsma, E. W., Diaz, H., Melet, A., Papa, F., Vousdoukas, M., Athanasiou, P., Dada, O., Pedro Almeida, L., & Kestenare, E. (2021). A global analysis of extreme coastal water levels with implications for potential coastal overtopping. *Nature Communications*. https://doi.org/10.1038/s41467-021-24008-9

Amatulli, G., Domisch, S., Tuanmu, M.-N., Parmentier, B., Ranipeta, A., Malczyk, J., & Jetz, W. (2018). A suite of global, cross-scale topographic variables for environmental and biodiversity modeling. *Scientific Data*, *5*(1), 180040. https://doi.org/10.1038/sdata.2018.40

ArcGIS. (2022, June 18). *How inverse distance weighted interpolation works*. https://pro.arcgis.com/en/pro-app/latest/help/analysis/geostatistical-analyst/how-inverse-distance-weighted-interpolation-works.htm

Babiker, I. S., Mohamed, M. A. A., Hiyama, T., & Kato, K. (2005). A GIS-based DRASTIC model for assessing aquifer vulnerability in Kakamigahara Heights, Gifu Prefecture, central Japan. *Science of the Total Environment*, *345*(1–3), 127–140. https://doi.org/10.1016/j.scitotenv.2004.11.005

Baena-Ruiz, L., Pulido-Velazquez, D., Collados-Lara, A.-J., Renau-Pruñonosa, A., Morell, I., & Es, M. (2018). *Global Assessment of Seawater Intrusion Problems (Status and Vulnerability)*. https://doi.org/10.1007/s11269-018-1952-2

Baena-Ruiz, L., Pulido-Velazquez, D., Collados-Lara, A.-J., Renau-Pruñonosa, A., Morell, I., Senent-Aparicio, J., & Llopis-Albert, C. (2020). Summarizing the impacts of future potential global change scenarios on seawater intrusion at the aquifer scale. *Environmental Earth Sciences*, *79*, 99. https://doi.org/10.1007/s12665-020-8847-2

Barik, K. K., Panda, S. R., Nanda, S., Tripathy, J. K., Chhotaray, P. K., Annadurai, R., Mishra, S. P., & Mitra, D. (2021). GIS based saltwater vulnerability mapping of the northern coast of Odisha, East coast of India. *Arabian Journal of Geosciences*, *14*(14). https://doi.org/10.1007/s12517-021-07800-1

Barlow, P. M. (2003). *Ground Water in Freshwater-Saltwater Environments of the Atlantic Coast*. http://www.usgs.gov/

Barlow, P. M., & Reichard, E. G. (2010). Saltwater intrusion in coastal regions of North America. *Hydrogeology Journal*, *18*(1), 247–260. https://doi.org/10.1007/s10040-009-0514-3

BBVA Research. (2017). *Urbanization in Latin America*.

Bocanegra, E., da Silva, G. C., Custodio, E., Manzano, M., & Montenegro, S. (2010). State of knowledge of coastal aquifer management in South America. *Hydrogeology Journal*, *18*(1), 261–267. https://doi.org/10.1007/s10040-009-0520-5

Brindha, K., & Schneider, M. (2019). Impact of Urbanization on Groundwater Quality. In *GIS and Geostatistical Techniques for Groundwater Science* (pp. 179–196). Elsevier. https://doi.org/10.1016/B978-0-12-815413-7.00013-4

Buchhorn, M., Bruno, S., Bartels, L., de Roo, B., Lesiv, M., Tsendbazar, N., Li, L., & Tarko, A. (2020). *Copernicus Global Land Service: Land Cover 100m: Version 3 Globe 2015-2019: Product User Manual*. https://doi.org/10.5281/zenodo.3938963

Cao, T., Han, D., & Song, X. (2021). Past, present, and future of global seawater intrusion research: A bibliometric analysis. In *Journal of Hydrology* (Vol. 603). Elsevier B.V. https://doi.org/10.1016/j.jhydrol.2021.126844

Chachadi, A. G., & Lobo-Ferreira, P. L. (2007). Assessing aquifer vulnerability to sea-water intrusion using GALDIT method: Part 2-GALDIT Indicators Description. *The 4th Inter-Celtic Colloqoium on Hydrology and Management of Water Resources*.

Chang, S. W., Chung, I. M., Kim, M. G., Tolera, M., & Koh, G. W. (2019). Application of GALDIT in assessing the seawater intrusion vulnerability of Jeju Island, South Korea. *Water (Switzerland)*, *11*(9). https://doi.org/10.3390/w11091824

Chang, S. W., Chung, I. M., Kim, M. G., & Yifru, B. A. (2020). Vulnerability assessment considering impact of future groundwater exploitation on coastal groundwater resources in northeastern Jeju Island, South Korea. *Environmental Earth Sciences*, *79*(22). https://doi.org/10.1007/s12665-020-09254-2

Chen, Z., Auler, A. S., Bakalowicz, M., Drew, D., Griger, F., Hartmann, J., Jiang, G., Moosdorf, N., Richts, A., Stevanovic, Z., Veni, G., & Goldscheider, N. (2017). *The World Karst Aquifer Mapping project: concept, mapping procedure and map of Europe*. *25*, 771–785. https://doi.org/10.1007/s10040-016-1519-3

CIESIN. (2007). *Asia Climate Zone*.

Clark, J. R. (1992). Integrated management of coastal zones. *FAO Fisheries Technical Paper*.

Costall, A. R., Harris, B. D., Teo, B., Schaa, R., Wagner, M., & Pigois, J. P. (2020). Groundwater Throughflow and Seawater Intrusion in High Quality Coastal Aquifers. *Scientific Reports*. https://doi.org/10.1038/s41598-020-66516-6

Custodio, E. (2010). Coastal aquifers of Europe: an overview. *Hydrogeology Journal*, *18*(1), 269–280. https://doi.org/10.1007/s10040-009-0496-1

Damayanti, A. D., & Notodarmodjo, S. (2021). Metode G-ALDIT dan G-ALDITLcR untuk Evaluasi Kerentanan Air Tanah Dangkal Akibat Pengaruh Intrusi Air Laut (Studi Kasus: Air Tanah Dangkal Kawasan Pesisir Bagian Utara dan Selatan Kota Makassar). *Journal of Environment and Geological Hazard*, *12*(2), 107–123. http://jlbg.geologi.esdm.go.id/index.php/jlbg

de Graaf, I. E. M., Sutanudjaja, E. H., van Beek, L. P. H., & Bierkens, M. F. P. (2015). A high-resolution global-scale groundwater model. *Hydrology and Earth System Sciences*, *19*(2), 823–837. https://doi.org/10.5194/hess-19-823-2015

Deltares. (2017). *On fresh-saline groundwater in coastal zones*.

Disaster Management Centre (DMC). (2022). *Hazard Profiles of Sri Lanka*. http://www.dmc.gov.lk/hazard/hazard/Report.html

Dronkers, J. (2022, August 16). *Integrated Coastal Zone Management (ICZM)*. http://www.coastalwiki.org/wiki/Integrated_Coastal_Zone_Management_(ICZM)#ICZM_implementation

Elçi, A., & Polat, R. (2011). Assessment of the statistical significance of seasonal groundwater quality change in a karstic aquifer system near Izmir-Turkey. *Environmental Monitoring and Assessment*, *172*(1–4), 445–462. https://doi.org/10.1007/s10661-010-1346-2

Erkens, G., & Sutanudjaja, E. H. (2015). Towards a global land subsidence map. *Proceedings of the International Association of Hydrological Sciences*, *372*, 83–87. https://doi.org/10.5194/piahs-372-83-2015

Fan, Y., Li, H., & Miguez-Macho, G. (2013). Global Patterns of Groundwater Table Depth. *Science*, *339*(6122), 940–943. https://doi.org/10.1126/science.1229881

Fatema, S. (2019). *Vulnerability assessment of the coastal aquifers in the Cox's Bazar area, Bangladesh using hydrochemical tools and the GALDIT model*. https://creativecommons.org/licenses/

Freeze, R., & Cherry, J. A. (1979). *GROUNDWATER* (C. Brenn & K. McNeily, Eds.). Prentice-Hall, Inc.

Gleeson, T., Moosdorf, N., Hartmann, J., & van Beek, L. P. H. (2014). A glimpse beneath earth's surface: GLobal HYdrogeology MaPS (GLHYMPS) of permeability and porosity. *Geophysical Research Letters*, *41*(11), 3891–3898. https://doi.org/10.1002/2014GL059856

Gleeson, T., Smith, L., Moosdorf, N., Hartmann, J., Dürr, H. H., Manning, A. H., van Beek, L. P. H., & Jellinek, A. M. (2011). Mapping permeability over the surface of the Earth. *Geophysical Research Letters*, *38*(2). https://doi.org/10.1029/2010GL045565

Groen, J. (2002). *The Effects of Transgressions and Regressions on Coastal and Offshore Groundwater. A case study of Suriname and generic studies into groundwater flow systems, salinity patterns and paleo-groundwater*.

Gurmessa, S. K., MacAllister, D. J., White, D., Ourdraog, I., Lapworth, D., & MacDonald, A. (2022). Assessing groundwater salinity across Africa. *Science of the Total Environment*, *828*. https://doi.org/10.1016/j.scitotenv.2022.154283

Gutiérrez, J. M. , Jones, R. G., Narisma, G. T., Alves, L. M., Amjad, M., Gorodetskaya, I. V., Grose, M., Klutse, N. A. B., Krakovska, S., Li, . J., Martínez-Castro, D., Mearns, L. O., Mernild, S. H., Ngo-Duc, T., van den Hurk, B., & Yoon, J.-H. (2021). *In Climate Change 2021: The Physical Science Basis. Contribution of Working Group I to the Sixth Assessment Report of the Intergovernmental Panel on Climate Change*. Cambridge University Press; Cambridge University Press. http://interactive-atlas.ipcc.ch/

Haitjema, H. M., & Mitchell-Bruker, S. (2005). Are Water Tables a Subdued Replica of the Topography? *Ground Water*, *0*(0). https://doi.org/10.1111/j.1745-6584.2005.00090.x

Hassani, A., Azapagic, A., & Shokri, N. (2021). Global predictions of primary soil salinization under changing climate in the 21st century. *Nature Communications*, *12*(1), 6663. https://doi.org/10.1038/s41467-021-26907-3

Hendrikx, T. (n.d.). *MSc internship: Numerical computation of the influence of water management on land subsidence and saltwater intrusion in deltas using iMOD-WQ-SUBCR*.

Huscroft, J., Gleeson, T., Hartmann, J., & Börker, J. (2018). Compiling and Mapping Global Permeability of the Unconsolidated and Consolidated Earth: GLobal HYdrogeology MaPS 2.0 (GLHYMPS 2.0). *Geophysical Research Letters*, *45*(4), 1897–1904. https://doi.org/10.1002/2017GL075860

IPCC. (2021). *Summary for Policy Makers in: Climate Change 2021: The Physical Science Basis. The Sixth Assessment Report of the IPCC*.

Ivkovic, K. M., Marshall, S., Morgan, L., Werner, A., Carey, H., Cook, S., Sundaram, B., Norman, R., Wallace, L., Caruana, L., Dixon-Jain, P., & Simon, D. (2012). *National-scale vulnerability assessment of seawater intrusion: Summary report*.

Jakovovic, D., Werner, A. D., de Louw, P. G. B., Post, V. E. A., & Morgan, L. K. (2016). Saltwater upconing zone of influence. *Advances in Water Resources*, *94*, 75–86. https://doi.org/10.1016/j.advwatres.2016.05.003

Javadi, S., Kardan Moghaddam, H., & Neshat, A. (2022). A new approach for vulnerability assessment of coastal aquifers using combined index. *Geocarto International*, *37*(6), 1681–1703. https://doi.org/10.1080/10106049.2020.1797185

Javadi, S., Kavehkar, N., Mohammadi, K., Khodadadi, A., & Kahawita, R. (2011). Calibrating DRASTIC using field measurements, sensitivity analysis and statistical methods to assess groundwater vulnerability. *Water International*, *36*(6), 719–732. https://doi.org/10.1080/02508060.2011.610921

Khaleel, Z. (2021). *South Asian Seas Programme (SASP)*.

Kirlas, M. C., Karpouzos, · D K, Georgiou, · P E, & Katsifarakis, · K L. (2022). A comparative study of groundwater vulnerability methods in a porous aquifer in Greece. *Applied Water Science*, *12*, 123. https://doi.org/10.1007/s13201-022-01651-1

Kooi, H., Groen, J., & Leijnse, A. (2000). Modes of seawater intrusion during transgressions. *Water Resources Research*, *36*(12), 3581–3589. https://doi.org/10.1029/2000WR900243

Lobo-Ferreira, J. P., Chachadi, A. G., Diamantino, C., & Henriques, M. J. (2005). *Assessing aquifer vulnerability to seawater intrusion using the GALDIT method: part 1-application to the Portuguese Monte Gordo aquifer* (Vol. 310). IAHS Publ. http://www.teriin.org/teri-wr/coastin/newslett/-

Luo, T., Winsemius, H., & Ward, P. (2015). *Aqueduct Global Flood Risk Maps*. https://www.wri.org/data/aqueduct-global-flood-risk-maps

Luoma, S., Okkonen, J., & Korkka-Niemi, K. (2017). Comparison of the AVI, modified SINTACS and GALDITvulnerability methods under future climate-change scenariosfor

a shallow low-lying coastal aquifer in southern Finland. *Hydrogeology Journal*, *25*(1), 203–222. https://doi.org/10.1007/s10040-016-1471-2

Michael, H. A., Russoniello, C. J., & Byron, L. A. (2013). Global assessment of vulnerability to sea-level rise in topography-limited and recharge-limited coastal groundwater systems. *Water Resources Research*, *49*(4), 2228–2240. https://doi.org/10.1002/wrcr.20213

Minderhoud, P. S. J., Erkens, G., Pham, V. H., Bui, V. T., Erban, L., Kooi, H., & Stouthamer, E. (2017). Impacts of 25 years of groundwater extraction on subsidence in the Mekong delta, Vietnam. *Environmental Research Letters*, *12*(6). https://doi.org/10.1088/1748-9326/aa7146

Mirzavand, M., Ghasemieh, · H, Sadatinejad, · S J, & Bagheri, · R. (2020). An overview on source, mechanism and investigation approaches in groundwater salinization studies. *International Journal of Environmental Science and Technology*, *17*(3), 2463–2476. https://doi.org/10.1007/s13762-020-02647-7

Moeck, C., Grech-Cumbo, N., Podgorski, J., Bretzler, A., Gurdak, J. J., Berg, M., & Schirmer, M. (2020). A global-scale dataset of direct natural groundwater recharge rates: A review of variables, processes and relationships. *Science of the Total Environment*, *717*. https://doi.org/10.1016/j.scitotenv.2020.137042

Moghaddam, H. K., Jafari, F., & Javadi, S. (2017). Vulnerability evaluation of a coastal aquifer via GALDIT model and comparison with DRASTIC index using quality parameters. *Hydrological Sciences Journal*, *62*(1), 137–146. https://doi.org/10.1080/02626667.2015.1080827

Morgan, L. K., & Werner, A. D. (2015). A national inventory of seawater intrusion vulnerability for Australia. *Journal of Hydrology: Regional Studies*, *4*, 686–698. https://doi.org/10.1016/j.ejrh.2015.10.005

Muis, S., Verlaan, M., Winsemius, H. C., Aerts, J. C. J. H., & Ward, P. J. (2016). A global reanalysis of storm surges and extreme sea levels. *Nature Communications*, *7*. https://doi.org/10.1038/ncomms11969

Natural Earth. (2022). *Coastline*. https://www.naturalearthdata.com/downloads/10m-physical-vectors/10m-coastline/

Nicholls, R. J., & Klein, R. J. T. (2005). *Climate change and coastal management on Europe's coast*. http://www.eurosion.org

Nicholls, R. J., Poh Wong, P., Burkett, V., Codignotto, J., Hay, J., McLean, R., Ragoonaden, S., Woodroffe, C. D., Abuodha, P., Dronkers, J., Wong, P., Burkett, V., Codignotto, J., Hay, J., McLean, R., Ragoonaden, S., Woodroffe, C., Parry, M., Canziani, O., … Hanson, C. (2007). *Coastal systems and low-lying areas. Climate Change 2007: Impacts, Adaptation and Vulnerability.*

Nogueira, G., Stigter, T. Y., Zhou, Y., Mussa, F., Juizo, D., & Virgílio Cruz, J. (2019). Understanding groundwater salinization mechanisms to secure freshwater resources in the water-scarce city of Maputo, Mozambique. *Science of the Total Environment*, *661*, 723–736. https://doi.org/10.1016/j.scitotenv.2018.12.343

Noor, N. M., & Abdul Maulud, K. N. (2022). Coastal Vulnerability: A Brief Review on Integrated Assessment in Southeast Asia. In *Journal of Marine Science and Engineering* (Vol. 10, Issue 5). MDPI. https://doi.org/10.3390/jmse10050595

Oude Essink, G. H. P. (2001). *Density Dependent Groundwater Flow Salt Water Intrusion and Heat Transport*.

Parizi, E., Hosseini, S. M., Ataie-Ashtiani, B., & Simmons, C. T. (2019). Vulnerability mapping of coastal aquifers to seawater intrusion: Review, development and application. *Journal of Hydrology*, *570*, 555–573. https://doi.org/10.1016/j.jhydrol.2018.12.021

Pilla, G., & Torrese, P. (2022). Hydrochemical-geophysical study of saline paleo-water contamination in alluvial aquifers. *Hydrogeology Journal*, *30*(2), 511–532. https://doi.org/10.1007/s10040-021-02446-5

Pool, M., & Carrera, J. (2010). Dynamics of negative hydraulic barriers to prevent seawater intrusion. *Hydrogeology Journal*, *18*(1), 95–105. https://doi.org/10.1007/s10040-009-0516-1

Post, V. E. A., Essink, G. O., Szymkiewicz, A., Bakker, M., Houben, G., Custodio, E., & Voss, C. (2018). Celebrating 50 years of SWIMs (Salt Water Intrusion Meetings). *Hydrogeology Journal*. https://doi.org/10.1007/s10040-018-1800-8

Richts, A., Struckmeier, W. F., & Zaepke, M. (2011). WHYMAP and the Groundwater Resources Map of the World 1:25,000,000. In *Sustaining Groundwater Resources* (pp. 159–173). Springer Netherlands. https://doi.org/10.1007/978-90-481-3426-7_10

Seenipandi, K., Nainarpandian, C., Kandathil, R. K., & Sellamuthu, S. (2019). Seawater intrusion vulnerability in the coastal aquifers of southern India—an appraisal of the GALDIT model, parameters' sensitivity, and hydrochemical indicators. *Environmental Science and Pollution Research*, *26*(10), 9755–9784. https://doi.org/10.1007/s11356-019-04401-0

Setiawan, T., Yermia, E., Joko Purnomo, B., & Haryadi Tirtomihardjo, dan. (2017). *Seawater Intrusion in the Confined Aquifer System of Jakarta Graundwater Basin Base on Hydrochemical and Hydroisotope*. *27*(1), 1–14. https://doi.org/10.4203/risetgeotam

Siebert, S., Kummu, M., Porkka, M., Döll, P., Ramankutty, N., & Scanlon, B. R. (2015). A global data set of the extent of irrigated land from 1900 to 2005. *Hydrology and Earth System Sciences*, *19*(3), 1521–1545. https://doi.org/10.5194/hess-19-1521-2015

Sinaga, T. P. T., Nugroho, A., Lee, Y. W., & Suh, Y. (2011). GIS mapping of tsunami vulnerability: Case study of the Jembrana regency in Bali, Indonesia. *KSCE Journal of Civil Engineering*, *15*(3), 537–543. https://doi.org/10.1007/s12205-011-0741-8

Sprenger, C., Hartog, N., Hernández, M., Vilanova, E., Grützmacher, G., Scheibler, F., & Hannappel, S. (2017). Inventaire des sites de gestion des aquifères par recharge en Europe: développement historique, situation actuelle et perspectives. *Hydrogeology Journal*, *25*(6), 1909–1922. https://doi.org/10.1007/s10040-017-1554-8

Stigter, T. (2021, November 28). *Managing the invisible: Groundwater salinity in coastal areas*. Https://Www.Un-Ihe.Org/Stories/Managing-Invisible-Groundwater-Salinity-Coastal-Areas.

Stuyfzand, P. J., & van der Schans, M. L. (2018). Effects of intake interruptions on dune infiltration systems in the Netherlands, their quantification and mitigation. *Science of the Total Environment*, *630*, 757–773. https://doi.org/10.1016/j.scitotenv.2018.02.104

Sutanudjaja, E. H., van Beek, R., Wanders, N., Wada, Y., Bosmans, J. H. C., Drost, N., van der Ent, R. J., de Graaf, I. E. M., Hoch, J. M., de Jong, K., Karssenberg, D., López López,

P., Peßenteiner, S., Schmitz, O., Straatsma, M. W., Vannametee, E., Wisser, D., & Bierkens, M. F. P. (2018). PCR-GLOBWB 2: a 5 arcmin global hydrological and water resources model. *Geoscientific Model Development*, *11*(6), 2429–2453. https://doi.org/10.5194/gmd-11-2429-2018

Tasnim, Z., & Tahsin, S. (2016). Application of the Method of Galdit for Groundwater Vulnerability Assessment: A Case of South Florida. *South Florida Asian Journal of Applied Science and Engineering*, *5*(1), 27–40. https://doi.org/10.18034

Taylor, R. G., Scanlon, B., Döll, P., Rodell, M., van Beek, R., Wada, Y., Longuevergne, L., Leblanc, M., Famiglietti, J. S., Edmunds, M., Konikow, L., Green, T. R., Chen, J., Taniguchi, M., Bierkens, M. F. P., Macdonald, A., Fan, Y., Maxwell, R. M., Yechieli, Y., … Treidel, H. (2013). Ground water and climate change. In *Nature Climate Change* (Vol. 3, Issue 4, pp. 322–329). https://doi.org/10.1038/nclimate1744

Tebaldi, C., Ranasinghe, R., Vousdoukas, M., Rasmussen, D. J., Vega-Westhoff, B., Kirezci, E., Kopp, R. E., Sriver, R., & Mentaschi, L. (2021). Extreme sea levels at different global warming levels. *Nature Climate Change*, *11*(9), 746–751. https://doi.org/10.1038/s41558-021-01127-1

Thorslund, J., & van Vliet, M. T. H. (2020). A global dataset of surface water and groundwater salinity measurements from 1980–2019. *Scientific Data*, *7*(1). https://doi.org/10.1038/s41597-020-0562-z

Todd, D. K., & Mays, L. W. (2005). *Groundwater Hydrology* (B. Zobrist, J. Welter, & V. A. Vargas, Eds.; 3rd ed.). John Wiley & Sons.

Trabelsi, N., Triki, I., Hentati, I., & Zairi, • Moncef. (2016). Aquifer vulnerability and seawater intrusion risk using GALDIT, GQI SWI and GIS: case of a coastal aquifer in Tunisia. *Environmental Earth Sciences*, *75*. https://doi.org/10.1007/s12665-016-5459-y

Verkaik, J., Sutanudjaja, E. H., Oude Essink, G. H. P., Lin, H. X., & Bierkens, M. F. P. (2021). Implementing a transient PCR-GLOBWB-MODFLOW global groundwater model on a 1 km resolution using high performance computing. *AGU Fall Metting 2021*.

Vithanage, M., Engesgaard, P., Villholth, K. G., & Jensen, K. H. (2012). The Effects of the 2004 Tsunami on a Coastal Aquifer in Sri Lanka. *Ground Water*, *50*(5), 704–714. https://doi.org/10.1111/j.1745-6584.2011.00893.x

von Glasow, R., Jickells, T. D., Baklanov, A., Carmichael, G. R., Church, T. M., Gallardo, L., Hughes, C., Kanakidou, M., Liss, P. S., Mee, L., Raine, R., Ramachandran, P., Ramesh, R., Sundseth, K., Tsunogai, U., Uematsu, M., & Zhu, T. (2013). Megacities and large urban agglomerations in the coastal zone: Interactions between atmosphere, land, and marine ecosystems. In *Ambio* (Vol. 42, Issue 1, pp. 13–28). https://doi.org/10.1007/s13280-012-0343-9

Vrba, J., & Zaporožec, A. (1994). *Guidebook on mapping groundwater vulnerability*. Heise.

Wada, Y., van Beek, L. P. H., Sperna, F. C., Chao, B. F., Wu, Y.-H., Bierkens, M. F. P., van Beek, L. P. H., Sperna, F. C., Chao, B. F., Wu, Y.-H., & Bierkens, M. F. P. (2012). *Past and future contribution of global groundwater depletion to sea-level rise*. https://doi.org/10.1029/2012GL051230

Wada, Y., Wisser, D., & Bierkens, M. F. P. (2014). Global modeling of withdrawal, allocation and consumptive use of surface water and groundwater resources. *Earth System Dynamics*, *5*(1), 15–40. https://doi.org/10.5194/esd-5-15-2014

Weerasekera, W. L. (2017). *3D Variable-density Groundwater Modelling of the Red River Delta, Vietnam*.

Werner, A. D., Bakker, M., Post, V. E. A., Vandenbohede, A., Lu, C., Ataie-Ashtiani, B., Simmons, C. T., & Barry, D. A. (2013). Seawater intrusion processes, investigation and management: Recent advances and future challenges. *Advances in Water Resources*, *51*, 3–26. https://doi.org/10.1016/j.advwatres.2012.03.004

Wetzelhuetter, C. (2013). Groundwater in the Coastal Zones of Asia-Pacific. In *Coastal Research Library* (Vol. 7). http://www.springer.com/series/8795

WHO. (2003). *Total dissolved solids in Drinking-water Background document for development of WHO Guidelines for Drinking-water Quality*.

Wijaya, A., Kuntoro, A. A., & Gondodinoto, E. A. S. (2019). Pemodelan Intrusi Air Asin Pada Akuifer Pantai (Studi Kasus: DKI Jakarta). *JURNAL TEKNIK HIDRAULIK*, *10*(1), 15–28. https://doi.org/10.32679/jth.v10i1.583

Wu, H., Lu, C., Kong, J., & Werner, A. D. (2020). Preventing Seawater Intrusion and Enhancing Safe Extraction Using Finite-Length, Impermeable Subsurface Barriers: 3D Analysis. *Water Resources Research*, *56*(11). https://doi.org/10.1029/2020WR027792

Xiao, H., Tang, Y., Li, H., Zhang, L., Ngo-Duc, T., Chen, D., & Tang, Q. (2021). Saltwater intrusion into groundwater systems in the Mekong Delta and links to global change. In *Advances in Climate Change Research* (Vol. 12, Issue 3, pp. 342–352). National Climate Center. https://doi.org/10.1016/j.accre.2021.04.005

Zamrsky, D. (2013). *Coastal vulnerability to tsunami impacts and modelling SWI in aquifers situated in the most vulnerable areas*.

Zamrsky, D., Karssenberg, M. E., Cohen, K. M., Bierkens, M. F. P., & Oude Essink, G. H. P. (2020). Geological Heterogeneity of Coastal Unconsolidated Groundwater Systems Worldwide and Its Influence on Offshore Fresh Groundwater Occurrence. *Frontiers in Earth Science*, *7*. https://doi.org/10.3389/feart.2019.00339

Zamrsky, D., Oude Essink, G. H. P., & Bierkens, M. F. P. (2018). Estimating the thickness of unconsolidated coastal aquifers along the global coastline. *Earth System Science Data*, *10*(3), 1591–1603. https://doi.org/10.5194/essd-10-1591-2018

Zamrsky, D., Oude Essink, G. H. P., Sutanudjaja, E. H., van Beek, L. P. H., & Bierkens, M. F. P. (2021). Offshore fresh groundwater in coastal unconsolidated sediment systems as a potential fresh water source in the 21st century. *Environmental Research Letters*, *17*(1). https://doi.org/10.1088/1748-9326/ac4073

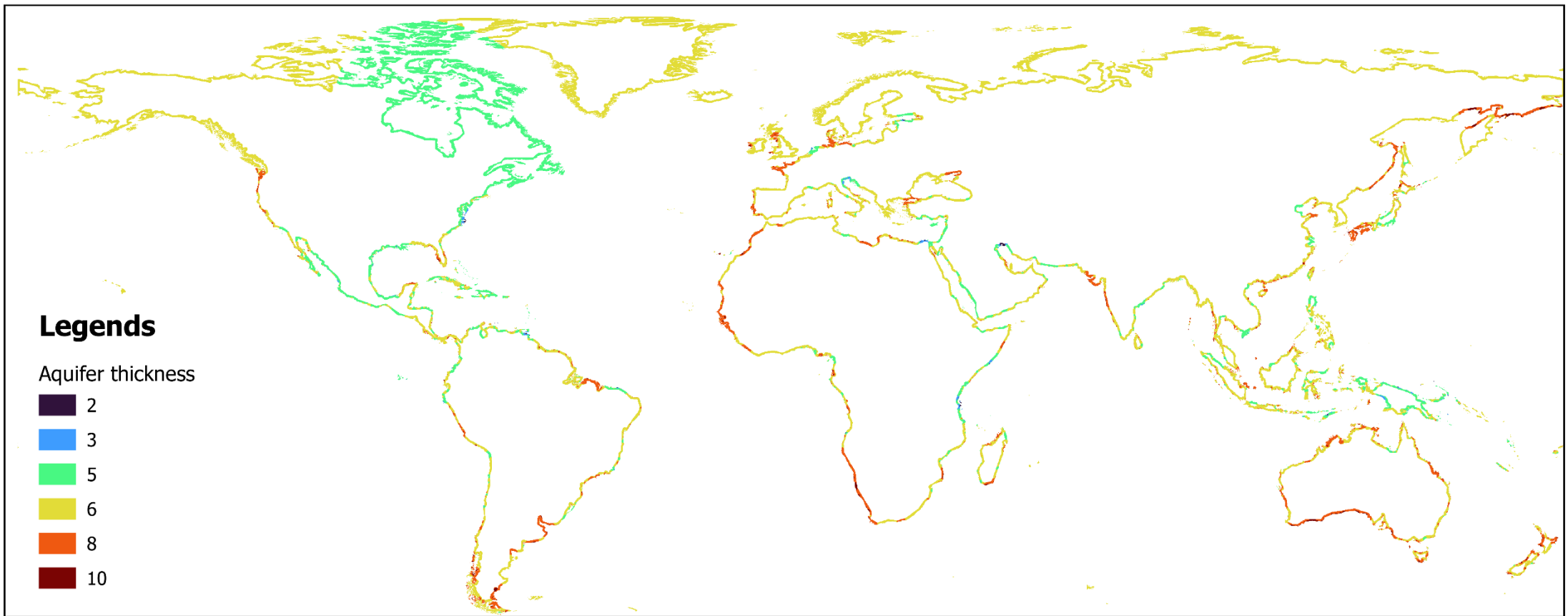Zomer, R. J., & Trabucco, A. (2022). *Global Aridity Index and Potential Evapo-Transpiration (ET0) Database v3*. https://cgiarcsi.community/2019/01/24/global-

Appendices

Appendix A. -   Global vulnerability map before reclassified into 5 categories

Legends

Vulnerability index

7.576277

2.081577

Legends

Aquifer type

- 4
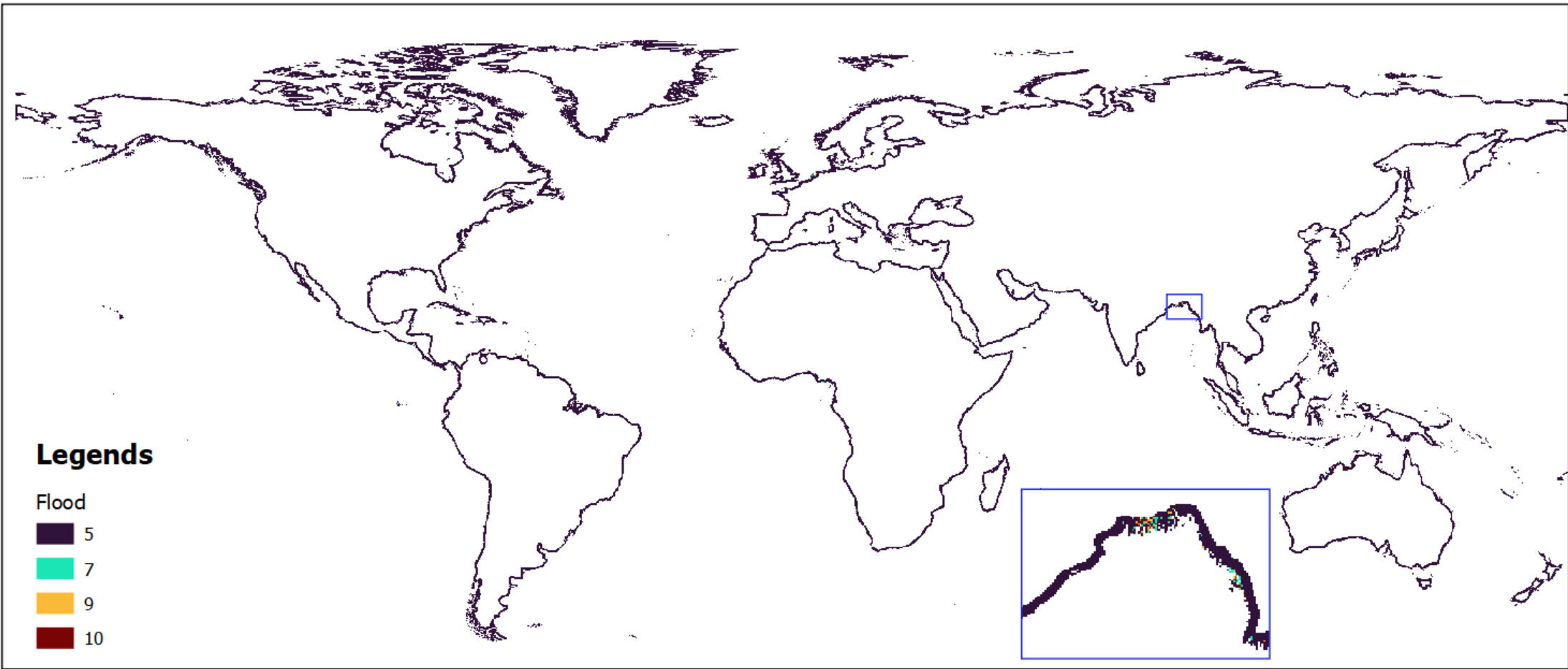- 6
- 8
- 10
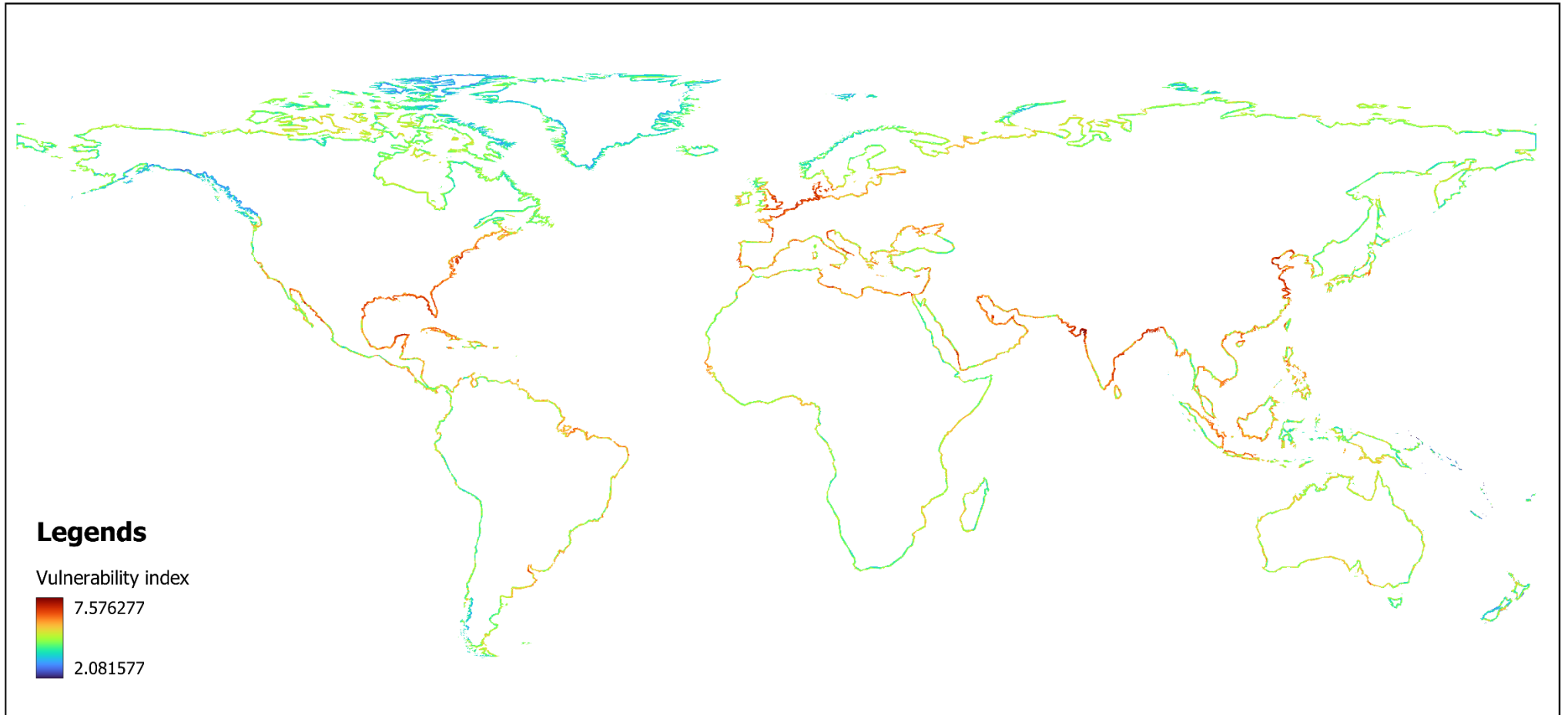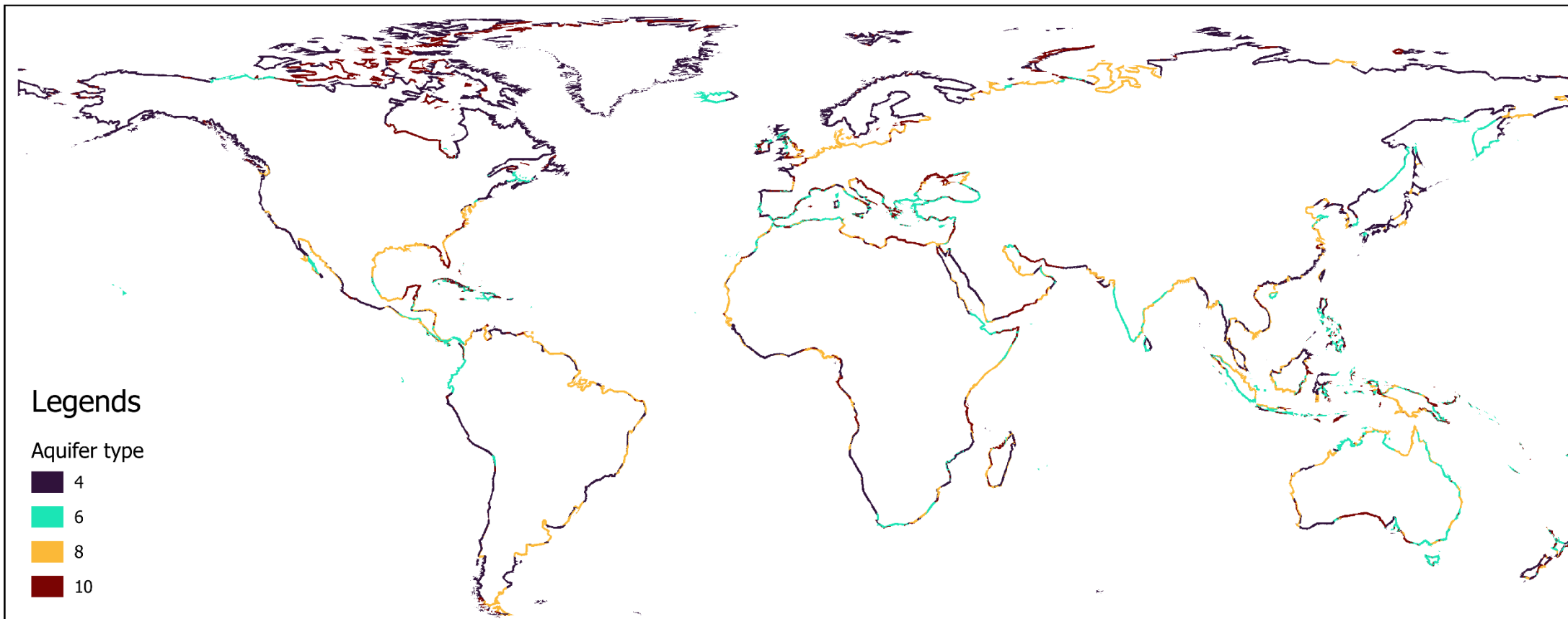
B-1. Reclassified aquifer type in coastal zone
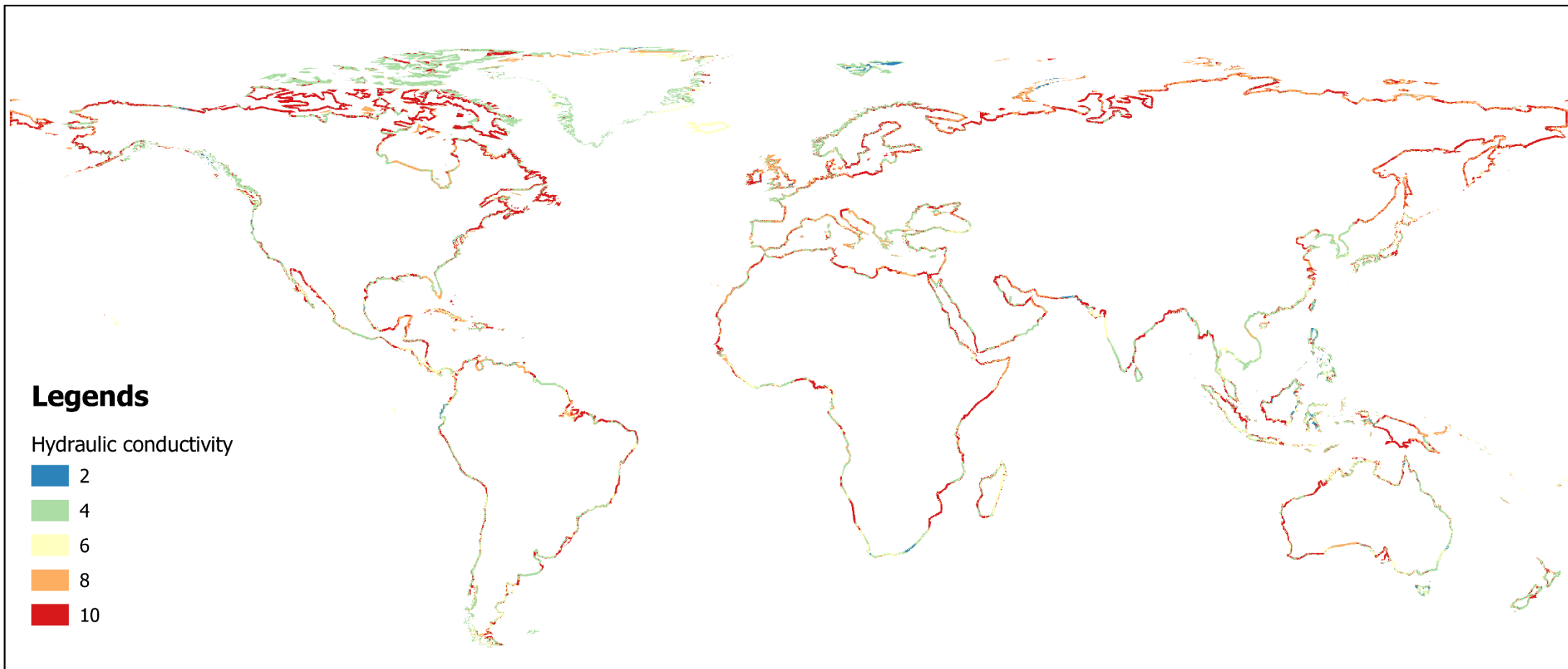
B-2. Reclassified aquifer thickness in coastal zone
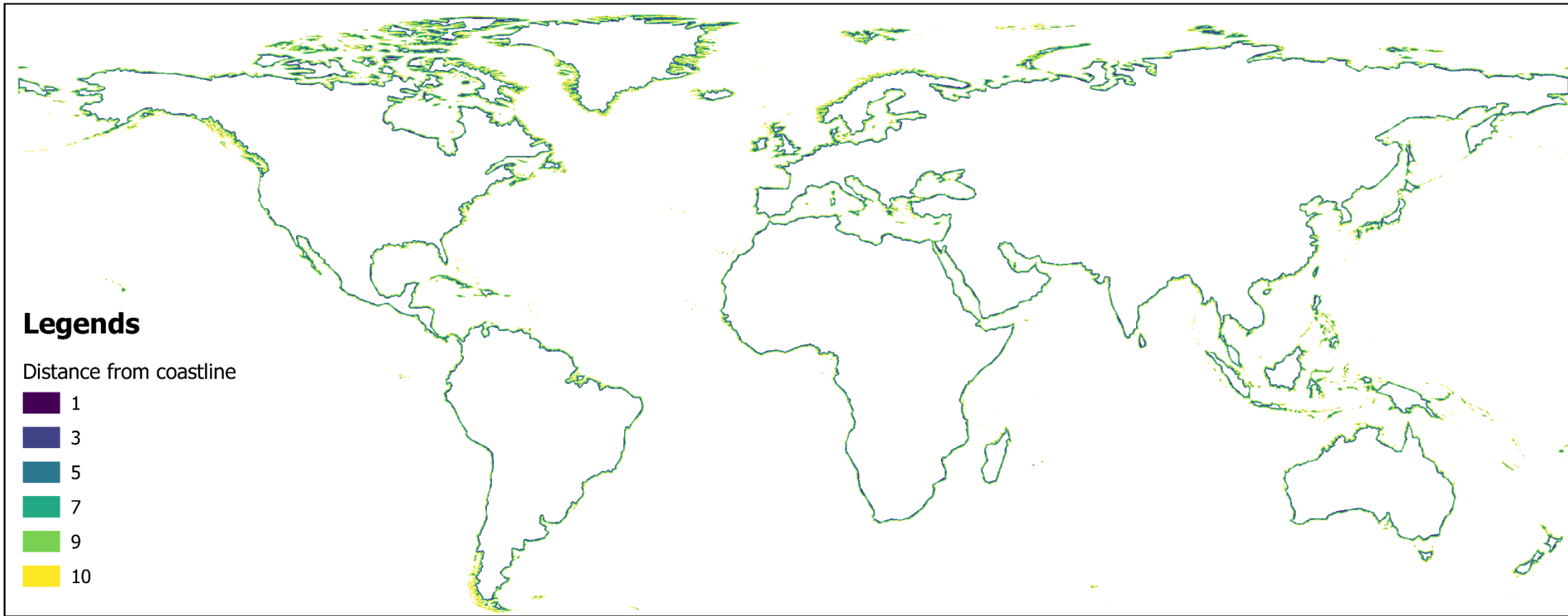
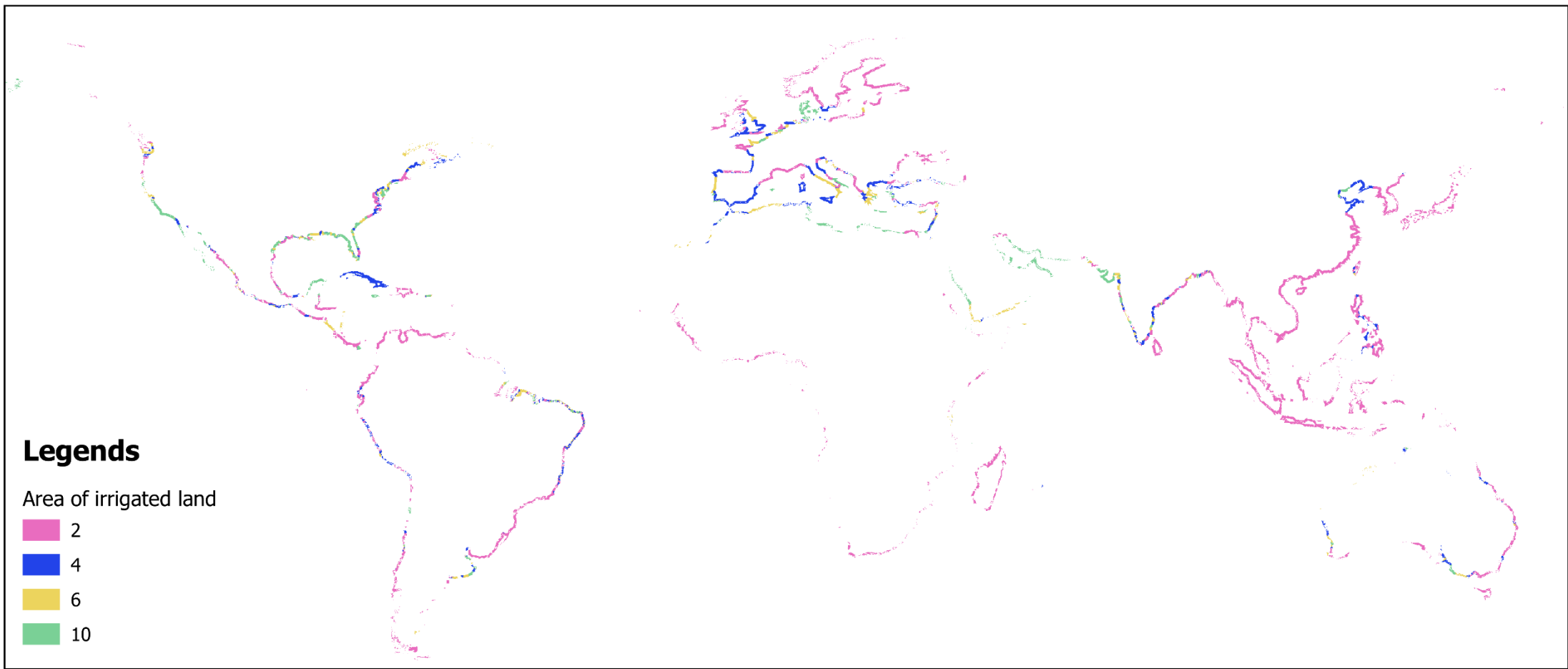B-3. Reclassified distance from coastline in coastal zone
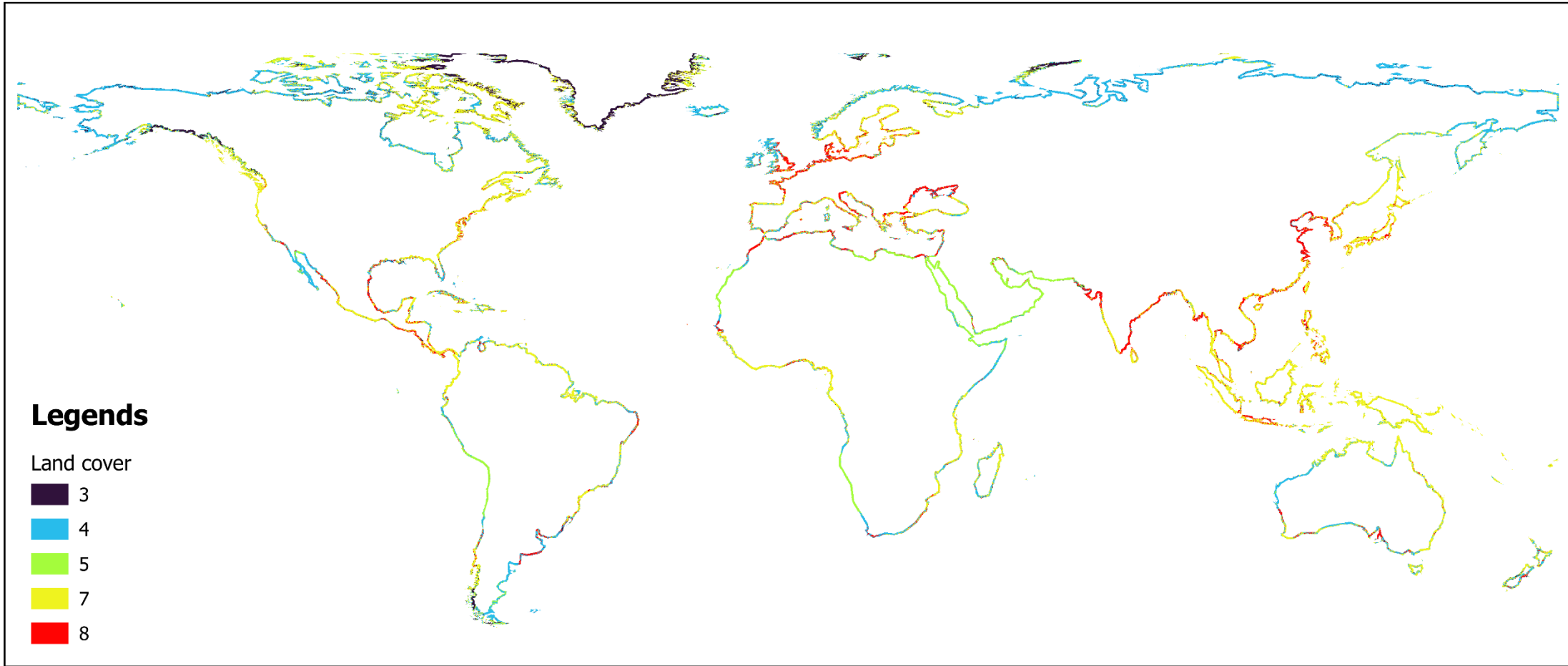
B-4. Reclassified flood in coastal zone
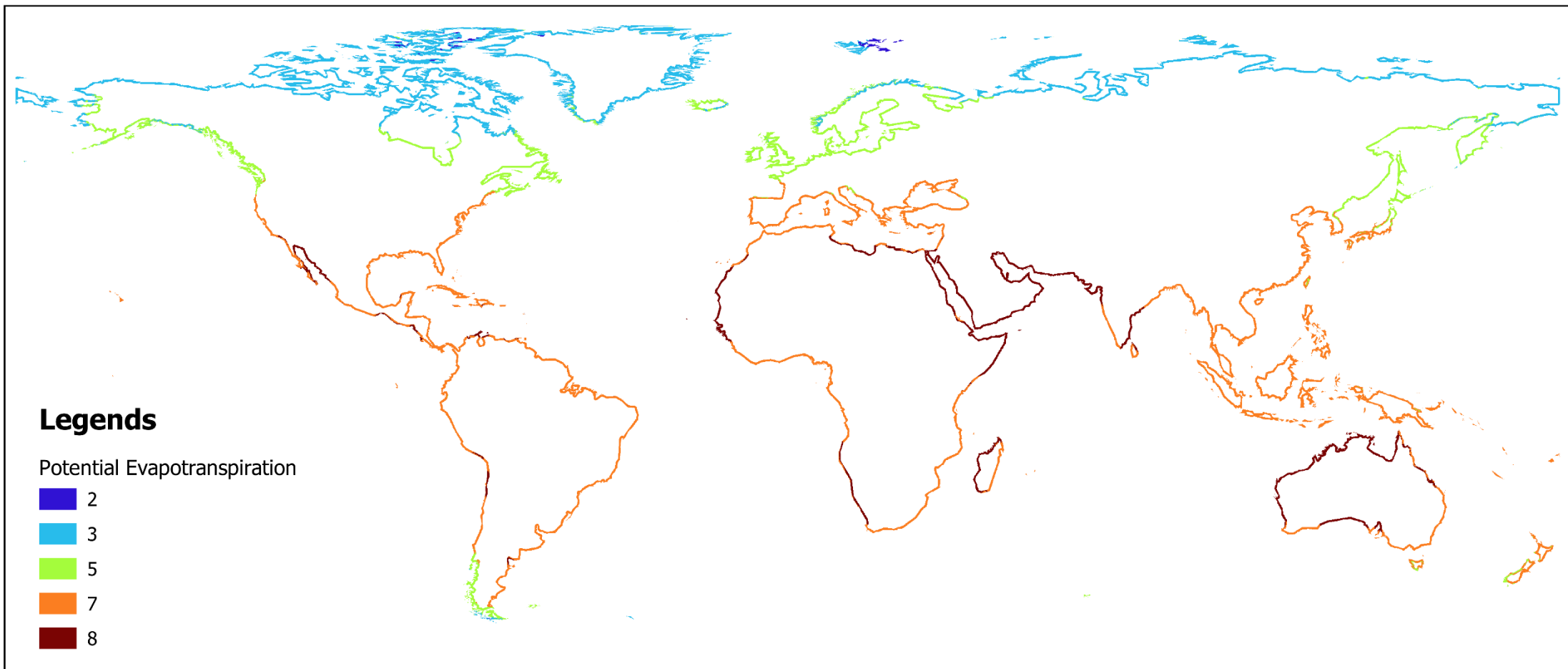
B-5. Reclassified groundwater abstraction in coastal zone

B-6. Reclassified hydraulic conductivity in coastal zone

B-7. Reclassified area of irrigated land in coastal zone

B-8. Reclassified land cover in coastal zone

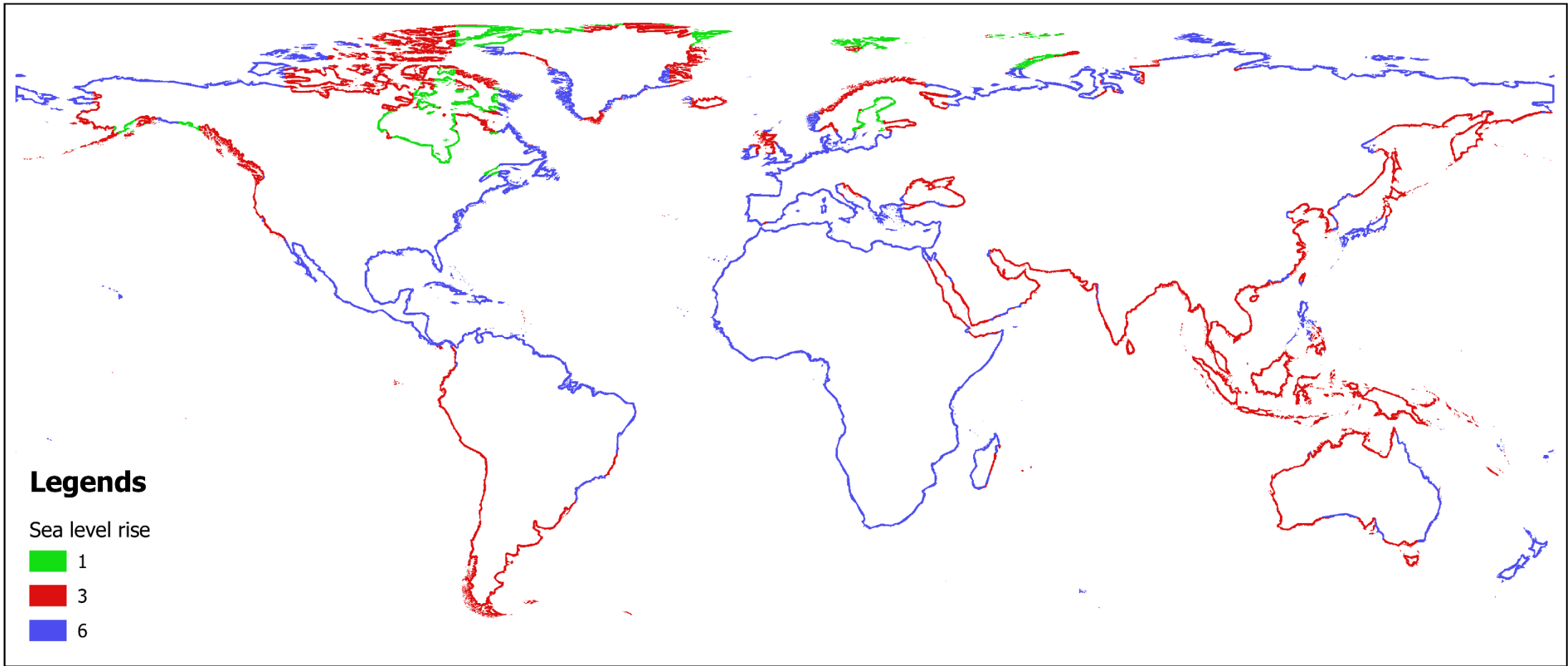B-9. Reclassified potential evapotranspiration in coastal zone
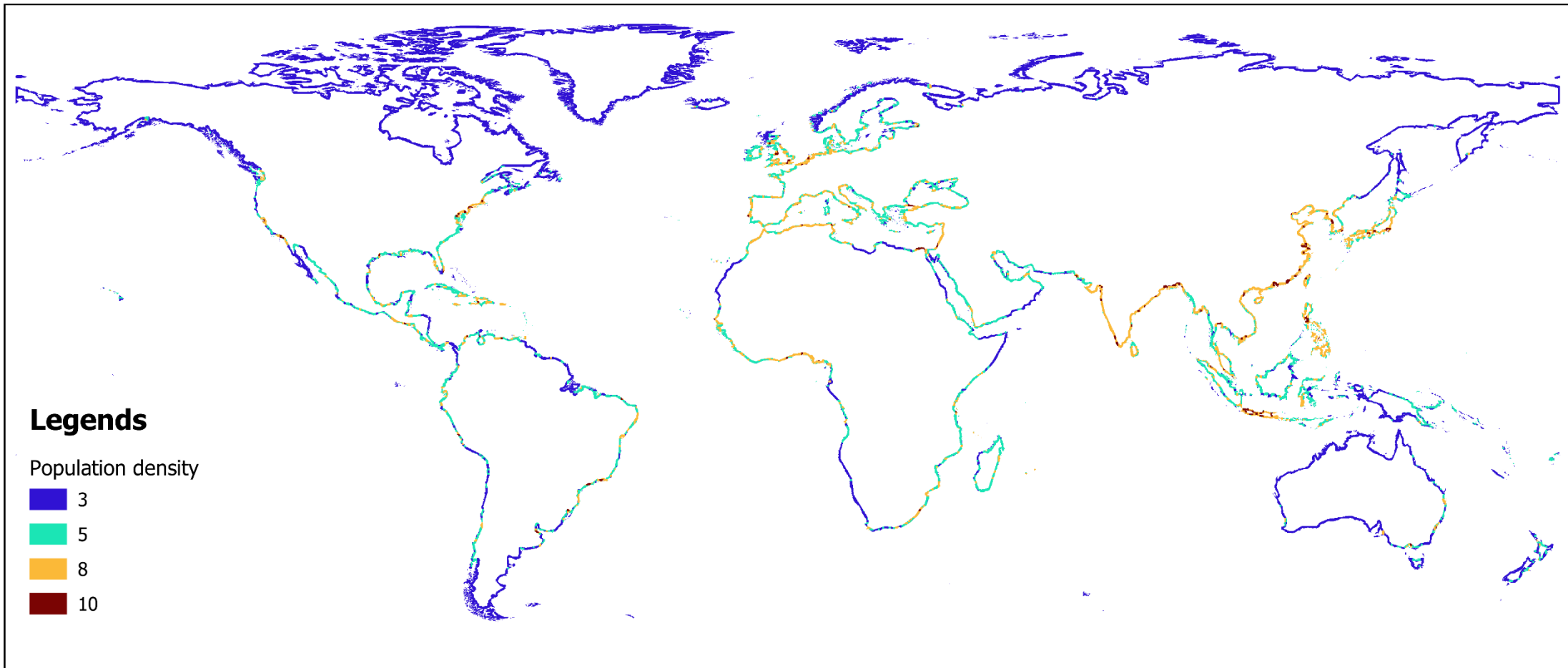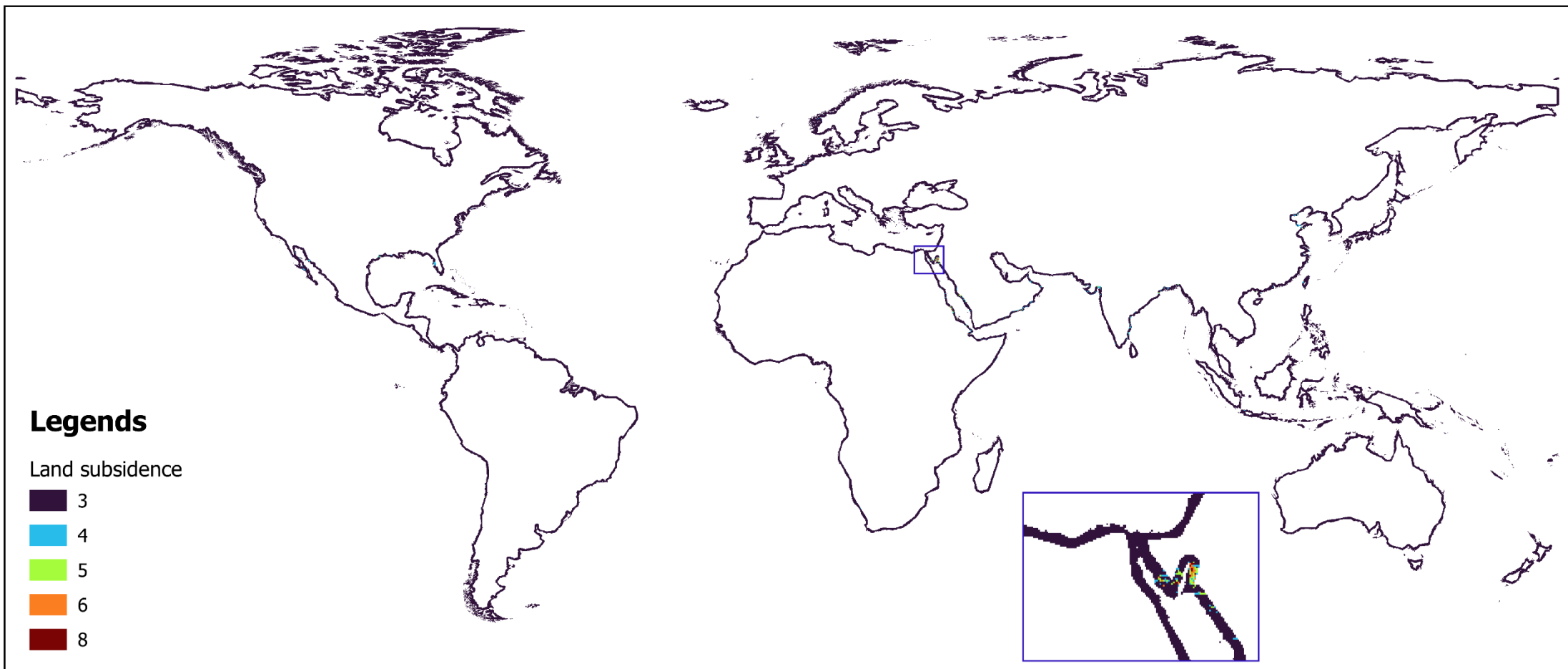
B-10. Reclassified population density in coastal zone

Legends

Population density
- 3
- 5
- 8
- 10
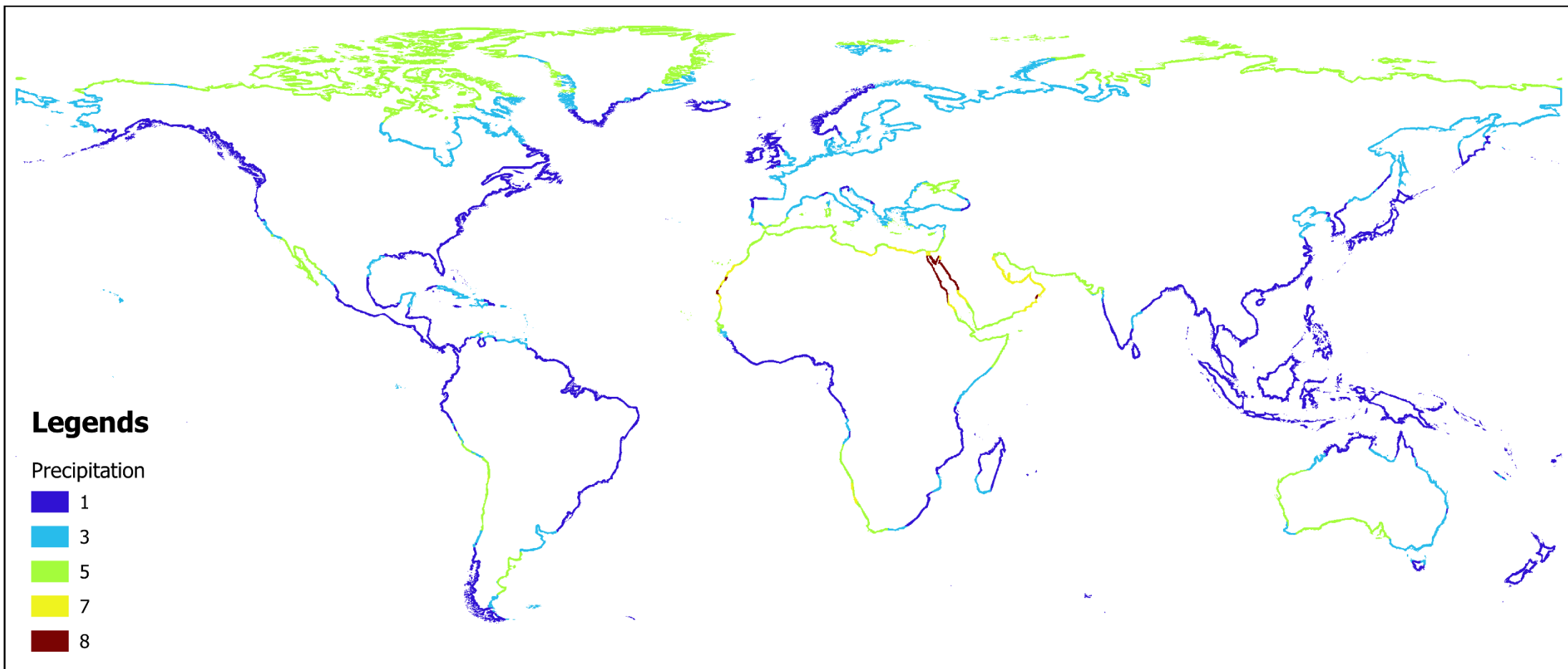
B-11. Reclassified precipitation in coastal zone

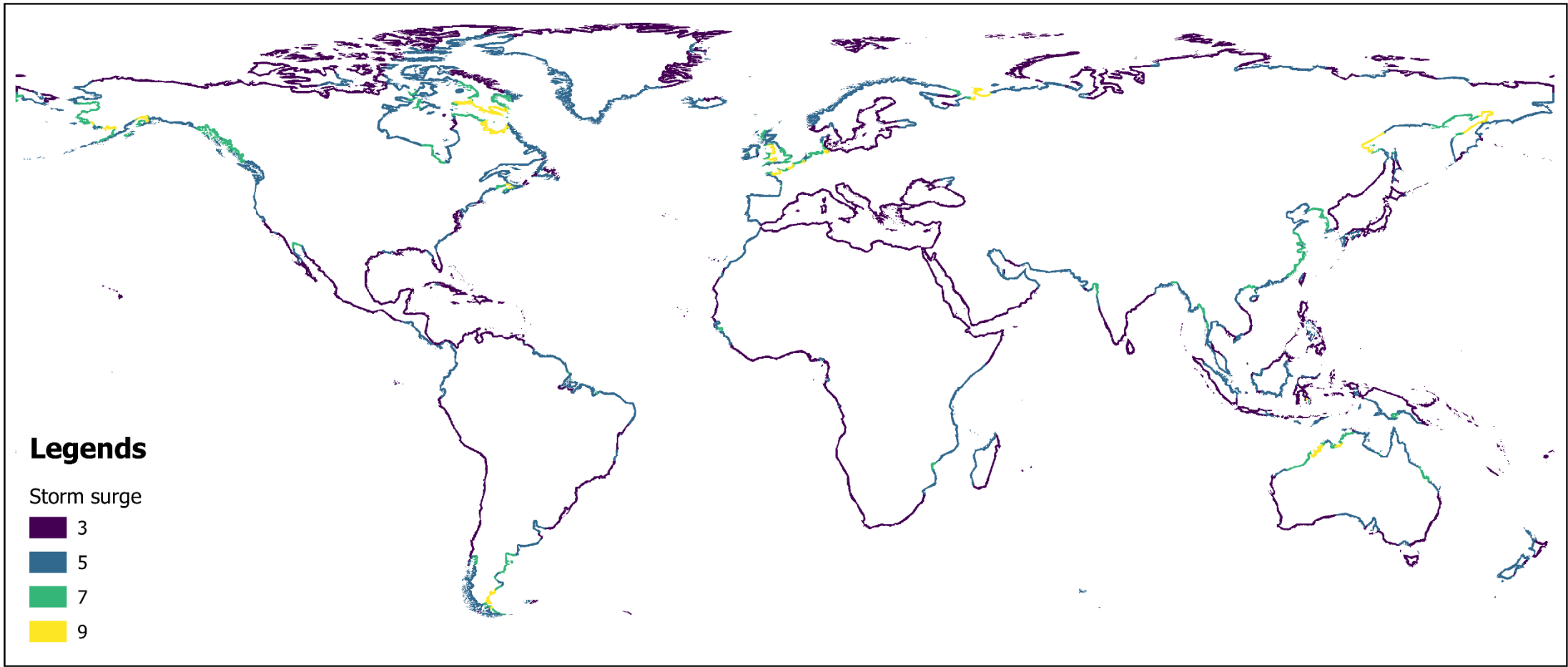Legends
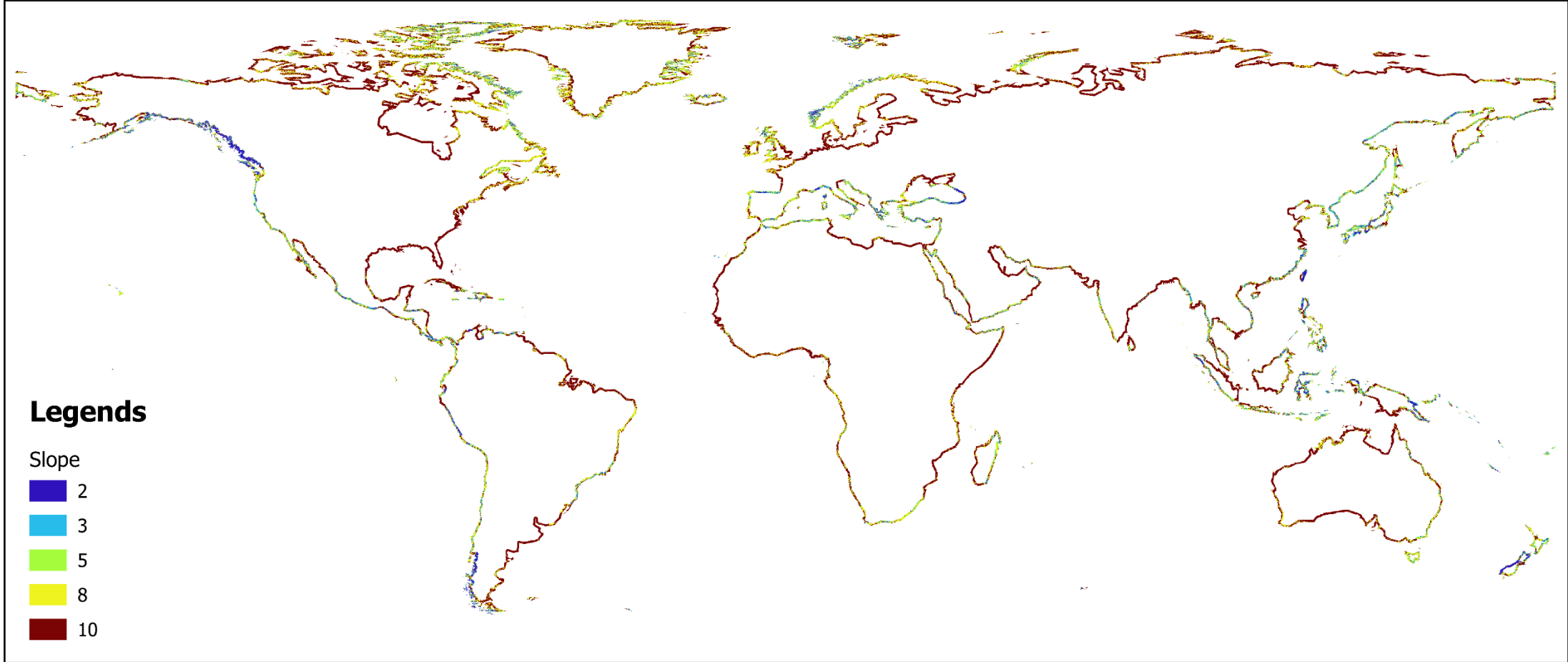
Slope
- 2
- 3
- 5
- 8
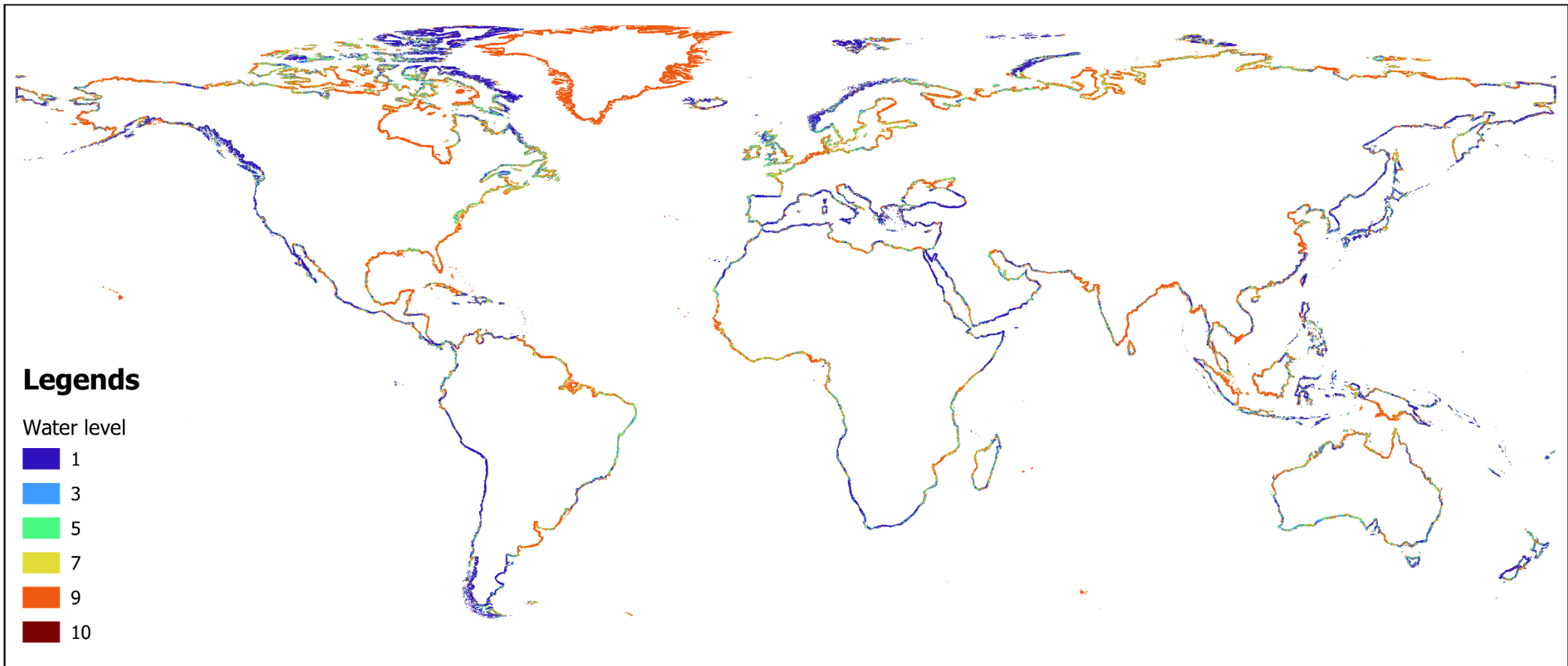- 10

B-12. Reclassified surface slope in coastal zone

B-13. Reclassified sea level rise along the coastline, interpolated toward coastal zone

B-14. Reclassified land subsidence in coastal zone

B-15. Reclassified storm surges along the coastline interpolated landward

B-16. Reclassified water level in coastal zone